

JANNE HAAPANEN

Control of Wettability Using Flame Generated Multicomponent Nanoparticle Coatings

JANNE HAAPANEN

Control of Wettability Using Flame Generated Multicomponent Nanoparticle Coatings

ACADEMIC DISSERTATION

To be presented, with the permission of
the Faculty of Engineering and Natural Sciences
of Tampere University,

for public discussion in the Auditorium TB109
of the Tietotalo Building, Korkeakoulunkatu 1, 33720 Tampere,
on 15 September 2023, at 12 o'clock.

ACADEMIC DISSERTATION
Tampere University, Faculty of Engineering and Natural Sciences
Finland

*Responsible
supervisor
and Custos*

Professor
Jyrki Mäkelä
Tampere University
Finland

Pre-examiners

Associate Professor
Adam Boies
University of Cambridge
United Kingdom

Docent
Jorma Joutsensaari
University of Eastern Finland
Finland

Opponent

Professor Dr.-Ing.
Einar Kruis
University of Duisburg-Essen
Germany

The originality of this thesis has been checked using the Turnitin OriginalityCheck service.

Copyright ©2023 Janne Haapanen

Cover design: Roihu Inc.

ISBN 978-952-03-3016-3 (print)
ISBN 978-952-03-3017-0 (pdf)
ISSN 2489-9860 (print)
ISSN 2490-0028 (pdf)
<http://urn.fi/URN:ISBN:978-952-03-3017-0>



Carbon dioxide emissions from printing Tampere University dissertations have been compensated.

PunaMusta Oy – Yliopistopaino
Joensuu 2023

PREFACE

The work of this thesis was performed at the Aerosol Physics Laboratory of Tampere University (former Tampere University of Technology). Work was mainly carried out in the NANORATA2 project, funded by TEKES. In addition to this project, I have had a possibility to take part in several other projects with relatively broad spectrum of different nanocoatings and applications, especially nLABS project funded by Academy of Finland. Jenny and Antti Wihuri Foundation is gratefully acknowledged for additional financial support.

First, I want to thank you my supervisor, Prof. Jyrki Mäkelä for hiring me to Aerosol Synthesis group as M.Sc. thesis worker. Inspiring and experimental research group and atmosphere in the lab, guided me for continuing my research further. Second, I want to thank Prof. Jorma Keskinen keeping up the positive attitude as the head of the laboratory. I would like to thank my pre-examiners Assoc. Prof. Adam Boies and Doc. Jorma Joutsensaari for the valuable comments and remarks for my thesis.

I have been blessed with excellent co-workers and co-authors throughout my time at the university. Dr. Mikko Aromaa is acknowledged for introduction to flame synthesis analysis methods and showing that almost anything can be nanocoated. I want to thank Dr. Hannu Teisala and Dr. Mikko Tuominen for the excellent collaboration in roll-to-roll coatings and the fruitful discussions. I want to thank Dr. Milena Stepien and Dr. Mari Honkanen for the hours and hours spent on the electron microscopes. All other co-authors are also acknowledged for their valuable contribution to the publications. Special thanks to our “Cut and Paste” group: Dr. Paxton Juuti, Dr. Miika Sorvali and Mr. Markus Nikka for the almost endless work with sample preparations.

I would like to thank our coffee break team Mikko, Juha, Jaakko, Kaisa and Jonna for making it enjoyable to join the research group. I would like to thank the whole OQ group, including my long-time roommate Anssi Järvinen for creating an excellent atmosphere at work.

I want to thank my fellow cigar aficionados in Finland and Denmark, as well as my fishing buddies and Mystic Tampere friends for keeping the balance between work and free time.

Finally, I want to thank my family for the endless support during all these years. My parents Irma and Esko and my sister Sanna have provided me the perfect base for problem solving and other useful researcher's skills. My deepest gratitude belongs to my wife Niina and my children Justus and Nelli for all the support and flexibility during these years. I love you all.

Tampere, August 2023
Janne Haapanen

ABSTRACT

Control of wettability of surfaces has been a hot research topic for years. Developing superhydrophobic and superhydrophilic surfaces are originally inspired by nature. Most common way to control the wettability of a surface is to produce functional nanocoatings on different substrates. In this work, aerosol synthesis method Liquid Flame Spray (LFS) was used for fabricating functional nanocoatings on paperboard, wood and glass substrates. Superhydrophobic and superhydrophilic nanocoatings have been previously produced by LFS method, but in this work the structure of the nanocoating was researched more closely to gain better understanding of the stability of the coating. Furthermore, minimum amount of coating for wettability modification was determined. Wettability of a surface was significantly changed even if the surface was only partly covered with nanoparticles.

Stability and wear resistance of functional nanocoatings is generally quite poor, so this was one of the research topics of this work. Stability of a coating depends on the adhesion and cohesion of the coating. Adhesion describes the interaction between a coating and a substrate and cohesion describes particle-to-particle interactions in the coating layer. This work focused on improving the cohesion of the nanocoatings by modifying the material composition of produced nanoparticles. Previously superhydrophobic TiO_2 nanocoatings have been fabricated by LFS, but in this work TiO_2 nanocoating was doped with SiO_2 , to improve the cohesion between agglomerated nanoparticles. Cohesion was successfully improved without losing the desired porosity or wetting properties.

LFS method was also combined with other coating methods. By combining LFS with other coating methods, superamphiphobic behavior was achieved, meaning that nanocoated surface repelled also other liquids than water. Nanoparticle layer formed optimal, porous layer on a surface and nanoparticle layer was afterwards modified by plasma treatment or chemical vapor deposition to obtain needed chemical composition of the coating. By combining different coating methods, excellent repellency for water, olive oil, ethylene glycol (EG), diiodomethane (DIM) and n-Hexadecane was observed. Stability of multicomponent coatings was tested with thousands of water droplets and coating remained unharmed. This indicates relatively good adhesion and cohesion of the multicomponent coatings.

TIIVISTELMÄ

Pintojen kastuvuuden muokkaaminen on ollut yksi tärkeimmistä tutkimusaiheista jo vuosia. Kehitysidea vettähylykiviin ja vesihakuisiin pintoihin on tullut alun perin luonnon esimerkeistä. Yleisin tapa muokata pinnan kastumista on valmistaa pinnalle toiminnallinen nanopinnoite. Tässä työssä valmistettiin toiminnallisia nanopinnoitteita kartonki-, puu- ja lasipinnoille. Menetelmänä käytettiin nesteliiekkiruiskutusta (Liquid Flame Spray, LFS), jossa nanohiukkasia muodostetaan aerosolimenetelmällä. Superhydrofobisia eli vettähylykiviä ja superhydrofiilisiä eli vesihakuisia pinnoitteita on tehty jo aiemmin nesteliiekkiruiskutuksella, mutta tässä työssä tutkittiin tarkemmin pinnoitteen rakennetta ja selvitettiin mikä on minimimäärä pinnoitetta, jolla pinnan kastumista saadaan muokattua. Pinnan kastuvuus muuttui radikaalisti, vaikka pinta oli vain osittain nanohiukkasten peitossa.

Pinnoitteen pysyvyys ja kulutuskestävyys ovat perinteisesti nanopinnoitteiden suurimpia ongelmia, joten ne ovat tämänkin työn tutkimusaiheita. Pinnoitteen kestävyys riippuu pääosin pinnoitteen adheesiosta ja koheesiosta. Adheesiolla tarkoitetaan pinnoitteen kiinnittymistä materiaalin pintaan ja koheesiolla hiukkasten keskinäistä kiinnipysyvyyttä nanopinnoitteessa. Tässä työssä koheesiota on pyritty parantamaan muokkaamalla nanopinnoitteen hiukkarakennetta. Aiemmissa töissä superhydrofobinen pinnoite on saatu aikaan TiO_2 nanohiukkasilla, mutta tässä työssä TiO_2 nanopinnoitteen agglomeraattien kestävyyttä parannettiin lisäämällä pinnoitteeseen myös SiO_2 nanohiukkasia. Tällä tavoin pinnoitteen koheesiota saatiin parannettua niin että pinnoitteen huokoisuus ja vettähylykyvyys säilyivät lähes ennallaan.

Tässä työssä LFS-menetelmää yhdisteltiin myös muiden pinnoitusmenetelmien kanssa. Yhdistämällä useiden pinnoitusmenetelmien hyviä puolia, saatiin aikaan superamfifobinen pinnoite eli pinnoite hylki myös muita nesteitä kuin vain vettä. LFS-menetelmällä valmistettiin huokoinen nanorakenne, jonka pintaa parannettiin plasmakäsittelyllä tai kemiallisella kaasufaasipinnoituksella (Chemical Vapor Deposition, CVD). Näillä yhdistelmäpinnoituksilla pinta saatiin hylkimään vettä, oliiviöljyä, etyleeniglykolia, diodometaania sekä n-heksadekaania. Yhdistelmäpinnoitteiden pysyvyyttä testattiin pisaratesteillä, joissa pinnoille pudotettiin tuhansia

vesipisaroita. Pinnoite pysyi vahingoittumattomana, joten yhdistelmäpinnoitteella voitiin todeta olevan kohtuullisen hyvä adheesio ja koheesio.

CONTENTS

1	Introduction	1
2	Nanoparticle Synthesis	5
2.1	Liquid Flame Spray	5
2.2	Other Synthesis Methods	8
3	Coating Methods	11
3.1	Liquid Flame Spray	11
3.1.1	Deposition Process	11
3.1.2	Substrate Options	13
3.1.3	Multi-component Coatings	14
3.1.4	Up-scalability	14
3.2	Other Coating Methods	15
3.2.1	Plasma Treatment	16
3.2.2	Chemical Vapor Deposition (CVD)	17
4	Analysis and Characterization Methods	19
4.1	Determination of Wettability	20
4.2	Scanning Electron Microscopy (SEM)	21
4.3	Transmission Electron Microscopy (TEM)	21
4.4	Chemical Analysis	21
4.5	Inductively Coupled Plasma Optical Emission Spectrometry (ICP-OES)	22
4.6	UV-Transmission Measurement	22
5	Functionality of Fabricated Nanocoatings	25
5.1	Wetting	25
5.2	Effect of the Coating Amount	27
5.3	Multi-component Nanocoatings	30
5.4	Combining Different Coating Methods	32
5.5	Stability	34
6	Conclusions	39
	References	43

SYMBOLS AND ABBREVIATIONS

SYMBOLS

γ	Surface tension of the liquid (mN/m)
θ	Water Contact Angle (WCA, °)

ABBREVIATIONS

ACVD	Atmospheric Pressure Chemical Vapor Deposition
AgNO ₃	Silver nitrate
ALD	Atomic Layer Deposition
CA	Contact angle
CCVD	Combustion Assisted Chemical Vapor Deposition
CVD	Chemical Vapor Deposition
DC-SPU	Direct Current Sputtering
EDS/EDX	Energy-dispersive X-ray Spectroscopy
EG	Ethylene glycol
EVP	Evaporation
FSP	Flame Spray Pyrolysis
Hexa	n-Hexadecane
HWLP	Hot Wall Aerosol Reactor and Low-Pressure Impactor
IAD	Ion Beam Sputtering Ion Assisted Deposition
ICP-OES	Inductively Coupled Plasma Optical Emission Spectrometry
LFS	Liquid Flame Spray
MBE	Molecular Beam Epitaxy
OMCVD	Organometallic Chemical Vapor Deposition
PECVD	Plasma Enhanced Chemical Vapor Deposition
PFH	Perfluorohexane
PLD	Pulsed Laser Deposition
PVD	Physical Vapor Deposition

RA	Roll-off angle
RF-SPU	Radio Frequency Sputtering
RGTO	Rheotaxial Growth and Thermal Oxidation
SCBD	Supersonic Cluster Beam Deposition
SEM	Scanning Electron Microscopy
Si	Silicon
SiO ₂	Silicon dioxide
SP	Spray Pyrolysis
TEOS	Tetraethyl orthosilicate
TEM	Transmission Electron Microscopy
Ti	Titanium
TiO ₂	Titanium dioxide
TTIP	Titanium tetraisopropoxide
UV	Ultraviolet
WCA	Water Contact Angle
XPS	X-ray Photoelectron Spectroscopy
XRD	X-ray Diffraction Spectroscopy

ORIGINAL PUBLICATIONS

- Paper I **Janne Haapanen**, Mikko Aromaa, Hannu Teisala, Paxton Juuti, Mikko Tuominen, Markus Sillanpää, Milena Stepien, Jarkko J. Saarinen, Martti Toivakka, Jurkka Kuusipalo, Jyrki M. Mäkelä, "On the limit of superhydrophobicity: defining the minimum amount of TiO₂ nanoparticle coating", *Materials Research Express*, 6, 035004, 2019
- Paper II **Janne Haapanen**, Mikko Aromaa, Hannu Teisala, Mikko Tuominen, Milena Stepien, Jarkko J. Saarinen, Mikko Heikkilä, Martti Toivakka, Jurkka Kuusipalo, Jyrki M. Mäkelä, "Binary TiO₂/SiO₂ nanoparticle coating for controlling the wetting properties of paperboard", *Materials Chemistry and Physics*, 149, pp. 230-237, 2015
- Paper III Mikko Tuominen, Hannu Teisala, **Janne Haapanen**, Jyrki M. Mäkelä, Mari Honkanen, Minnamari Vippola, Stig Bardage, Magnus E.P. Wälinder, Agne Swerin, "Superamphiphobic overhang structured coating on a biobased material", *Applied Surface Science*, Volume 389, pp. 135-143, 2016
- Paper IV Hannu Teisala, Florian Geyer, **Janne Haapanen**, Paxton Juuti, Jyrki M. Mäkelä, Doris Vollmer, Hans-Jürgen Butt, "Ultrafast Processing of Hierarchical Nanotexture for a Transparent Superamphiphobic Coating with Extremely Low Roll-Off Angle and High Impalement Pressure", *Advanced Materials*, 30, 1706529, 2018

REVIEW OF THE PAPERS AND AUTHOR'S CONTRIBUTION

- I. Paper I presents fabrication of superhydrophobic nanocoatings by Liquid Flame Spray in roll-to-roll coating process, with up to 300 m/min line speed. Minimum amount of TiO₂ nanoparticles for creating superhydrophobicity was obtained to be ~20 mg/m². Coating process was carried out by the author and H. Teisala. Analyses were performed mainly by M. Stepien and M. Sillanpää. The author carried out a major part of the data analysis and writing the manuscript, under supervision of J.M. Mäkelä.
- II. Paper II presents modification of paperboard wettability by changing the ratio of TiO₂/SiO₂ in the nanocoatings, fabricated by Liquid Flame Spray in roll-to-roll process. Coating process was carried out with M. Aromaa, H. Teisala and M. Tuominen. Part of the analyses were performed by M. Stepien and M. Heikkilä. The author had a major role in designing the experiments, data analysis and writing the manuscript.
- III. Paper III presents the combination of Liquid Flame Spray method with plasma treatment for superamphiphobic coating on wood substrate. Plasma treatments and a major part of the measurements, analyses and writing the manuscript were carried out by M. Tuominen. The author was responsible for Liquid Flame Spray coatings and contributed to the writing of the manuscript.
- IV. Paper IV presents a method for fabricating transparent superamphiphobic nanocoating on glass substrate by combining Liquid Flame Spray and Chemical Vapor Deposition methods. H. Teisala was responsible for designing the experiments and had the major part in measurements and writing the manuscript. The author designed and carried out the Liquid Flame Spray coatings and contributed to the writing of the manuscript.

1 INTRODUCTION

Functional nanocoatings have been inspired by nature. One of the most well known example of a functional nanostructure is on the water-repellent surface of a lotus leaf [1-5]. Other similar structures are found in other species as well [6, 7]. Rose petal is common example of similar water repellency as lotus leaf [8-10]. Also structures of shark skin [11], gecko feet [12] and butterfly wings [11, 13, 14] have received lot of attention in the past few years. Researchers around the world have used different techniques to fabricate similar surface structures by mimicking the natural functional surfaces. All these examples from nature are related to surface wettability. Liquid repellent surfaces have significant role in protecting the surface from contamination. Wet surfaces are more prone to bacterial and mold growth. Liquid repellent surfaces are also easy to clean since rolling droplets clean the surface from dirt and dust.

There are several methods for fabricating functional nanocoatings, such as Atomic Layer Deposition (ALD) [15-17], Chemical Vapor Deposition (CVD) [18], sol-gel method [19, 20], spray techniques [21] and etching [22]. Functional nanocoating is relatively simple to fabricate by various methods, but major challenge has been a poor wear resistance and/or high manufacturing costs [23-25]. Nanocoatings cover the surface partly or fully, depending on the method and used parameters. Especially in this thesis, in the case of fully covered surface, coating usually consist of porous layer of nanoparticles. Figure 1 shows an example of a porous nanoparticle layer on pigment coated paperboard. Porous nanoparticle layer contains large surface area compared to mass of the coating. Downside of these porous structures is that the adhesion between particles and a surface or the cohesion between particles is often relatively poor. Adhesion and cohesion may be improved by additives or pre-/after-treatment methods, but these methods are often complicated and time-consuming processes. Finding new solutions to this problem has been one of the key points in this thesis.

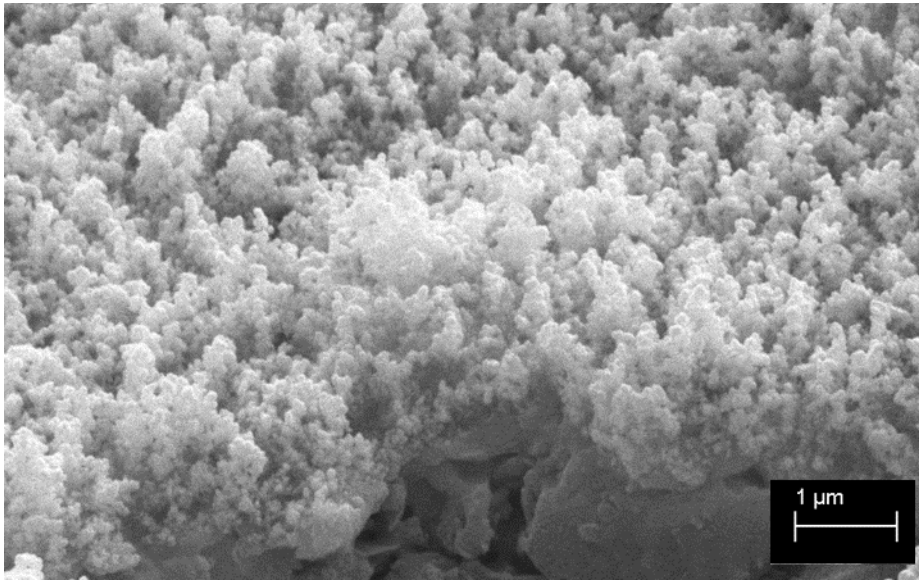


Figure 1. Tilted view of a porous nanoparticle coating on paperboard

Nanoparticles are widely used in industrial field. Especially carbon black and titanium dioxide are used in high quantities as a pigment in several industrial applications, such as inks, car tyres and paints [25, 26]. These two nanoparticle materials are produced and used millions of tons every year.

Nanoparticles have long history. Carbon black has been used as a pigment for thousands of years. Industrial manufacturing of nanoparticles started in 19th century and quantity and selection of industrial nanoparticles has increased ever since [27]. Nanoparticles are present practically everywhere. Even forests produce nanoparticles, mainly during a daytime [28].

Two-component nanocoatings are relatively easy way to improve the cohesion between nanoparticles in LFS method. Also combining LFS with other coating methods has shown promising results in adhesion and wear resistance improvement. Wear resistance is one of the key challenges in nanocoatings development [29-31].

One of the major advantages in LFS is robustness and high nanoparticle production rate. These features enable using LFS as a single-step coating method in roll-to-roll process. Roll-to-roll line speeds up to 300 m/min have been successfully used. Such a high line speed have not been reported before in the case of functional nanoparticle coatings, which is an important result also in the industrial point of view [32].

Target of this thesis is to evaluate Liquid Flame Spray (LFS) as a method for surface wetting modification technique in high roll-to-roll line speeds and to observe LFS as a method for fabricating optimal surface structure for superamphiphobic coatings. Superhydrophobic and superamphiphobic repel water and other liquids, respectively. Such surfaces have many practical applications and surfaces are easy to clean or even have self-cleaning properties. Figure 2 demonstrates superamphiphobic wood surface with oil and water droplets. Droplets bounce off from the clean surface (A-H) and remove dirt from surface effectively (I-P).

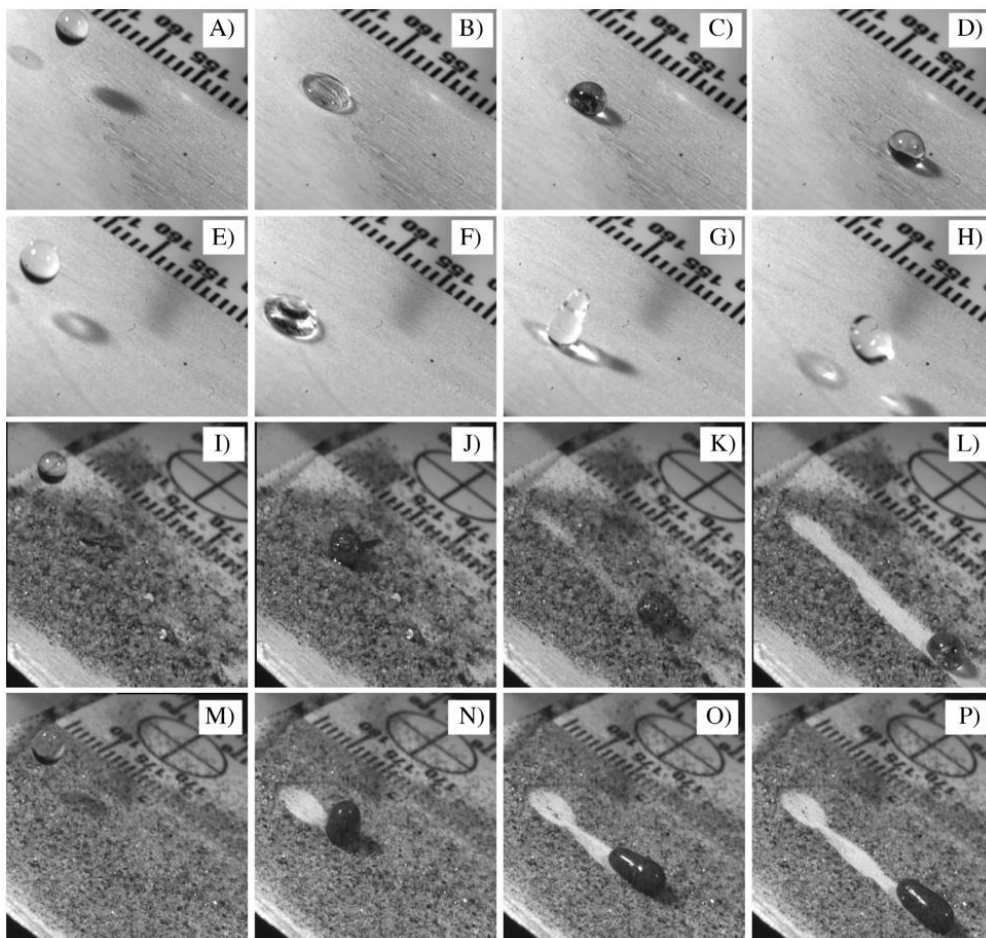


Figure 2. Example of self-cleaning properties of functional nanocoating. A–D: oil droplet on $3 \times \text{TiO}_2$ -PFH coated wood, E–H: water droplet on $3 \times \text{TiO}_2$ -PFH coated wood surface, I–L: self-cleaning using oil droplet on $3 \times \text{TiO}_2$ -PFH coated wood (I and J: 1st droplet, K: 2nd droplet, L: 5th droplet) and M–P: self-cleaning using water droplet in the longitudinal direction on $3 \times \text{TiO}_2$ -PFH coated wood. [Paper III]

Challenges faced in this thesis are relatively universal. Finding the minimum amount of nanoparticles for desired functionality is extremely important for energy efficiency. Excess amount of nanoparticles in a nanocoating is a waste of resources and material. It is also important to be able to minimize nanoparticle amounts to prevent possible negative health effects.

Combining different coating methods is one option for manufacturing nanocoating with optimal physical and chemical properties. One method can be used for optimal structure and porosity and another method for optimizing chemical composition of a nanocoating. Combination of several coating methods is always a challenge since the methods may not be compatible with each other and second method might modify the first one to lose the desired properties.

Main research objectives of this thesis:

To define what is the optimal structure of the nanocoating and how much nanoparticles are needed for the sufficient controlling of the wettability.

To discover if there is an advantage in using multi-component nanocoatings.

To achieve amphiphobic nanocoating by combining different coating methods.

To obtain new information on the stability of the functional nanocoatings by using multi-component nanoparticle coatings and combining different coating methods.

2 NANOPARTICLE SYNTHESIS

Synthesis of nanoparticles is defined as fabrication of particles with diameter in the range of nanometers to submicron. Nanoparticles have many unique properties compared to bulk materials. Most important factor in nanoparticles is extremely high surface to volume ratio. Many reactions and phenomenon takes place on the surface of the material. Nanoparticles have large surface area, even with small quantities. Many material properties are different between nanoparticles and bulk materials, such as melting temperature and optical properties [33-36]. There is great variety of different synthesis methods for fabricating nanoparticles. This chapter mainly focuses on Liquid Flame Spray, which is in the key role in this thesis.

2.1 Liquid Flame Spray

Liquid Flame Spray (LFS) is a gaseous synthesis method for nanoparticle generation. In LFS, liquid precursor is fed into turbulent hydrogen-oxygen flame. High-velocity hydrogen stream disperses liquid as small droplets, which evaporate, decompose and form new compounds in the hot flame [37]. After rapid cooling in the flame, evaporated gas becomes supersaturated and nucleation starts forming solid nanoparticles. Depending on the process parameters, coagulation, sintering and agglomeration of nanoparticles occur in the flame. Schematic picture of the LFS flame with aerosol processes occurring between the burner and a substrate is presented in Figure 3.

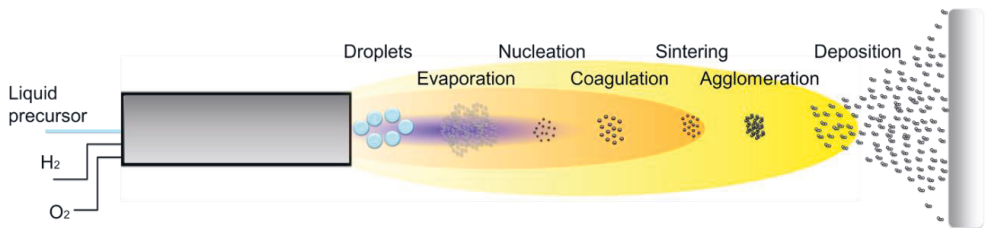


Figure 3. Schematic picture of Liquid Flame Spray (LFS) method. [Paper II]

LFS method was originally developed for glass coloring at Tampere University of Technology [38]. Thin layer of coloring nanoparticle layer was deposited between two layers of molten glass. Later this method has been applied in several different applications, e.g. source for test aerosol [39] and generation of functional nanocoatings, which is discussed in more detail in the next chapter.

Parameters of the LFS process affect the properties of the generated nanoparticles [40-42]. Gas flow rates and ratio can be adjusted for stoichiometric value or flame can be also oxygen-rich or oxygen-lean. Fraction of oxygen in the flame affects oxidation of nanoparticles, but also flame size and temperature. Flame size and temperature have an effect on the size of the formed nanoparticles. LFS offers a great variety of precursors available. Process parameters affect greatly on nanoparticle size. By varying process parameters, primary particle size varies from 2 nm to 200 nm. Agglomerated nanoparticles consist of several primary nanoparticles and size of an agglomerate can be in micrometer range. Process parameters have an effect on amount of material in the flame as well as flame temperature. These both have effect on aerosol processes happening in the flame. Part of the processes depend also on particle material properties, e.g. sintering of primary and/or agglomerated nanoparticles.

LFS is operated in open atmosphere causing the oxidation of synthesized nanoparticles in most cases. Noble metals such as silver, gold, platinum and palladium do not oxidize, producing metallic nanoparticles. Other precursor materials oxidize more easily and formed nanoparticles are usually oxides. However, level of oxidization can be modified in some level by tuning the combustion gases to less oxidative.

There are other similar flame methods as well, such as Flame Spray Pyrolysis (FSP). In FSP, the carrier flame itself is relatively small. Most of the energy for the FSP flame comes from a precursor [43, 44]. In FSP, usually methane is used as a base gas for the flame and oxygen is used as a dispersion and combustion gas. Advantage of LFS compared to other flame synthesis methods is relatively high flow rate of combustion gases. This enables using even water based precursors. Especially generation of silver nanoparticles is more economic, when silver nitrate (AgNO_3) diluted in water can be used as a precursor. Wide selection of precursor materials enables production of multi-component nanoparticles with broad selection of materials.

Titanium dioxide (TiO_2) and silicon dioxide (SiO_2) are the main materials for nanoparticles used in this thesis. Titanium tetraisopropoxide (TTIP) and Tetraethyl orthosilicate (TEOS) diluted in isopropanol were used as precursors for TiO_2 and SiO_2 , respectively. SiO_2 synthesized by LFS is amorphous, but TiO_2 has two main crystalline forms, anatase and rutile. Brookite is the rarest polymorph of TiO_2 and it has not been observed as a product of TiO_2 synthesis by LFS. Rutile is thermodynamically most stable form of TiO_2 , but since the crystal formation in flame synthesis is extremely fast, formed TiO_2 nanoparticles are mainly anatase, with small fraction of rutile present [27, 45]. Crystalline form of collected TiO_2 powder was analyzed by X-ray diffraction spectroscopy (XRD) in Paper II (Figure 4). Anatase is often more favorable crystalline form of TiO_2 since it has higher photocatalytic activity. Photocatalytic activity of LFS-made TiO_2 nanocoatings has been studied quite extensively in previous studies by changing the wettability of TiO_2 -nanocoated paperboard by UV exposure [46-48]. In photocatalysis, carbonaceous compounds are removed from the TiO_2 surface and more OH-groups are formed [49]. Combination of these two phenomena changes the wettability of a surface from hydrophobic to hydrophilic [50].

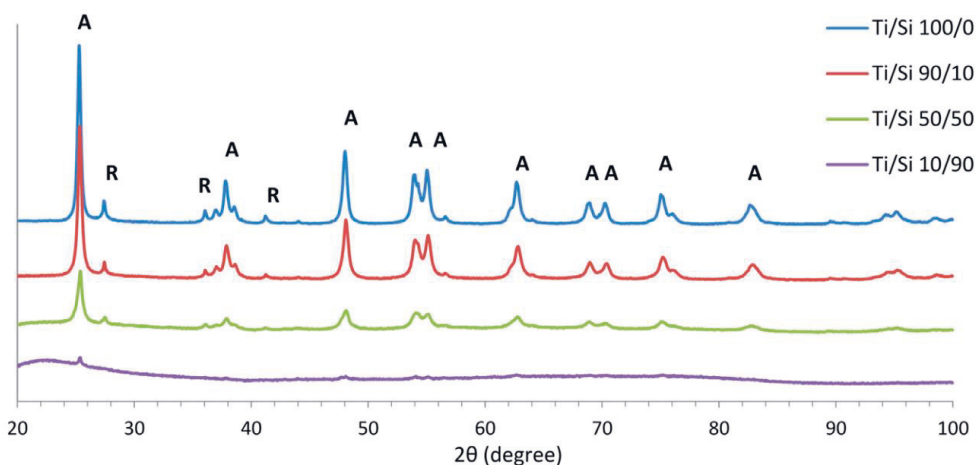


Figure 4. XRD graphs of $\text{TiO}_2/\text{SiO}_2$ nanoparticles with different fractions of Ti/Si. Peaks of anatase (A) and rutile (R) are marked on the figure. [Paper II]

2.2 Other Synthesis Methods

Selection of methods for nanoparticle synthesis is extremely wide. Usually different synthesis methods suit better for a certain nanoparticles or applications. Synthesis methods can be divided into two groups: wet chemistry and gas phase synthesis methods. In wet chemistry methods, chemical reactions occur in the liquid, forming nanoparticles or nano-sized structures and afterwards suspension is applied on the surface to form a coating. [51-53]

In gas phase synthesis methods, nanoparticles are formed through the gas phase. Origin of the nanoparticle material can be in solid, liquid or gas phase, depending on the method. [54-56]

Furnace method is one of the simplest way to produce nanoparticles. This type of synthesis can be performed e.g. in tube furnace where solid metal evaporates due to heating and when vapor is transferred to cooler part by background gas, solid nanoparticles are formed by nucleation and coagulation. Depending on the carrier gas, nanoparticles can be metals or oxides. This method can also be called as evaporation-condensation reaction. [55]

In **Laser ablation**, nanoparticles and vapor are released from solid substrate by laser, usually pulsed laser beam. This method can be used in atmospheric conditions, in controlled atmosphere or even in liquid. Produced nanoparticles can be collected from air with filter or deposited directly on a surface. If laser ablation is used under water, nanoparticles are also collected into water. [57-60]

Spark discharge generation is a method where metals are vaporized from the electrodes by arc. Quantity of synthesized nanoparticles is relatively low, but production rate is stable with good reproducibility. This method has been up-scaled by using several parallel spark discharge units. [61-63]

In **Plasma synthesis** method precursors are injected into thermal plasma that decomposes precursor into atoms. When supersaturated vapor cools down, nanoparticles are formed. Vapor or produced nanoparticles can be deposited directly on a surface. [64-66]

Hot-wall reactor is similar to tube furnace, but precursor is usually introduced into a reactor in liquid form. Precursor either evaporates, decomposes and nucleates after

chemical reactions and cooling or liquid droplet dries out into a solid residual particle. Depending on the particle material, morphology and crystallinity of particles may differ which route they are formed. [67-69]

In **Spray pyrolysis**, liquid precursor is sprayed on a hot substrate as liquid droplets or as particles. Precursor reacts on the hot surface and solvent evaporates or decomposes. Precursor solution may contain one or several different precursor materials and temperature of a surface enables chemical reactions between different compounds. This technique is used e.g. TiO₂ and ZnO coatings. [70-72]

In **Electrospray** method, liquid precursor is injected through a capillary needle and high voltage between needle and a substrate forms Taylor cone type of jet with proper parameters. Process parameters depend on the properties of the liquid (surface tension, dielectric constant and electrical conductivity), liquid flow rate and applied voltages. Liquid precursor may contain nanoparticles or residual nanoparticles are formed by droplet evaporation after cone tip. Castillo et al. have used electrospray for fabricating porous nanoparticle coatings on various materials. [21, 73]

Comparison of these methods and some key features are presented in Table 1. Values in the Table 1 are based on Friedlander [74].

Table 1. Comparison of different nanoparticle synthesis methods; (based on Friedlander [74])

	Flame	Evap/Cond reaction	Laser ablation	Spark discharge	Plasma	Hot wall	Spray pyrolysis	Electrospray
Max size, μm	1	0.1-10	1	0.1-1	1	10	0.10 – 100	0.1-10
Spread	broad	narrow	narrow	narrow	broad	narrow	broad	narrow
Morphology	solid agglomerates	solid	solid	solid	solid agglomerates	spherical solid	spherical solid porous hollow	spherical liquid solid
Max temp, K	2500	<2000	2000	60000	25000	2000	1600	~500
Material	oxides	metals oxides	non-oxides oxides	metals oxides	non-oxides oxides semiconductors	non-oxides oxides semiconductors	non-oxides oxides	non-oxides oxides
Complexity	low	low	medium	low	high	low	Low	medium
Synthesis amount	medium	low	low	low	low	low	high	medium

3 COATING METHODS

There are several different coating methods available. Thermal sprays and other similar coating methods are used widely in industry for relatively thick and wear resistant coatings. Nanocoatings are important since functionality of a surface can be done with a small amount of material. Nanocoating can be thin, homogeneous layer or consists of porous layer of nanoparticles. This chapter focuses mainly on Liquid Flame Spray (LFS) and other methods for thin nanocoatings. LFS was used in all publications of this thesis to generate porous layer of nanoparticles on different substrates. Plasma treatment and chemical vapor deposition (CVD) were used as additional coating methods on top of LFS-fabricated nanoparticle layer in Papers III and IV, respectively. Stability of a nanoparticle coating depends on two main factors, adhesion and cohesion. Adhesion typically refers to interaction with nanocoating and a substrate. Cohesion stands for interaction between nanoparticles in a nanocoating. Both adhesion and cohesion play important role in the stability of nanocoatings and will be discussed more closely in later chapters

3.1 Liquid Flame Spray

Previously, Liquid Flame Spray (LFS) was introduced as a versatile synthesis method for nanoparticles. In addition to synthesis method, LFS is also method for fabricating functional nanocoatings on various substrates. This chapter introduces LFS as a coating method for functional nanocoatings.

3.1.1 Deposition Process

Deposition of nanoparticles play an important role on fabricating nanocoatings. Deposition may occur by impaction, interception, Brownian diffusion, thermophoresis, or electrical and gravitational forces between a particle and a surface. [32, 75]

Nanoparticle size has a big role in most of the deposition methods. Impaction and gravitational forces are more important in larger particles ($>1\ \mu\text{m}$) and diffusion is the most important deposition method for small nanoparticles ($<10\ \text{nm}$). Electrical forces are dependent on particle charge and electric field near the surface. In flame processes, part of the particles are charged, but most of the particles are neutral in charge [76]. Since the flame process includes large amount of heat, temperature gradient between hot particles and cool surface is relatively high, making thermophoresis the most important deposition method in LFS coating process [32, 75].

Various deposition methods and their importance in flame processes are described more detailed by Mädler et al. [75], Thybo et al. [77] and Mäkelä et al. [32]. All these publications show that thermophoresis is the main deposition method in flame processes. In roll-to-roll process, substrate passes flame rapidly and since the heat sensitive substrate is not damaged by the heat, temperature difference between the flame and the substrate is in the range of 1000°C . Such a high temperature gradient enables high process yield and up to 40% of the produced nanoparticles are deposited onto paperboard surface (Paper I). Yield of the process depends on the line speed of roll-to-roll process. Yield results based on Inductively Coupled Plasma Optical Emission Spectrometry (ICP-OES) analysis of 30 cm wide samples are marked on Table 2.

Table 2. Yield of the LFS coating in roll-to-roll process with different line speeds. [Paper I]

Line speed (m/min)	50	100	200	300
Amount of TiO_2 in the coating (mg/m^2)	23.6	9.2	7.1	4.1
Coated area (m^2/min) from a 30 cm wide sample	15	30	60	90
Yield of the process (%)	36.4	28.4	43.8	38.0

Deposited amount of TiO_2 has large spatial variation. Since the flame is hotter and precursor is fed in the in the centerline of the coating, more nanoparticles are deposited in the middle of the coating line. Spatial distribution of the TiO_2 nanocoating was analyzed in Paper I (Figure 5a), and correlation between the water contact angle (WCA) and TiO_2 amount was confirmed.

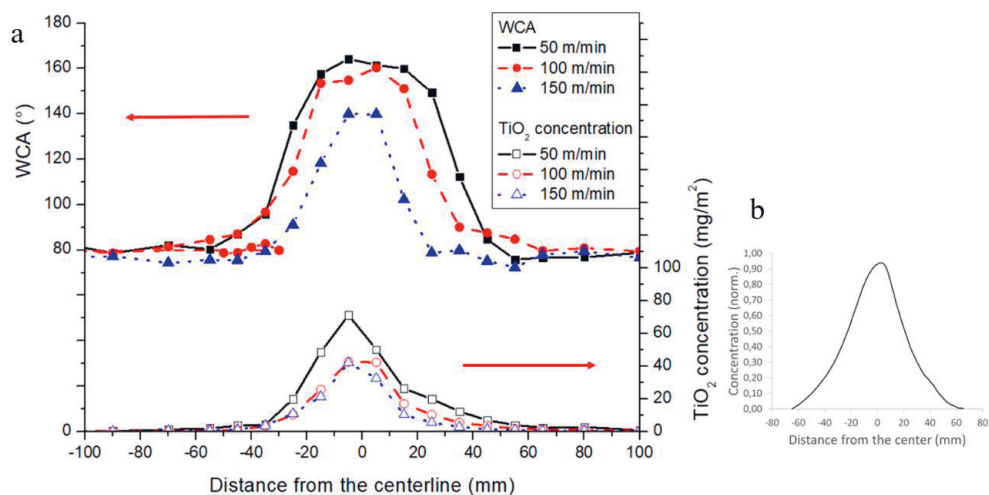


Figure 5. Spatial distribution of TiO₂ nanocoating in roll-to-roll process. Graphs in a) are based on ICP-OES analysis and WCA measurements of TiO₂ coating. In insert b), colour intensity of deposited iron oxide was analyzed optically. [Paper I]

Spatial distribution of the coating amount was also observed in iron oxide coated paperboard (Figure 5b). Iron oxide forms brown-coloured coating even in nano size. By analyzing the darkness of the coating colour, it was clear that coating in the middle of the coating line is thicker and coating gets thinner as the distance from the centerline increases.

3.1.2 Substrate Options

Variety of substrate materials are available for LFS coatings. Paper and paperboard have been used in several studies as a substrate for superhydrophobic and superhydrophilic LFS nanocoatings [47-50, 78-82]. Commercially available pigment-coated paperboard (200 g/m²) was also used as a substrate in Papers I and II. Wood was used as a substrate in Paper III. Wood is relatively similar substrate to paperboard, since both are heat sensitive and colour of the substrate changes if too much heat is transferred from the flame to the substrate.

Other common substrates in LFS process are glass [29, 30, 83] and steel [31]. Both of these substrate materials stand heat better than paperboard or wood, but some changes on the substrate occur if they absorb enough heat. Glass surface melts in high temperature, which may cause nanoparticle penetration in to the substrate.

This can be desired or unwanted phenomenon, depending on the purpose of the nanoparticles. Hot flame may cause changes on steel substrate surface structure and this may change the colour and the properties of the substrate. Usually changes in substrate colour or structure are unwanted features.

Recently, polymer materials have been used as substrates in the LFS process [84, 85]. Different polymer materials have different properties, for instance melting temperature. Heat from the flame process softens topmost layer of the polymer surface and nanoparticles are able to penetrate to the substrate partly or fully.

3.1.3 Multi-component Coatings

One of the advantages of LFS process is the possibility for multi-component nanocoatings in one step. Different precursor can be mixed into one solution with desired ratio. Mixed precursor solution is injected into the flame and multi-component nanoparticles are formed. Vapor pressure of the nanoparticle materials play a big role in multi-component nanoparticle formation. $\text{TiO}_2/\text{SiO}_2$ multi-component nanocoatings were fabricated in Paper II. TiO_2 and SiO_2 nanoparticles are formed in similar temperatures and analyses showed that TiO_2 and SiO_2 were relatively evenly mixed in nanoparticles.

In the case of mixing precursor materials with different vapor pressures, one of the materials nucleate before others. In these cases, the results may be core-shell structure or decorated nanoparticles. Keskinen et al. presented results of TiO_2/Ag nanoparticle synthesis by LFS and TiO_2 nanoparticles were formed first and Ag nanoparticles formed small dots on top of the TiO_2 nanoparticles. [86]

3.1.4 Up-scalability

Up-scalability is extremely important factor if basic research results need to be commercialized. Flame based nanoparticle synthesis is widely used in generation of nanoparticle powders, such as TiO_2 and carbon black. These nanoparticle powders are synthesized and used millions of tons every year [25, 26]. However, flame methods are not widely used as direct coating methods for functional nanocoatings. Flame methods for direct deposition of nanoparticles are used in glass fiber industry for preform manufacturing, but not widely used elsewhere.

Robustness and a high production rate of nanoparticles in LFS process is a good start for up-scalability of the functional nanocoating manufacturing. In Papers I and

II, LFS was operated in pilot-scale roll-to-roll paper converting machine. Maximum line speed of the pilot-scale machine was 300 m/min and even with this line speed, superhydrophobic nanocoating was successfully fabricated onto paperboard substrate in one-step coating process. By improving the process parameters and adding more burners to the coating step, even higher line speeds are feasible.

One of the main features of the LFS coating is uneven spatial distribution of the coating. As presented in Figure 5, LFS form thicker coating in the middle. Coating is homogeneous in the coating direction. Homogeneous spatial coating thickness is nearly impossible to produce by depositing nanoparticles directly from the flame to a substrate. However, some properties of a functional coating do not need uniform coating on a substrate. For example, wetting properties do not vary much if the coating thickness is different from one point to another, as long as there is at least some amount of coating at every point. Spatial homogeneity could be improved using several burners side by side, but this was not tested in this work.

3.2 Other Coating Methods

There are several different coating methods available nowadays. Thermal sprays are one of the most commonly used coating method for various applications. Choosing the right coating method depends on the application and the substrate. Figure 6 lists some of the most common coating methods and their working pressure and temperature of a coated surface. Listed methods in the figure 6 are Atmospheric Pressure Chemical Vapor Deposition (APCVD), Atomic Layer Deposition (ALD), Combustion Assisted Chemical Vapor Deposition (CCVD), Direct Current Sputtering (DC-SPU), Evaporation (EVP), Flame Spray Pyrolysis (FSP), Hot Wall Aerosol Reactor and Low-Pressure Impactor (HWLP), Ion Beam Sputtering Ion Assisted Deposition (IAD), Molecular Beam Epitaxy (MBE), Organometallic Chemical Vapor Deposition (OMCVD), Plasma enhanced Chemical Vapor Deposition (PECVD), Pulsed Laser Deposition (PLD), Radio Frequency Sputtering (RF-SPU), Rheotaxial Growth and Thermal Oxidation (RGTO), Supersonic Cluster Beam Deposition (SCBD) and Spray Pyrolysis (SP) [87].

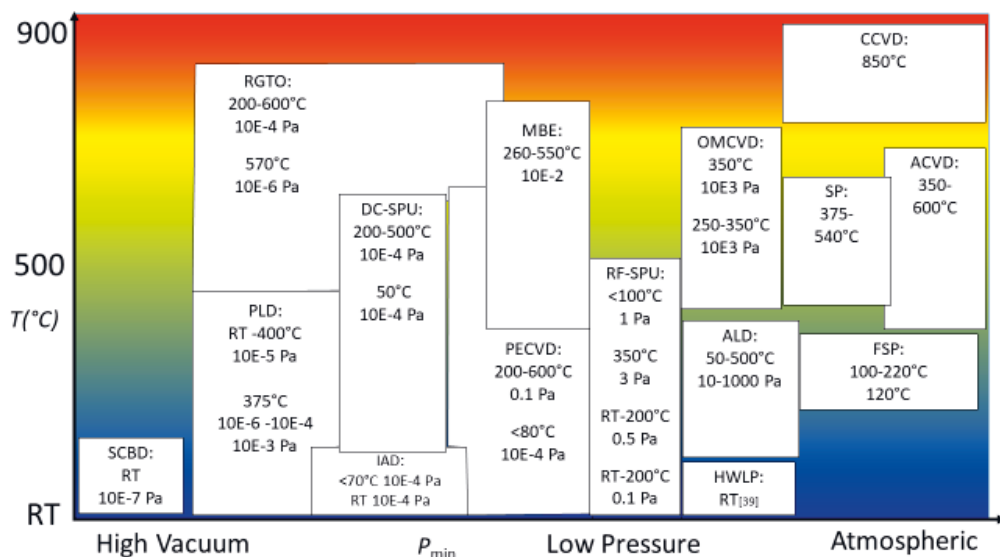


Figure 6. Comparison of different thin film methods with different operating temperatures and pressures. Abbreviations of the different thin film methods are described in Chapter 3.2. Figure is adapted from Tricoli et al. [87].

3.2.1 Plasma Treatment

In Paper III, plasma treatment was combined with LFS to further modify the chemical composition of the nanocoating. Low-pressure plasma deposition was carried out using an in-house reactor. The reactor consists of a glass vessel connected to a double-stage rotary vacuum pump (Leybold-Heraeus D 65 B). Two externally wrapped, capacitively coupled, copper electrode bands were powered by a 13.56 MHz radio-frequency power generator (ENI, Model ACG-3). Perfluorohexane (PFH, Apollo Scientific) monomer was used as a precursor. During the plasma deposition, generator power was 40 W, the pressure was 18 Pa and treatment time was 5 minutes. These plasma deposition parameters were chosen, based on previous experience, to provide a uniform and homogeneous coverage with a thickness of 30 nm.

3.2.2 Chemical Vapor Deposition (CVD)

In typical chemical vapor deposition (CVD), substrate is placed inside a chamber with one or several volatile compounds. By lowering the pressure in the chamber, volatile compounds turn into vapor and then deposited on the substrate. CVD method was chosen for modification of the chemical composition of the porous nanocoating, generated by LFS. In Paper IV, CVD treatment was combined with LFS to further modify the chemical composition of the nanocoating. In this study, 100 μl of fluorosilane was placed in the desiccator with nanocoated glass samples and pressure was lowered to 200 mbar for 2 h. After CVD process, samples were placed in vacuum oven at 60 $^{\circ}\text{C}$ for 2 h to remove unreacted silane. Nanocoated samples were treated with oxygen plasma prior to CVD process to activate the surface.

4 ANALYSIS AND CHARACTERIZATION METHODS

Functionality of the surface is often combination of physical and chemical properties. Various different analysis and characterization methods, used in this thesis, are introduced in this chapter. Figure 7 presents main analysis and characterization methods used in this thesis. Different methods give different information about the nanocoatings. Methods are divided roughly based on their given information about chemical and physical properties of the coating. Also, different methods are optimized for a certain size range.

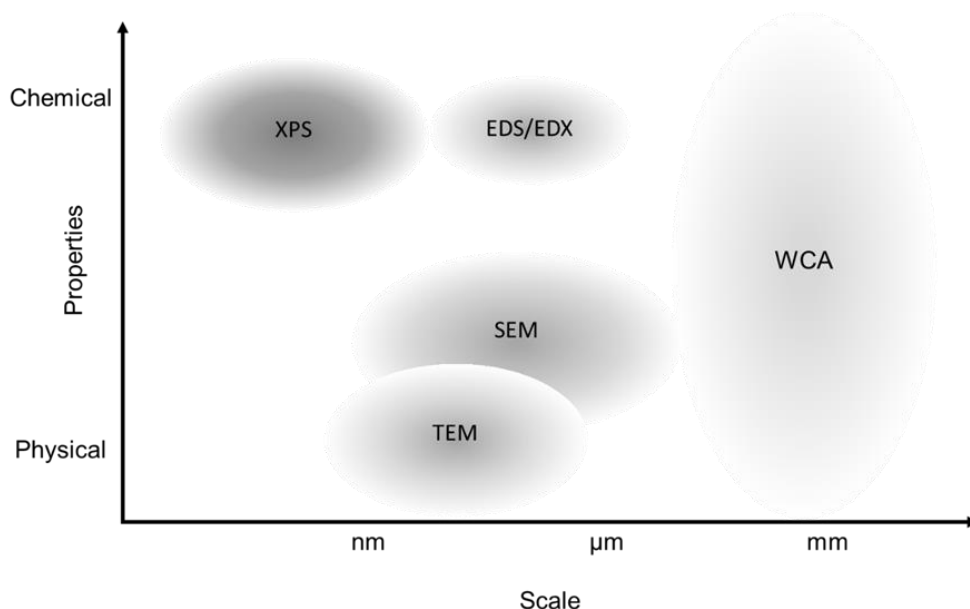


Figure 7. Analysis and characterization methods, used in this work, categorized based on their size range and features to give information about chemical and/or physical properties of the analyzed sample. Darkness of the shapes indicate the complexity of the method. Abbreviations in the graph are X-ray photoelectron spectroscopy (XPS), Energy-dispersive X-ray spectroscopy (EDS/EDX), Scanning electron microscopy (SEM), Transmission electron microscopy (TEM) and Water contact angle (WCA).

4.1 Determination of Wettability

Wettability of the surfaces is most often defined with water contact angle (WCA). WCA is usually measured with goniometer where droplet of water is placed on top of the surface and macroscopic WCA is determined by analyzing the angle between the surface and the droplet. If the measured angle is below 90° , surface is termed hydrophilic and if the contact angle is above 90° , surface is termed hydrophobic. Figure 8 illustrates the difference between hydrophilicity and hydrophobicity. Superhydrophilic surface has a contact angle less than 10° and superhydrophobic surface greater than 150° . Term superhydrophobic often requires also low water sliding angle ($< 10^\circ$). Sliding angle is most often measured by placing droplet on a horizontal surface and after that the surface is tilted until droplet falls off. Wettability is usually combination of two factors that affect the wetting: surface energy and surface roughness. Certain roughness is needed for both superhydrophobicity and superhydrophilicity.

Many surfaces in nature are superhydrophobic and nature has been a great source of enthusiasm for developing similar structures artificially, e.g. Lotus leaf [2]. Wettability often refers to water behavior, but it includes other liquids as well. Prepared nanocoatings were tested with water on Papers I&II, but Papers III&IV include also testing the wetting with other liquids, e.g. oil, ethylene glycol and n-hexadecane.

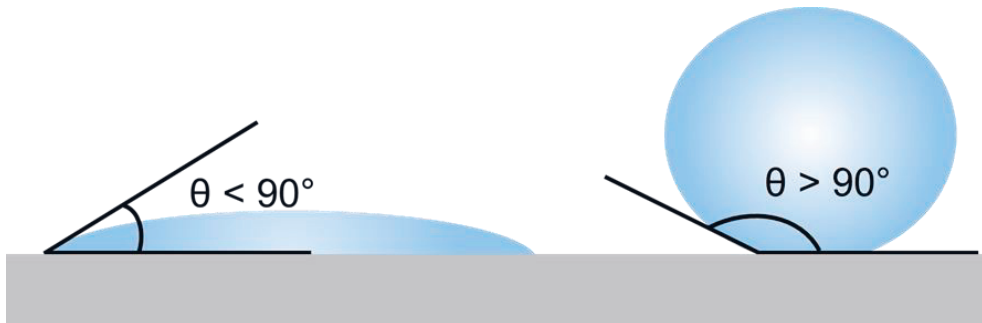


Figure 8. Definition of wettability: if water contact angle $\theta < 90^\circ$, surface is termed hydrophilic and if $\theta > 90^\circ$, surface is termed hydrophobic

4.2 Scanning Electron Microscopy (SEM)

In scanning electron microscopy (SEM), surface is exposed to focused beam of electrons [88, 89]. Electrons interact with a surface and produce various different signals to measure. SEM was used as one of the main analysis methods in all publications of this thesis. SEM was mainly used for analyzing the morphology of the samples. Prior to SEM imaging, samples are usually sputtered with thin layer of carbon or gold to ensure proper conductivity of a sample. Depending on the sputtering material and amount of sputtered coating, size of the analyzed nanoparticles may increase significantly. SEM is often equipped with additional energy-dispersive X-ray spectroscopy (EDS/EDX) system to analyze atomic composition of a sample. However, EDS/EDX is not particularly surface sensitive analysis method and part of the measured information is obtained from the substrate if the substrate is covered with only thin layer of nanoparticles ($< 1 \mu\text{m}$). SEM was used as one of the analysis methods in all publications of this thesis (Paper I-IV).

4.3 Transmission Electron Microscopy (TEM)

In transmission electron microscopy (TEM), electron beam is focused through a sample [88, 89]. Sample is usually deposited on 3 mm diameter TEM grid, which is a copper mesh covered with a thin carbon film. Usually TEM is used for analyzing size and shape of nanoparticles. Depending on the TEM equipment, even single atoms can be observed in TEM graphs. TEM can include separate EDS/EDX analysis equipment and atomic composition of single nanoparticle can be measured. TEM was used as an analysis method in Papers II and IV.

4.4 Chemical Analysis

The degree of oxidation and chemical composition of the treated samples were determined by X-ray photoelectron spectroscopy (XPS) using a Physical Electronics Quantum 200 ESCA (Paper I-II) and Kratos AXIS UltraDLD (Paper III) instruments, equipped with a monochromatic Al $K\alpha$ X-ray source. XPS is surface sensitive method and measured values are from the few nanometer topmost layer. In Paper I, the XPS measurements were performed one day and 90 days after the LFS treatments to analyze chemical changes on the surface.

4.5 Inductively Coupled Plasma Optical Emission Spectrometry (ICP-OES)

Inductively coupled plasma optical emission spectroscopy (ICP-OES) [90, 91] was used for analyzing nanocoating amount quantitatively from the TiO₂ coated paperboard. In ICP-OES, sample is first diluted or transformed to liquid form prior to actual analysis of composition and fractions of elements in the sample. This analysis had two main challenges: nano-sized TiO₂ is difficult to dilute and pigment-coated paperboard included TiO₂ as a white pigment. Prior to microwave digestion (Milestone, Italy), 2 ml of nitric acid and 2 ml of sulphuric acid were added. The digestion was operated at 240 °C and 40 bar for 45 min. After 15-min cooling, deionized milli-Q water was added until 30 ml total volume was reached. With this procedure, TiO₂ was fully dissolved and precise analysis was possible. Substrate without nanocoating was used as a reference to define TiO₂ content in the substrate. Inductively coupled plasma mass spectrometry (ICP-MS) is similar equipment, but the analysis part is different.

4.6 UV-Transmission Measurement

The transmittance spectra of nanocoated glass samples were measured in Papers III-IV using a UV/VIS spectrometer [92]. UV/VIS spectrometer typically scans desired wavelength spectrum in visible light and UV-A range. Usually thin nanoparticle coatings are nearly transparent. By increasing the coating amount, transparency decreases as the coating disperses and absorbs more light. Figure 9 presents transmittance spectra from TiO₂ and TiO₂+PFH coated glass samples from Paper III. Transmittance decreases significantly below 400 nm wavelengths since TiO₂ is absorbing UV light. TiO₂ is widely used as UV shield in many applications.

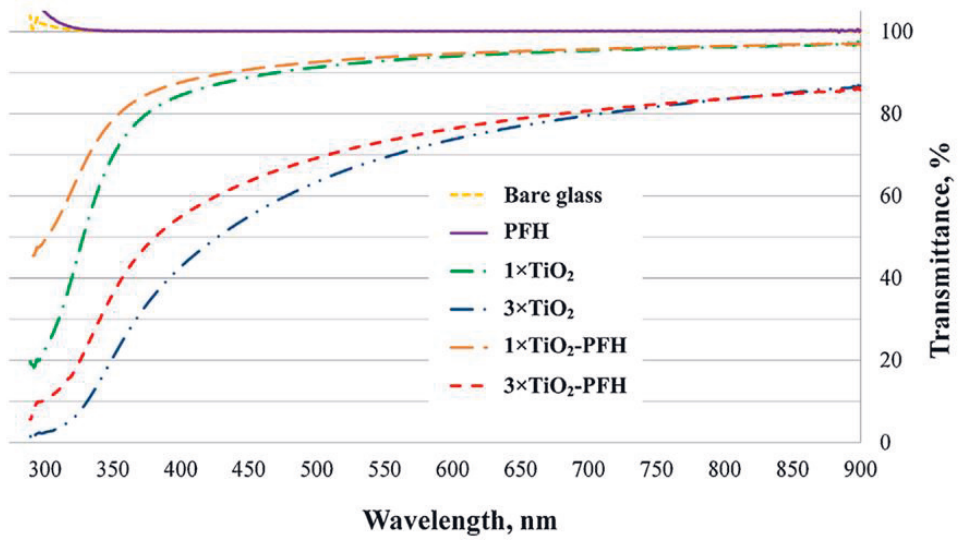


Figure 9. Transmittance spectra of TiO₂-PFH coated glass plates with different TiO₂ coating amounts with and without PFH coating. (Paper III)

5 FUNCTIONALITY OF FABRICATED NANOCOATINGS

5.1 Wetting

Hydrophobicity describes surface behavior with water, but recently repellency against other liquids has been in high interest in both scientific and industrial fields. Oleo- or amphiphobic surfaces repel also other liquids, such as oils, alcohols and liquids with low surface tension [93]. Oleophobic surface does not necessarily repel water, hence the term superamphiphobic is used for surfaces that repel both water and oils (amphi = both). Requirement of the superamphiphobic surface structure is different from superhydrophobic surface [94, 95]. Surface tension of water is relatively high ($\gamma = 72.8 \text{ mN/m}$) compared to other liquids, such as ethylene glycol ($\gamma = 48.3 \text{ mN/m}$) and n-hexadecane ($\gamma = 27.6 \text{ mN/m}$). Most common definition for superamphiphobic surface is the repellency for liquids with surface tension γ higher than 30 mN/m [93]. Omniphobic surfaces repel all possible liquids, even liquids with very low surface tension.

Superhydrophobic surface requires certain hierarchial surfaces structure. Superhydrophobic surface usually has both micro- and nanoscale roughness [96] [79]. Air pockets are formed on top and inside the hierarchial structure to minimize the water-surface interaction area. In addition to desired surface structure, also surface chemistry plays a role. Based on the results of Paper II, superhydrophobic and superhydrophilic surface look similar in SEM graphs. Difference in wetting behavior can be explained by different surface chemistry. TiO_2 -rich nanoparticle coating is contaminated by carbonaceous matter during the coating process, forming a thin layer of carbon/hydrocarbons on top of the nanoparticles. This is mainly due to chemically reactant TiO_2 surface with OH-groups. Similar behavior was not observed with SiO_2 -rich nanoparticle coatings and the surface remained superhydrophilic.

Wetting behavior depends also on the used liquid. A simple estimation on a surface consisting of spherical, randomly aggregated particles shows that this combination ensures low penetration depth and wetted contact area of both polar and nonpolar liquids on the solid substrate (Figure 10).

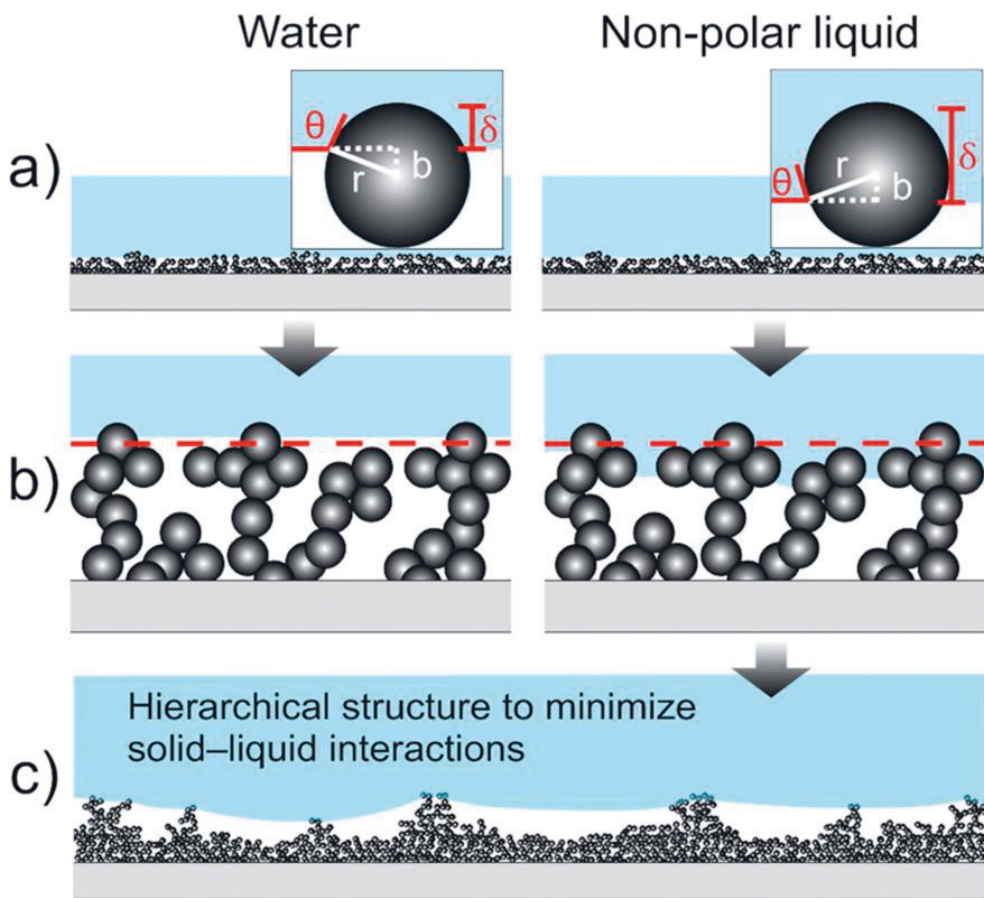


Figure 10. Schematic illustration of wetting of a model surface by water and a nonpolar liquid. The surface consists of spherical particles. Penetration depth δ of the liquid around a single particle with radius r depends on the intrinsic wettability of the material, characterized by the Young contact angle θ . a) Water (large θ) wets small fraction of individual particles within the first particle layer, indicated by the dashed line in (b). A nonpolar liquid (small θ) wets large fraction of individual particles and b) invades from one particle to the other into the texture of the solid until θ is reached at the overhangs. c) Hierarchical roughness of the surface has critically important role in reducing the overall solid–liquid contact area and pinning of low-surface-tension liquids on randomly structured super-amphiphobic surfaces. (Paper IV)

Superamphiphobic surfaces require more complex surface structure to avoid low-tension liquids to penetrate through the coating layer onto the substrate. So called overhang structure has been discussed in the literature in the past few years [97, 98]. In overhang structure, certain overhanging shape of coating is needed for keeping the liquid away from the substrate surface. One example of an overhang structure is

presented in Figure 11, where combination of TiO₂ nanoparticles and plasma coating form overhanging structure on top of the wood fibers.

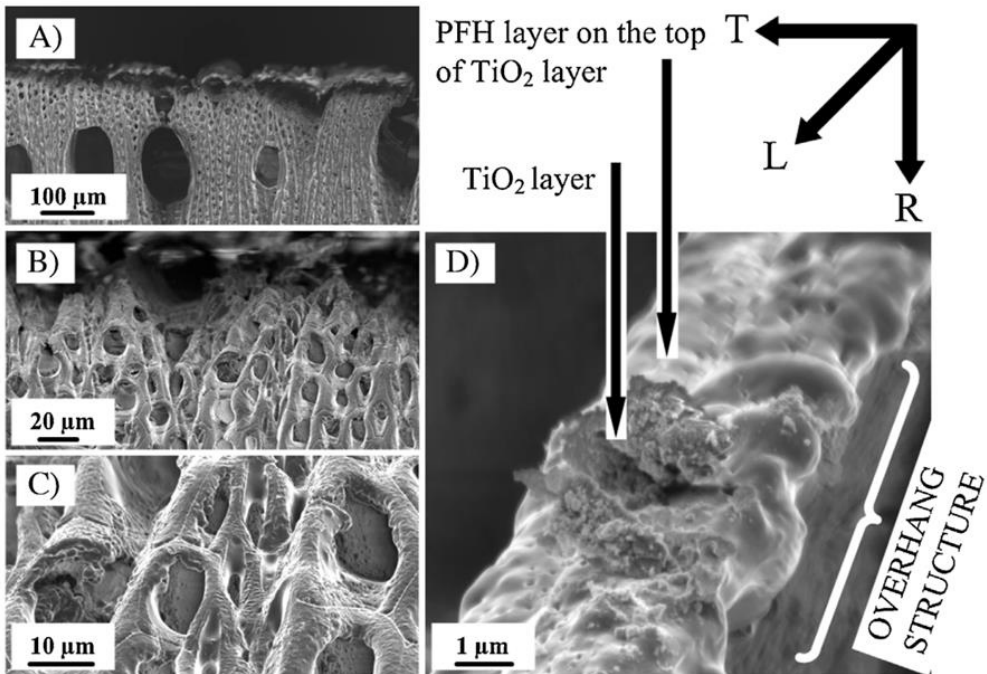


Figure 11. FEG-SEM images of the cross section of the coated wood samples at successive magnifications of 3× TiO₂-PFH coated wood. The overhang structure is seen in D. In addition, the individual TiO₂ and PFH layers are clearly seen in a small area where the PFH-TiO₂ coating has been damaged. T: tangential direction, L: longitudinal (fiber orientation of wood) direction and R: radial direction. (Paper III)

5.2 Effect of the Coating Amount

Minimizing the coating amount without losing the wanted properties of the coatings is important factor when aiming for the industrial scale production. Minimal amount of functional nanocoating makes process more economically and environmentally friendly. By using LFS as method for nanocoating fabrication, there are several options for varying amount of nanocoating. Precursor concentration and feed rate affect the amount of produced nanoparticles, which have an effect on nanocoating amount. However, these changes in process parameters have also an effect on synthesized particles. If precursor concentration or feed rate decreases, produced

nanoparticles are smaller and less agglomerated. Also distance between the burner and a substrate has an effect on deposition efficiency, thus affecting deposited nanoparticle amount on the surface. Nanoparticles have also more time to agglomerate if distance between the burner and a substrate is increased.

In Paper I, samples were fabricated in roll-to-roll process with different line speeds and all other process parameters were kept constant. By increasing the line speed, substrate residence time in the flame decreases, which has significant effect on deposited coating amount. This way size and structure of deposited remain fairly constant and different coating amount are obtained. Figure 12 shows SEM graphs of paperboard samples coated with TiO₂ nanoparticles with different line speeds. Right column of the figure presents conceptual side view of the coating with different line speeds. TiO₂ nanoparticles form tree-like structures with lower line speeds and surface is fully covered with highly porous nanoparticle layer. With increased line speeds (> 200 m/min), surface is only partly covered by agglomerated nanoparticles. Surface was still superhydrophobic even if surface was only partly covered. This information is essential if superhydrophobic surfaces will be produced in large quantities with low cost. It is also important that surface is superhydrophobic with excess amount of TiO₂ nanocoating. With this result, it is easier to generate superhydrophobic coatings with multiple burner system, because coating amount does not need to be constant in all parts of the surface.

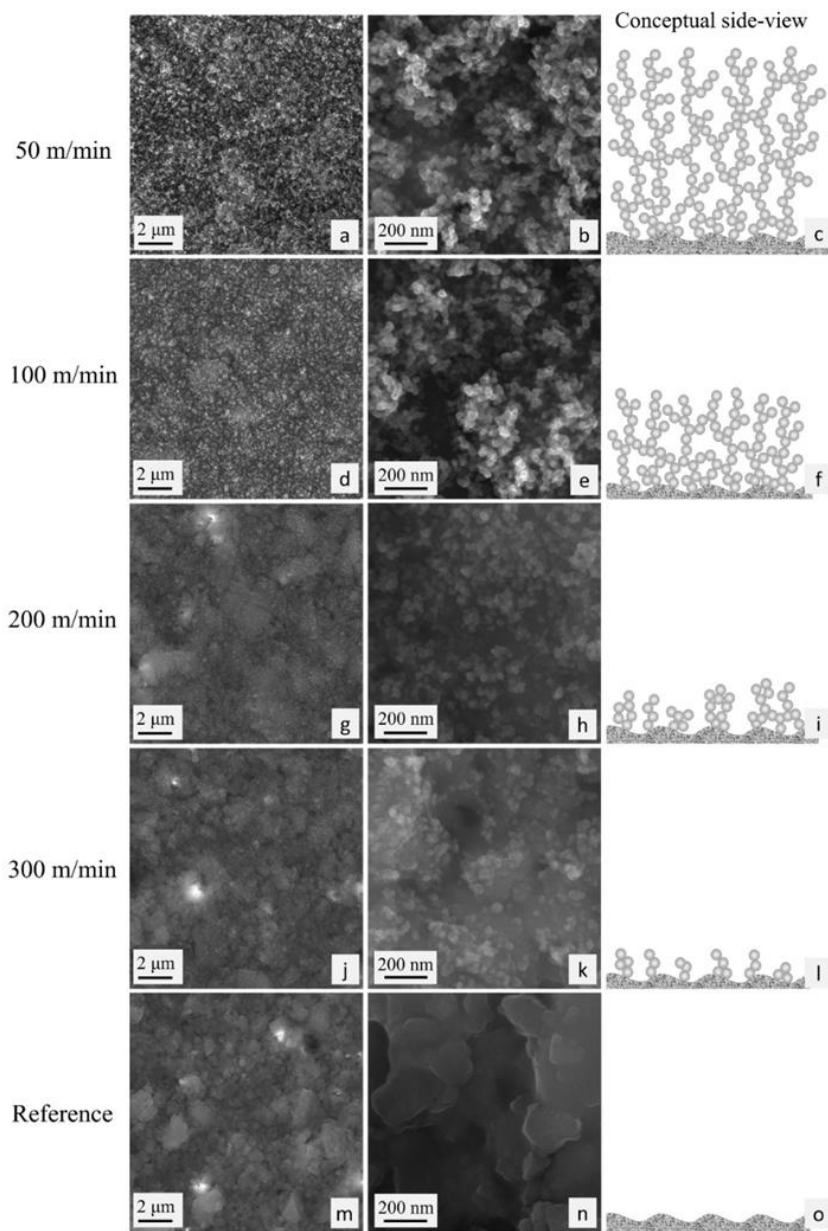


Figure 12. FE-SEM images of the paperboard surfaces coated at various line speeds. The left column (a), (d), (g), (j) and (m) is with lower magnification (scale bar 2 μm) and the middle column (b), (e), (h), (k) and (n) with higher magnification (scale bar 200 nm). Conceptual side view is presented in the right column (c), (f), (i), (l), and (o). (Paper I)

5.3 Multi-component Nanocoatings

Multi-component nanocoatings were first tested in Paper II. Pigment-coated paperboard was coated with $\text{TiO}_2/\text{SiO}_2$ nanoparticles with different fractions of Ti and Si in the precursors. From previous studies it was well known that TiO_2 nanoparticles form superhydrophobic coating and SiO_2 nanoparticles a superhydrophilic coating on paperboard. Coatings were carried out in roll-to-roll process with different Ti/Si ratios in the precursor. Wetting behavior of these coatings are presented in Figure 13. Result was a S-type curve, that can be explained partly by surface structure of nanocoatings. Paperboard has some micro-scale roughness and nanoparticles form porous layer on top. Such hierarchical structure improve both superhydrophilicity and superhydrophobicity. TEM-graphs of agglomerated nanoparticles with Ti/Si ratios of 1/99, 50/50 and 99/1 are shown in Figure 13 as inserts. With Ti/Si 1/99 primary nanoparticles are clearly sintered together without any separate spherical nanoparticles present. With Ti/Si 99/1, spherical primary nanoparticles are present and agglomerates form pearl necklace type of structure.

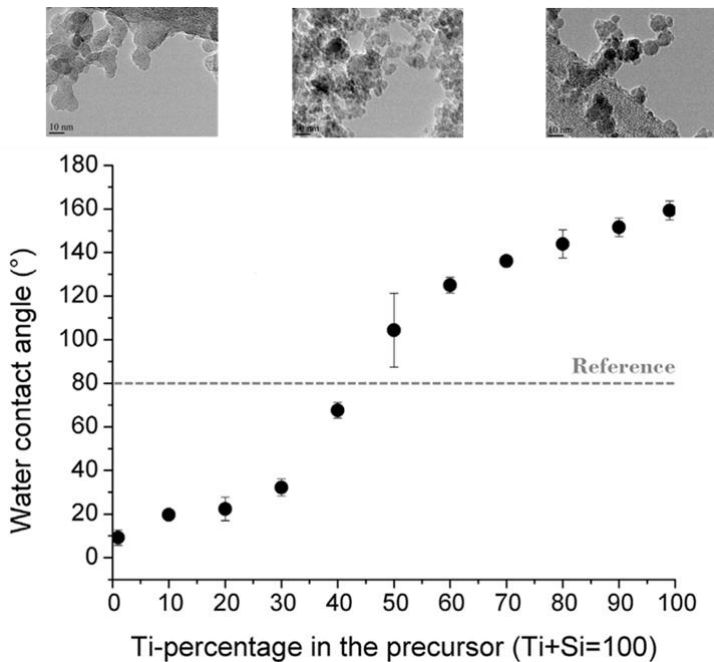


Figure 13. Dependence of water contact angle (WCA) on Ti-percentage in the precursor. Value 100 in the x-axis indicates 100% of Ti and 0% of Si. TEM graphs show shape of nanoparticles with Ti/Si ratios of 1/99, 50/50 and 99/1. (Paper II)

With high fraction of Si in the precursor, agglomerates are more sintered together. This improves the cohesion between the primary nanoparticles, but also decreases surface area and nanoscale roughness of the coating. This information was used when tuning the process parameters nanoparticle layer for samples used in Paper IV. Figure 14 presents effect of Ti/Si ratio in LFS-generated nanocoating after CVD coatings. With increased Ti/Si ratio, agglomerated primary particles are more separate and coating forms more porous structure. Increasing porosity increases air gaps in the coating that improves superamphiphobicity of the surface.

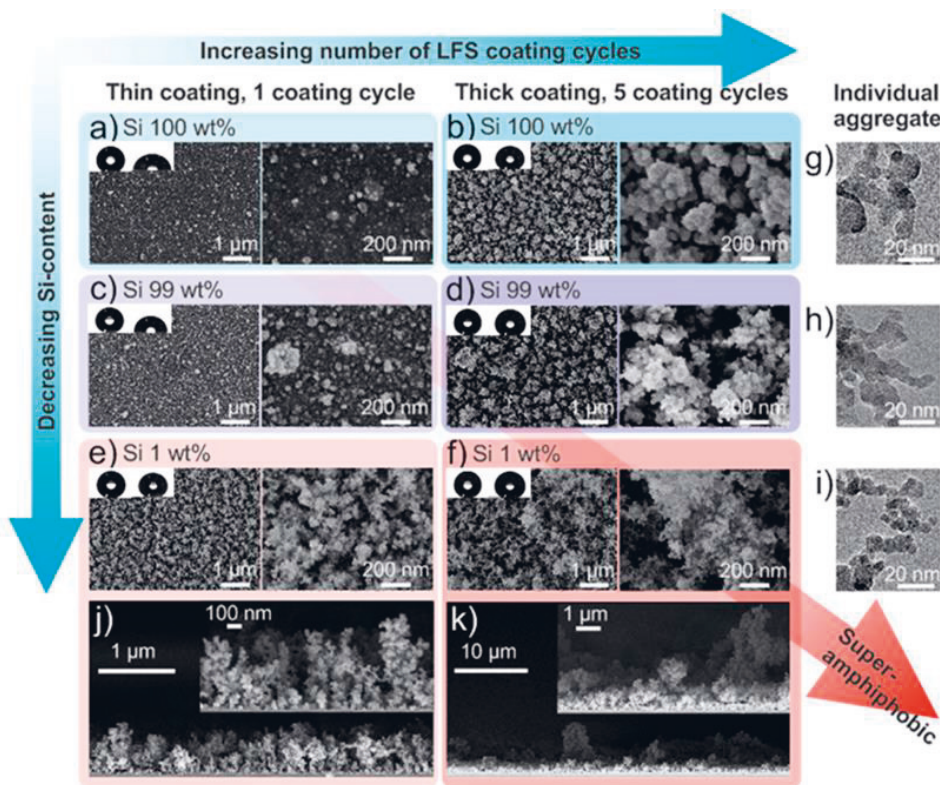


Figure 14. Top-view scanning electron microscopy (SEM) images of the coatings with different silicon dioxide content and thickness after chemical vapor deposition (CVD) of the fluorosilane. a,b Si 100 wt%; c,d Si 99 wt%; and e,f Si 1 wt% coating. Insets: the shape of 5 μL water (left) and n-hexadecane (right) drops resting on the respective surfaces. TEM images show different degree of sintering and overhang morphology of the particle aggregates: g) Si 100 wt%, h) Si 99 wt%, and i) Si 1 wt% coating. Side-view SEM images of j) Si 1 wt% thin coating (coated 1 time) and k) Si 1 wt% thick coating (coated 5 times). (Paper IV)

Ti/Si fractions of single nanoparticles were analyzed in Paper II by EDS analysis from TEM grids with TiO₂/SiO₂ nanoparticles. Elemental analysis was in line with the Ti/Si ratio used in the precursors. Recent study by Fang et al. reported results about cluster formation in flame synthesis with TiO₂/SiO₂ mixture [99]. Results were in line with the hypothesis presented in Paper II. TiO₂ and SiO₂ are mixed already in early stage of particle formation. Decomposition of TTIP/TEOS mixture is more complex than decomposition of TTIP or TEOS. In flame, decomposition and chemical reactions occur in a short time period and TiO₂/SiO₂ nanoparticles are formed in the first few centimeters of the flame.

5.4 Combining Different Coating Methods

Combining different coating methods is essential to obtain superamphiphobicity. LFS method was used for fabricating optimal surface structure for wood (Paper III) and glass (Paper IV) samples. Figure 15 presents wettability of wood surface with different coating combinations. LFS-made TiO₂ coating transforms surface superhydrophobic, but surface does not repel other tested liquids than water. Bare PFH-plasma coating improves surface phobicity for all tested liquids, but contact angles remain still under 150°. By combining LFS and PFH-plasma treatments, surface repels water, ethylene glycol (EG), diiodomethane (DIM) and olive oil. Also CAs of hexadecane (Hexa) are above 130°. This result can be explained by combining best features of each coating method. TiO₂ nanoparticles form optimal porous overhang-type structure and PFH generates desired chemical composition on top of the nanoparticle layer.

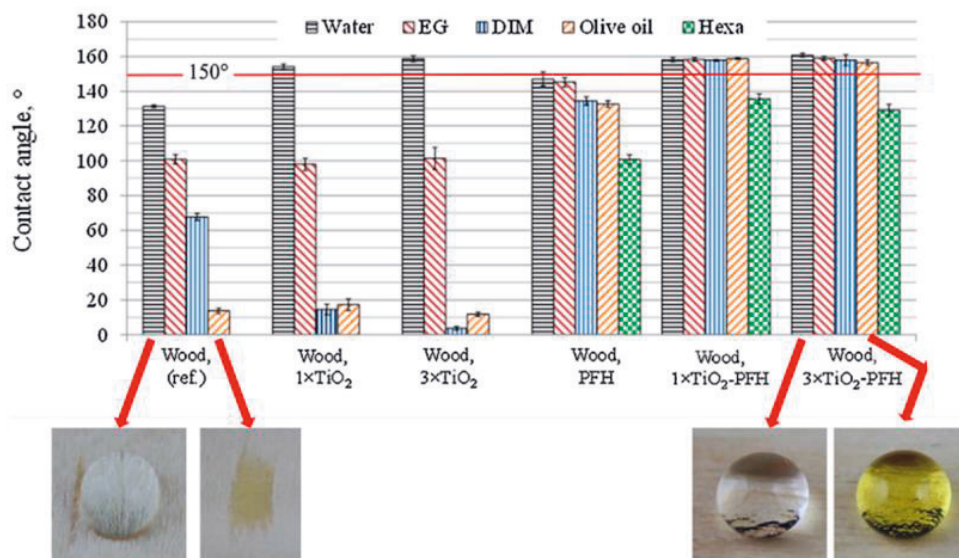


Figure 15. Static contact angles of water, ethylene glycol (EG), diiodomethane (DIM), olive oil and hexadecane (Hexa) on (1× and 3×) TiO₂-PFH coated wood. Static CA of hexadecane on wood, 1× and 3 × TiO₂ coated wood is <2°. Inset: ~10 mL drops of water and olive oil on uncoated and fully coated wood. (Paper III)

In Paper IV, CVD method was used for depositing fluorosilane on top of the TiO₂/SiO₂ nanocoating. This combination generated relatively good amphiphobicity on the surface. Ti/Si ratio and number of sweeps through the flame were varied in LFS coating. Measured contact angle values for different liquids are presented in Table 3. Thin coating stands for 1 sweep and thick coating for 5 sweeps in the LFS process. Thick coating improved amphiphobicity as well as higher Ti/Si ratio. Thick Si 1 wt% LFS coating consists of almost pure TiO₂ and thus has high porosity and surface area. Deposited fluorosilane layer covers nanoparticles and generates optimal low surface energy chemistry for amphiphobicity. Water repellency is high with almost all coating combinations, but EG and Hexa repellency is clearly improved with high Ti/Si ratio and increasing thickness of a nanoparticle coating. Low roll-off angle (RA) for Hexa was obtained only with Si 1 wt% thick nanoparticle layer. Measured RA 1° ± 1° is probably the lowest ever reported value for Hexa.

Table 3. Wettability of the liquid-repellent coatings. Apparent static contact angles (CA) and roll-off angles (RA) of 10 μ L drops of water, ethylene glycol, and n-hexadecane on coatings with different silicon dioxide content and thickness after chemical vapor deposition of the fluorosilane. “Thin” refers to a single LFS coating cycle. “Thick” refers to 5 subsequent LFS coating cycles. The standard deviations are given by individual contact angle goniometer measurements. Note that contact angles larger than $\approx 155^\circ$ cannot reliably be measured using the goniometer technique and thus the real error is larger. (Paper IV)

Coating	Water CA/RA [°]	Ethylene glycol CA/RA [°]	<i>n</i> -Hexadecane CA/RA [°]
Si 100 wt%, thin	138 \pm 3/–	118 \pm 1/–	83 \pm 1/–
Si 100 wt%, thick	168 \pm 1/<1	154 \pm 3/50 \pm 3	146 \pm 1/–
Si 99 wt%, thin	157 \pm 4/13 \pm 10	126 \pm 5/–	91 \pm 4/–
Si 99 wt%, thick	168 \pm 1/<1	160 \pm 5/6 \pm 1	153 \pm 2/–
Si 1 wt%, thin	163 \pm 2/3 \pm 1	154 \pm 2/12 \pm 1	151 \pm 2/29 \pm 7
Si 1 wt%, thick	167 \pm 1/<1	164 \pm 1/<1	157 \pm 4/1 \pm 1

In Paper IV only few different Ti/Si ratios were used and there is a lot of room for future studies in optimization of Ti/Si ratios for different coatings for different substrates. Si 1 wt% had the best performance among the tested coatings, but it is not necessarily the best possible Ti/Si ratio.

5.5 Stability

Stability of nanocoatings has been an issue for several decades [100, 101]. If a nanocoating consists of layer of nanoparticles, stability of a nanocoating depends on adhesion and cohesion of the nanoparticles. Adhesion is defined as stability between a nanoparticle and a surface, and cohesion as a stability of nanoparticles to each other. Especially the adhesion of the nanoparticle coatings has been an issue. Usually particles are attached on the substrate by relatively weak van der Waals forces and nanoparticles are easily removed by abrasion. Stepien et al. analyzed the stability of a LFS deposited TiO₂ nano-coating by Taber test, where a rolling wheel introduces abrasive wearing on the surface [100]. Most of the TiO₂ nanoparticle coating was easily removed from the surface and superhydrophobicity was lost. Part of the nanoparticles remained on the surface even if the substrate was damaged with excess amount of wear, but functionality of the nanocoating was destroyed.

Cohesion between nanoparticles in the coating can be improved by choosing the right nanoparticle materials. In Paper II, difference between TiO_2 and SiO_2 was analyzed from TEM graphs and SiO_2 nanoparticles form more combined structure than TiO_2 . Thick TiO_2 nanoparticle layer consists of agglomerates of several primary nanoparticles, forming tree-like structures. Individual TiO_2 nanoparticles remain relatively separate from each other causing the weak cohesion between primary particles. SiO_2 nanoparticles are strongly attached to each other forming strong bond. By mixing TiO_2 and SiO_2 precursors to same precursor solution, TEM graphs indicate that SiO_2 is acting partly as a binder material between the mixed $\text{TiO}_2/\text{SiO}_2$ nanoparticles. Even if the SiO_2 nanocoating is superhydrophilic and TiO_2 superhydrophobic, adding certain amount of SiO_2 into the coating, surface is still superhydrophobic. Figure 16 demonstrates clear difference in the shape of agglomerated $\text{TiO}_2/\text{SiO}_2$ nanoparticles. When the amount of SiO_2 increases, agglomerated nanoparticles are more sintered together and thus the cohesion between primary nanoparticles are improved. Structure of primary particles and agglomerates can be modified by choosing certain Ti/Si ratio for a precursor solution. This was first observed in Paper II and this knowledge was used in sample preparation for Paper IV.

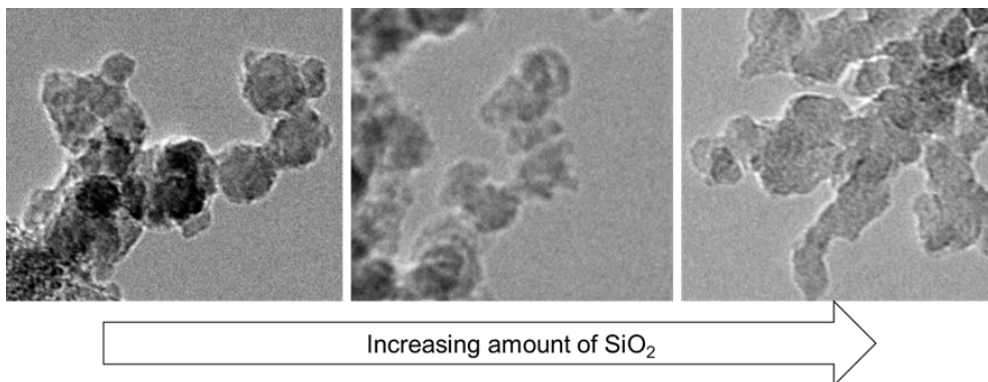


Figure 16. By increasing the Si content in the precursor, formed $\text{TiO}_2/\text{SiO}_2$ nanoparticle agglomerates are more sintered together. This improves the cohesion between the primary nanoparticles.

Several options for improving a nanoparticle coating stability are available. Substrate itself can improve the stability, e.g. in the case of using thermoplastics. Thermoplastics soften when it is introduced to a heat source. Substrate can be partly melted during the coating process, which was introduced by Brobbey et al. [85]. Substrate can be partly molten afterwards with extra heat treatment step, e.g. by

furnace, flame or lamination process [102]. These both methods improve the stability of a coating, but part of the active surface are is lost. Nanoparticles may be fully embedded into a substrate if the functionality of nanoparticles does not need direct contact. Embedded nanoparticles may be used e.g. in non-linear optical applications, when only interaction with light is needed.

Stability of a porous nanoparticle coating layer can be improved by after-treatment methods, such as ALD, CVD or plasma. Sorvali et al. [31] used ALD method for stabilizing porous TiO_2 nanoparticle layer with thin layer of Al_2O_3 . ALD treatment was followed by silanization to obtain desired low surface energy. Combined LFS+ALD+silanization coating was superamphiphobic and showed relatively good stability under wear stress. In Papers III and IV, porous nanoparticle coatings were after-treated with plasma and CVD methods, respectively. In Paper III, stability of plasma treated TiO_2 nanoparticle layer on wood substrate was tested with droplet test, where thousands of water droplets were dropped on the surface, without losing the superhydrophobicity.

Wood samples with TiO_2 +PFH coatings were tested with wetting durability test in Paper III. Samples were introduced to a set of 500000 water droplets. Wetting properties remained nearly identical before and after the wetting durability test. Schematic picture of test setup is presented in Figure 17.

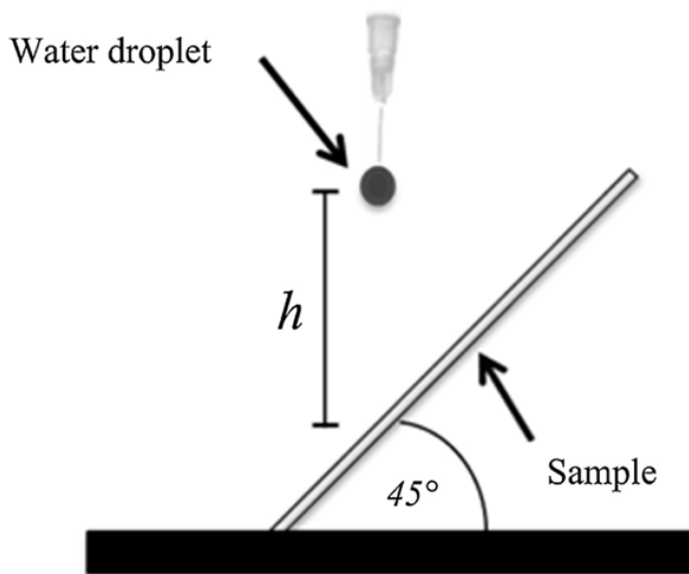


Figure 17. Sketch of the setup to test water drop impact resistance. $5 \mu\text{l}$ water drops were dispensed from a height (h) of 10 cm (impact velocity $U = 1.4 \text{ m/s}$). The tilting angle of the sample was 45° and the sequence was one drop every third second (Paper III).

Similar test setup was also used in Paper IV with good results. In Paper IV, 20000 droplets of 15 μl were dropped onto 10° tilted surface with Si 1 wt% thick coating. Roll-off angle (RA) was tested after 20000 droplets and values had decreased to 13° from initial 1° for water and Hexa pinned onto surface. After this test nanoparticle layer was coated by CVD with thin layer of SiO₂ prior to Fluorosilane coating to improve stability of the nanoparticle layer. With addition of SiO₂ layer between nanoparticle and Fluorosilane layer, surface remained undamaged during the new test with 20000 droplets and RA of water and Hexa were similar as before the droplet test. Water droplet test was also carried out for Si 100 wt% and Si 99 wt% samples. These samples remained undamaged during the droplet tests. This indicates that SiO₂ improves stability of the nanoparticle layer significantly. Future studies will include samples with more varied ratio of Ti/Si in the nano-particle layer to optimize good wettability and good stability without additional SiO₂ layer by CVD.

Other form of stability is how the samples behave as time goes by. In Paper I, surface wettability of samples was tested 1, 2, 7, 30, 90 and 365 days after the coating process. All samples were kept in constant conditions (dark, 50 %RH, 22°C) and WCAs of samples remained nearly the same or even increased. Measured WCAs of TiO₂ nanocoated samples with different line speeds are presented in Figure 18. WCA of reference samples remained stable at ~78°.

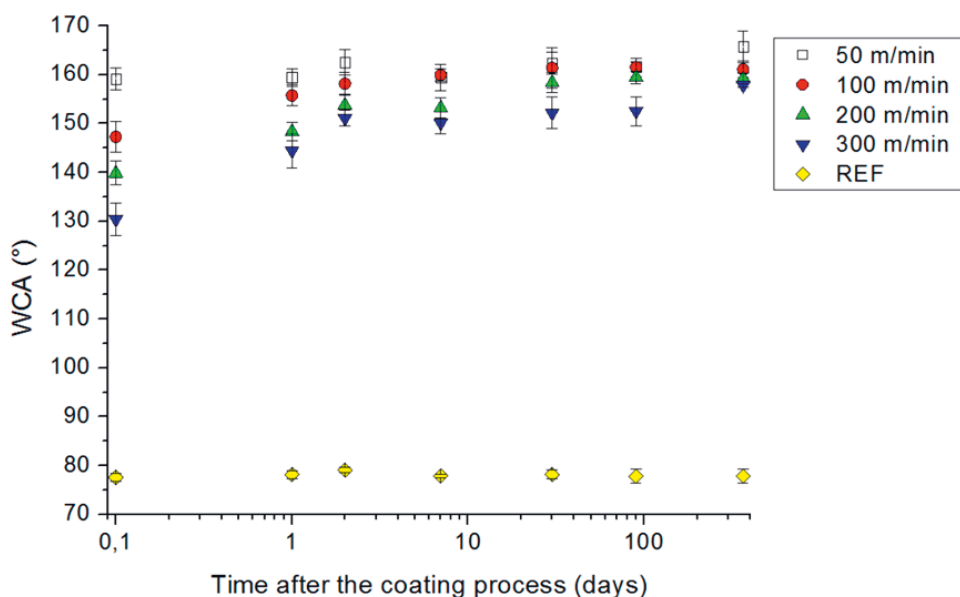


Figure 18. WCA values as a function of the time after the coating process with different line speeds (Paper I).

Explanation for increase in WCA values during time was analyzed by XPS. Analysis shows that C/O ratio increases in time. WCAs with C/O ratios 1 and 90 days after the coating process are presented in Figure 19. This result is in line with the hypothesis that superhydrophobicity of TiO₂ nanocoated paperboard is based on accumulation of carbonaceous compounds on top of the nanocoating. Clean TiO₂ surface is hydrophilic, similar to other oxides with high surface energy. Changes in the C/O ratio of reference sample (paperboard without nanocoating) was not observed so it can be concluded that chemical changes on the surface depend on the nanoparticle layer.

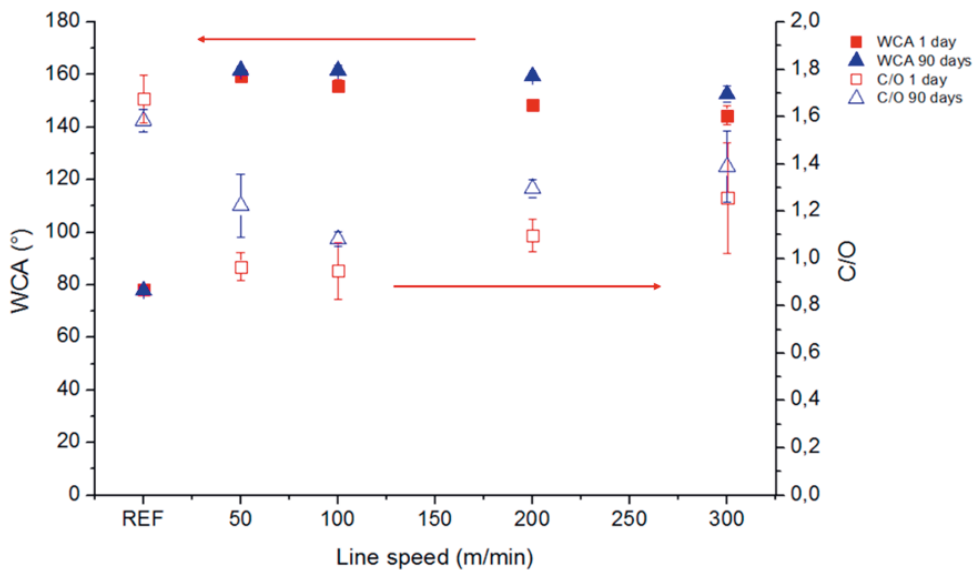


Figure 19. WCA and C/O ratio comparison between 1 day and 90 days after the LFS treatment (Paper I).

6 CONCLUSIONS

In this work, different approaches were used for controlling wettability of different surfaces. Liquid Flame Spray (LFS) was used as the main technique for fabricating porous nanoparticle coatings on paperboard, glass and wood substrates. Nanoparticle coatings were tested with various analysis methods and properties of nanocoatings were improved, based on the analysis results.

Changing the wettability of different surfaces was one of the main objectives and challenges since the beginning of this work. Different substrates were successfully coated with nanoparticles directly by the LFS coating process. Wetting behavior of paperboard was modified to superhydrophilic and superhydrophobic by changing the composition of nanoparticle coating. Water contact angle (WCA) changed as the Ti/Si ratio in the precursor solution was varied. Structural changes in the generated agglomerates were observed as well. Higher SiO₂ content in the nanocoating produced more sintered and stable nanoparticle agglomerates. This observation was used in later studies as LFS nanoparticle coating layer formed optimal porous structure for liquid repellency, even with improved stability of agglomerates. LFS nanocoating was further modified with optimal chemical compositions to enable repellency also for other liquids than water. Amphiphobic behavior was achieved in Papers III and IV for wood and glass substrates, respectively.

Stability of functional nanoparticle coatings have been one of the main issues for several years. Adhesion and cohesion play the key role in coating stability. This study revealed new information about problems and solutions to this stability problem. Cohesion between particles in a nanoparticle coating layer was greatly improved by mixing Ti and Si precursors in the same precursor solution, but adhesion still needs to be studied further. TiO₂/SiO₂ agglomerates formed different structures based on Ti/Si ratio used in the precursor solution. This was presented in Paper II and it was one of the main findings of this work. Optimized agglomerate structure was used in Paper IV for developing more stabilized, but still porous structure for excellent repellency for various liquids.

Key findings regarding the main research objectives of this thesis:

To define what is the optimal structure of the nanocoating and how much nano-particles are needed for the sufficient controlling of the wettability.

Optimal structure of a nanocoating depends partly on the substrate. If substrate has some micro-scale roughness, even partial coverage of surface is sufficient for superhydrophobicity. In the case of amphiphobicity, thicker, porous nanoparticle layer is needed. Porous layer of nanoparticles form overhang-type structure that inhibits even low-tension liquids penetrating on the substrate surface.

To discover if there is an advantage in using multi-component nanocoatings.

Multi-component nanocoatings improve cohesion of the nanoparticle layer. By changing the ratio of Ti/Si in the precursor, structure of TiO₂/SiO₂ multi-component nanoparticle agglomerates can be modified. With higher SiO₂ content, primary nanoparticles are more attached to each other. This decreases the porosity and surface area of nanoparticle layer, which can be positive or negative side-effect.

To achieve amphiphobic nanocoating by combining different coating methods.

Relatively good level of amphiphobicity was obtained by combining LFS with CVD or plasma coating. Nanoparticle layer by LFS generated optimal surface structure for wood and glass substrates. CVD and plasma treatment were used for stabilizing nanoparticle layer and for generating optimal chemical composition on the surface for amphiphobicity.

To obtain new information on the stability of the functional nanocoatings by using multi-component nanoparticle coatings and combining different coating methods.

Stability of functional nanocoatings was measured and improved. Superhydrophobicity of TiO₂ nanocoated paperboard remained in time or even improved. Wetting durability was tested for surfaces with multiple coating methods. By combining different coating methods, functional nanocoating were observed to withstand thousands of droplets of water. More research is needed for analyzing and improving stability of coatings in more abrasive wear tests. Cohesion between nanoparticles was greatly improved by optimizing the TiO₂/SiO₂ ratio in the nanoparticle coatings.

This work concentrated on the development of functional nanocoatings for the control of the wettability. Results were good, but further research is needed, especially for the stability of nanocoatings. Even if the cohesion between nanoparticles was improved during this work, adhesion between a nanocoating and a substrate remains as a universal problem. Improving the adhesion is a research topic which has plenty of different approaches to discover. Stability of functional nanocoating depends always on the application, but especially applications with abrasive wear conditions are problematic. Improving the adhesion has several routes to approach. Two of the most promising ways would be substrate modification prior to nanocoating process to ensure proper attachment of the nanocoating on the substrate surface. Other option is to carry out surface modification after the nanocoating process, but this often causes losing part of the porosity of a nanocoating.

Controlling the wettability of surfaces continues as a very important research topic as numerous applications include solid-liquid interactions. Superhydrophobic nanocoatings were successfully produced in roll-to-roll process with up to 300 m/min line speeds. This opens up new possibilities towards the industrial scale nanocoating processes. In addition to high line speeds, finding the minimum amount of nanocoating for superhydrophobicity enables developing functional nanocoatings more efficiently in the future. Research on functional nanocoatings continues and hopefully solutions for wear resistant superhydrophobic and superamphiphobic nanocoatings will be achieved in the near future.

REFERENCES

- [1] K. Koch, B. Bhushan, W. Barthlott, Multifunctional surface structures of plants: An inspiration for biomimetics, *Progress in Materials Science*, Vol. 54, Iss. 2, 2009, pp. 137-178.
- [2] W. Barthlott, C. Neinhuis, Purity of the sacred lotus, or escape from contamination in biological surfaces, *Planta*, Vol. 202, Iss. 1, 1997, pp. 1-8.
- [3] Y. Su, B. Ji, K. Zhang, H. Gao, Y. Huang, K. Hwang, Nano to micro structural hierarchy is crucial for stable superhydrophobic and water-repellent surfaces, *Langmuir*, Vol. 26, Iss. 7, 2010, pp. 4984-4989.
- [4] A. Solga, Z. Cerman, B.F. Striffler, M. Spaeth, W. Barthlott, The dream of staying clean: Lotus and biomimetic surfaces, *Bioinspiration and Biomimetics*, Vol. 2, Iss. 4, 2007, pp. S126-S134.
- [5] Y.T. Cheng, D.E. Rodak, C.A. Wong, C.A. Hayden, Effects of micro- and nano-structures on the self-cleaning behaviour of lotus leaves, *Nanotechnology*, Vol. 17, Iss. 5, 2006, pp. 1359-1362.
- [6] T. Darmanin, F. Guittard, Wettability of conducting polymers: From superhydrophilicity to superoleophobicity, *Progress in Polymer Science*, Vol. 39, Iss. 4, 2014, pp. 656-682.
- [7] T. Darmanin, F. Guittard, Superhydrophobic and superoleophobic properties in nature, *Materials Today*, Vol. 18, Iss. 5, 2015, pp. 273-285.
- [8] L. Feng, Y. Zhang, J. Xi, Y. Zhu, N. Wang, F. Xia, L. Jiang, Petal effect: A superhydrophobic state with high adhesive force, *Langmuir*, Vol. 24, Iss. 8, 2008, pp. 4114-4119.
- [9] S. Choo, H.-J. Choi, H. Lee, Replication of rose-petal surface structure using UV-nanoimprint lithography, *Materials Letters*, Vol. 121, 2014, pp. 170-173.
- [10] B. Bhushan, M. Nosonovsky, The rose petal effect and the modes of superhydrophobicity, *Philosophical Transactions of the Royal Society A: Mathematical, Physical and Engineering Sciences*, Vol. 368, Iss. 1929, 2010, pp. 4713-4728.

- [11] G.D. Bixler, B. Bhushan, Bioinspired rice leaf and butterfly wing surface structures combining shark skin and lotus effects, *Soft Matter*, Vol. 8, Iss. 44, 2012, pp. 11271-11284.
- [12] K. Liu, J. Du, J. Wu, L. Jiang, Superhydrophobic gecko feet with high adhesive forces towards water and their bio-inspired materials, *Nanoscale*, Vol. 4, Iss. 3, 2012, pp. 768-772.
- [13] G.D. Bixler, B. Bhushan, Rice- and butterfly-wing effect inspired self-cleaning and low drag micro/nanopatterned surfaces in water, oil, and air flow, *Nanoscale*, Vol. 6, Iss. 1, 2014, pp. 76-96.
- [14] Y. Zheng, X. Gao, L. Jiang, Directional adhesion of superhydrophobic butterfly wings, *Soft Matter*, Vol. 3, Iss. 2, 2007, pp. 178-182.
- [15] C.H.L. Goodman, M.V. Pessa, Atomic layer epitaxy, *Journal of Applied Physics*, Vol. 60, Iss. 3, 1986, pp. R65-R82.
- [16] S.M. George, Atomic layer deposition: An overview, *Chemical reviews*, Vol. 110, Iss. 1, 2010, pp. 111-131.
- [17] M. Kemell, V. Pore, M. Ritala, M. Leskelä, M. Lindén, Atomic layer deposition in nanometer-level replication of cellulosic substances and preparation of photocatalytic TiO₂/cellulose composites, *Journal of the American Chemical Society*, Vol. 127, Iss. 41, 2005, pp. 14178-14179.
- [18] K.L. Choy, Chemical vapour deposition of coatings, *Progress in Materials Science*, Vol. 48, Iss. 2, 2003, pp. 57-170.
- [19] C.J. Brinker, M.S. Harrington, Sol-gel derived antireflective coatings for silicon, *Solar Energy Materials*, Vol. 5, Iss. 2, 1981, pp. 159-172.
- [20] Y. Lu, R. Ganguli, C.A. Drewien, M.T. Anderson, C. Jeffrey Brinker, W. Gong, Y. Guo, H. Soyez, B. Dunn, M.H. Huang, J.I. Zink, Continuous formation of supported cubic and hexagonal mesoporous films by sol-gel dip-coating, *Nature*, Vol. 389, Iss. 6649, 1997, pp. 364-368.
- [21] J.L. Castillo, S. Martin, D. Rodriguez-Perez, F.J. Higuera, P.L. Garcia-Ybarra, Nanostructured porous coatings via electrospray atomization and deposition of nanoparticle suspensions, *Journal of Aerosol Science*, Vol. 125, 2018, pp. 148-163.

[22] A. del Campo, E. Arzt, Fabrication approaches for generating complex micro- and nanopatterns on polymeric surfaces, *Chemical reviews*, Vol. 108, Iss. 3, 2008, pp. 911-945.

[23] P. Van Broekhuizen, F. Van Broekhuizen, R. Cornelissen, L. Reijnders, Use of nanomaterials in the European construction industry and some occupational health aspects thereof, *Journal of Nanoparticle Research*, Vol. 13, Iss. 2, 2011, pp. 447-462.

[24] A. Barhoum, P. Samyn, T. Öhlund, A. Dufresne, Review of recent research on flexible multifunctional nanopapers, *Nanoscale*, Vol. 9, Iss. 40, 2017, pp. 15181-15205.

[25] A.J. Gröhn, S.E. Pratsinis, A. Sánchez-Ferrer, R. Mezzenga, K. Wegner, Scale-up of nanoparticle synthesis by flame spray pyrolysis: The high-temperature particle residence time, *Industrial and Engineering Chemistry Research*, Vol. 53, Iss. 26, 2014, pp. 10734-10742.

[26] F. Piccinno, F. Gottschalk, S. Seeger, B. Nowack, Industrial production quantities and uses of ten engineered nanomaterials in Europe and the world, *Journal of Nanoparticle Research*, Vol. 14, Iss. 9, 2012.

[27] J.-P. Nikkanen, S. Heinonen, E.H. Saarivirta, M. Honkanen, E. Levänen, Photocatalytically active titanium dioxide nanopowders: Synthesis, photoactivity and magnetic separation, *IOP Conference Series: Materials Science and Engineering*.

[28] P. Tunved, H.-. Hansson, V.-. Kerminen, J. Ström, M. Dal Maso, H. Lihavainen, Y. Viisanen, P.P. Aalto, M. Komppula, M. Kulmala, High natural aerosol loading over boreal forests, *Science*, Vol. 312, Iss. 5771, 2006, pp. 261-263.

[29] K.J. Brobbey, **J. Haapanen**, J.M. Mäkelä, M. Gunell, E. Eerola, E. Rosqvist, J. Peltonen, J.J. Saarinen, M. Tuominen, M. Toivakka, Effect of plasma coating on antibacterial activity of silver nanoparticles, *Thin Solid Films*, Vol. 672, 2019, pp. 75-82.

[30] K.J. Brobbey, **J. Haapanen**, M. Gunell, M. Toivakka, J.M. Mäkelä, E. Eerola, R. Ali, M.R. Saleem, S. Honkanen, J. Bobacka, J.J. Saarinen, Controlled time release and leaching of silver nanoparticles using a thin immobilizing layer of aluminum oxide, *Thin Solid Films*, Vol. 645, 2018, pp. 166-172.

- [31] M. Sorvali, L. Vuori, M. Pudas, **J. Haapanen**, R. Mahlberg, H. Ronkainen, M. Honkanen, M. Valden, J.M. Makela, Fabrication of ultrathin multilayered superomniphobic nanocoatings by liquid flame spray, atomic layer deposition, and silanization, *Nanotechnology*, Vol. 29, Iss. 18, 2018.
- [32] J.M. Mäkelä, M. Aromaa, H. Teisala, M. Tuominen, M. Stepien, J.J. Saarinen, M. Toivakka, J. Kuusipalo, Nanoparticle deposition from liquid flame spray onto moving roll-to-roll paperboard material, *Aerosol Science and Technology*, Vol. 45, Iss. 7, 2011, pp. 817-827.
- [33] K. Dick, T. Dhanasekaran, Z. Zhang, D. Meisel, Size-dependent melting of silica-encapsulated gold nanoparticles, *Journal of the American Chemical Society*, Vol. 124, Iss. 10, 2002, pp. 2312-2317.
- [34] Y. Sun, Y. Xia, Shape-controlled synthesis of gold and silver nanoparticles, *Science*, Vol. 298, Iss. 5601, 2002, pp. 2176-2179.
- [35] S. Nie, S.R. Emory, Probing single molecules and single nanoparticles by surface-enhanced Raman scattering, *Science*, Vol. 275, Iss. 5303, 1997, pp. 1102-1106.
- [36] C.L. Haynes, A.D. McFarland, M.T. Smith, J.C. Hulteen, R.P. Van Duyne, Angle-resolved nanosphere lithography: Manipulation of nanoparticle size, shape, and interparticle spacing, *Journal of Physical Chemistry B*, Vol. 106, Iss. 8, 2002, pp. 1898-1902.
- [37] J. Tikkanen, K.A. Gross, C.C. Berndt, V. Pitkänen, J. Keskinen, S. Raghu, M. Rajala, J. Karthikeyan, Characteristics of the liquid flame spray process, *Surface and Coatings Technology*, Vol. 90, Iss. 3, 1997, pp. 210-216.
- [38] K.A. Gross, J. Tikkanen, J. Keskinen, V. Pitkänen, M. Eerola, R. Sükamäki, M. Rajala, Liquid flame spraying for glass coloring, *Journal of Thermal Spray Technology*, Vol. 8, Iss. 4, 1999, pp. 583-589.
- [39] J.M. Mäkelä, M. Aromaa, A. Rostedt, T.J. Krinke, K. Janka, M. Marjamäki, J. Keskinen, Liquid flame spray for generating metal and metal oxide nanoparticle test aerosol, *Human and Experimental Toxicology*, Vol. 28, Iss. 6-7, 2009, pp. 421-431.
- [40] H. Keskinen, M. Aromaa, M.C. Heine, J.M. Mäkelä, Size and velocity measurements in sprays and particle-producing flame sprays, *Atomization and Sprays*, Vol. 18, Iss. 7, 2008, pp. 619-644.

- [41] H. Keskinen, J.M. Mäkelä, M. Vippola, M. Nurminen, J. Liimatainen, T. Lepistö, J. Keskinen, Generation of silver/palladium nanoparticles by liquid flame spray, *Journal of Materials Research*, Vol. 19, Iss. 5, 2004, pp. 1544-1550.
- [42] M. Aromaa, H. Keskinen, J.M. Mäkelä, The effect of process parameters on the Liquid Flame Spray generated titania nanoparticles, *Biomolecular engineering*, Vol. 24, Iss. 5, 2007, pp. 543-548.
- [43] L. Mädler, H.K. Kammler, R. Mueller, S.E. Pratsinis, Controlled synthesis of nanostructured particles by flame spray pyrolysis, *Journal of Aerosol Science*, Vol. 33, Iss. 2, 2002, pp. 369-389.
- [44] H.K. Kammler, L. Mädler, S.E. Pratsinis, Flame synthesis of nanoparticles, *Chemical Engineering and Technology*, Vol. 24, Iss. 6, 2001, pp. 583-596.
- [45] D.O. Scanlon, C.W. Dunnill, J. Buckeridge, S.A. Shevlin, A.J. Logsdail, S.M. Woodley, C.R.A. Catlow, M.J. Powell, R.G. Palgrave, I.P. Parkin, G.W. Watson, T.W. Keal, P. Sherwood, A. Walsh, A.A. Sokol, Band alignment of rutile and anatase TiO₂, *Nature Materials*, Vol. 12, Iss. 9, 2013, pp. 798-801.
- [46] J. Zhang, Q. Xu, Z. Feng, M. Li, C. Li, Importance of the relationship between surface phases and photocatalytic activity of TiO₂, *Angewandte Chemie - International Edition*, Vol. 47, Iss. 9, 2008, pp. 1766-1769.
- [47] H. Teisala, M. Tuominen, **J. Haapanen**, M. Aromaa, M. Stepien, J.M. Mäkelä, J.J. Saarinen, M. Toivakka, J. Kuusipalo, Switchable water absorption of paper via liquid flame spray nanoparticle coating, *Cellulose*, Vol. 21, Iss. 3, 2014, pp. 2033-2043.
- [48] M. Tuominen, H. Teisala, **J. Haapanen**, M. Aromaa, J.M. Mäkelä, M. Stepien, J.J. Saarinen, M. Toivakka, J. Kuusipalo, Adjustable wetting of liquid flame spray (LFS) TiO₂-nanoparticle coated board: Batch-type versus roll-to-roll stimulation methods, *Nordic Pulp and Paper Research Journal*, Vol. 29, Iss. 2, 2014, pp. 271-279.
- [49] H. Teisala, M. Tuominen, M. Stepien, **J. Haapanen**, J.M. Mäkelä, J.J. Saarinen, M. Toivakka, J. Kuusipalo, Wettability conversion on the liquid flame spray generated superhydrophobic TiO₂ nanoparticle coating on paper and board by photocatalytic decomposition of spontaneously accumulated carbonaceous overlayer, *Cellulose*, Vol. 20, Iss. 1, 2013, pp. 391-408.

- [50] M. Stepien, J.J. Saarinen, H. Teisala, M. Tuominen, M. Aromaa, **J. Haapanen**, J. Kuusipalo, J.M. Mäkelä, M. Toivakka, ToF-SIMS analysis of UV-switchable TiO₂-nanoparticle-coated paper surface, *Langmuir*, Vol. 29, Iss. 11, 2013, pp. 3780-3790.
- [51] V.N. Mochalin, Y. Gogotsi, Wet chemistry route to hydrophobic blue fluorescent nanodiamond, *Journal of the American Chemical Society*, Vol. 131, Iss. 13, 2009, pp. 4594-4595.
- [52] C.A. Morris, M.L. Anderson, R.M. Stroud, C.I. Merzbacher, D.R. Rolison, Silica sol as a nanoglue: Flexible synthesis of composite aerogels, *Science*, Vol. 284, Iss. 5414, 1999, pp. 622-624.
- [53] E. Hao, G.C. Schatz, J.T. Hupp, Synthesis and optical properties of anisotropic metal nanoparticles, *Journal of Fluorescence*, Vol. 14, Iss. 4, 2004, pp. 331-341.
- [54] F.E. Kruis, H. Fissan, A. Peled, Synthesis of nanoparticles in the gas phase for electronic, optical and magnetic applications - A review, *Journal of Aerosol Science*, Vol. 29, Iss. 5-6, 1998, pp. 511-535.
- [55] M.T. Swihart, Vapor-phase synthesis of nanoparticles, *Current Opinion in Colloid and Interface Science*, Vol. 8, Iss. 1, 2003, pp. 127-133.
- [56] R. Strobel, S.E. Pratsinis, Flame aerosol synthesis of smart nanostructured materials, *Journal of Materials Chemistry*, Vol. 17, Iss. 45, 2007, pp. 4743-4756.
- [57] T. Salminen, J. Dahl, M. Tuominen, P. Laukkanen, E. Arola, T. Niemi, Single-step fabrication of luminescent GaAs nanocrystals by pulsed laser ablation in liquids, *Optical Materials Express*, Vol. 2, Iss. 6, 2012, pp. 799-813.
- [58] T. Salminen, M. Honkanen, T. Niemi, Coating of gold nanoparticles made by pulsed laser ablation in liquids with silica shells by simultaneous chemical synthesis, *Physical Chemistry Chemical Physics*, Vol. 15, Iss. 9, 2013, pp. 3047-3051.
- [59] A.M. Morales, C.M. Lieber, A laser ablation method for the synthesis of crystalline semiconductor nanowires, *Science*, Vol. 279, Iss. 5348, 1998, pp. 208-211.
- [60] B.N. Chichkov, C. Momma, S. Nolte, F. Von Alvensleben, A. Tünnermann, Femtosecond, picosecond and nanosecond laser ablation of solids, *Applied Physics A: Materials Science and Processing*, Vol. 63, Iss. 2, 1996, pp. 109-115.

- [61] N.S. Tabrizi, M. Ullmann, V.A. Vons, U. Lafont, A. Schmidt-Ott, Generation of nanoparticles by spark discharge, *Journal of Nanoparticle Research*, Vol. 11, Iss. 2, 2009, pp. 315-332.
- [62] J.H. Byeon, J.H. Park, J. Hwang, Spark generation of monometallic and bimetallic aerosol nanoparticles, *Journal of Aerosol Science*, Vol. 39, Iss. 10, 2008, pp. 888-896.
- [63] B.O. Mueller, M.E. Messing, D.L.J. Engberg, A.M. Jansson, L.I.M. Johansson, S.M. Norlén, N. Tureson, K. Deppert, Review of spark discharge generators for production of nanoparticle aerosols, *Aerosol Science and Technology*, Vol. 46, Iss. 11, 2012, pp. 1256-1270.
- [64] D. Vollath, Plasma synthesis of nanoparticles, *KONA Powder and Particle Journal*, Vol. 25, Iss. March, 2007, pp. 39-55.
- [65] N. Petermann, N. Stein, G. Schierning, R. Theissmann, B. Stoib, M.S. Brandt, C. Hecht, C. Schulz, H. Wiggers, Plasma synthesis of nanostructures for improved thermoelectric properties, *Journal of Physics D: Applied Physics*, Vol. 44, Iss. 17, 2011.
- [66] L. Jia, F. Gitzhofer, Nano-particle sizing in a thermal plasma synthesis reactor, *Plasma Chemistry and Plasma Processing*, Vol. 29, Iss. 6, 2009, pp. 497-513.
- [67] K.J. Hüttinger, CVD in Hot Wall Reactors - The Interaction between Homogeneous Gas-Phase and Heterogeneous Surface Reactions, *Chemical Vapor Deposition*, Vol. 4, Iss. 4, 1998, pp. 151-158.
- [68] V. De Pauw, B. Reznik, S. Kalhöfer, D. Gerthsen, Z.J. Hu, K.J. Hüttinger, Texture and nanostructure of pyrocarbon layers deposited on planar substrates in a hot-wall reactor, *Carbon*, Vol. 41, Iss. 1, 2003, pp. 71-77.
- [69] T.E. Wilke, K.A. Turner, C.G. Takoudis, Chemical vapor deposition of silicon under reduced pressure in hot-wall reactors, *Chemical Engineering Science*, Vol. 41, Iss. 4, 1986, pp. 643-650.
- [70] G.L. Messing, S.-C. Zhang, G.V. Jayanthi, Ceramic Powder Synthesis by Spray Pyrolysis, *Journal of the American Ceramic Society*, Vol. 76, Iss. 11, 1993, pp. 2707-2726.
- [71] P.S. Patil, Versatility of chemical spray pyrolysis technique, *Materials Chemistry and Physics*, Vol. 59, Iss. 3, 1999, pp. 185-198.

- [72] K. Okuyama, I.W. Lenggoro, Preparation of nanoparticles via spray route, *Chemical Engineering Science*, Vol. 58, Iss. 3-6, 2003, pp. 537-547.
- [73] S. Martin, A. Perea, P.L. Garcia-Ybarra, J.L. Castillo, Effect of the collector voltage on the stability of the cone-jet mode in electrohydrodynamic spraying, *Journal of Aerosol Science*, Vol. 46, 2012, pp. 53-63.
- [74] S. Friedlander, *Smoke, dust and haze. Fundamentals of aerosol behaviour*. 1977.
- [75] L. Mädler, A. Roessler, S.E. Pratsinis, T. Sahm, A. Gurlo, N. Barsan, U. Weimar, Direct formation of highly porous gas-sensing films by in situ thermophoretic deposition of flame-made Pt/SnO₂ nanoparticles, *Sensors and Actuators, B: Chemical*, Vol. 114, Iss. 1, 2006, pp. 283-295.
- [76] M.M. Maricq, Size and charge of soot particles in rich premixed ethylene flames, *Combustion and Flame*, Vol. 137, Iss. 3, 2004, pp. 340-350.
- [77] S. Thybo, S. Jensen, J. Johansen, T. Johannessen, O. Hansen, U.J. Quaade, Flame spray deposition of porous catalysts on surfaces and in microsystems, *Journal of Catalysis*, Vol. 223, Iss. 2, 2004, pp. 271-277.
- [78] M. Aromaa, A. Arffman, H. Suhonen, **J. Haapanen**, J. Keskinen, M. Honkanen, J.-P. Nikkanen, E. Levänen, M.E. Messing, K. Deppert, H. Teisala, M. Tuominen, J. Kuusipalo, M. Stepien, J.J. Saarinen, M. Toivakka, J.M. Mäkelä, Atmospheric synthesis of superhydrophobic TiO₂ nanoparticle deposits in a single step using Liquid Flame Spray, *Journal of Aerosol Science*, Vol. 52, 2012, pp. 57-68.
- [79] J.M. Mäkelä, **J. Haapanen**, J. Harra, P. Juuti, S. Kujanpää, Liquid flame spray—a hydrogen-oxygen flame based method for nanoparticle synthesis and functional nanocoatings, *KONA Powder and Particle Journal*, Vol. 2017, Iss. 34, 2017, pp. 141-154.
- [80] M. Stepien, J.J. Saarinen, H. Teisala, M. Tuominen, **J. Haapanen**, J.M. Mäkelä, J. Kuusipalo, M. Toivakka, Compressibility of porous TiO₂ nanoparticle coating on paperboard, *Nanoscale Research Letters*, Vol. 8, Iss. 1, 2013, pp. 1-6.
- [81] H. Teisala, M. Tuominen, **J. Haapanen**, M. Aromaa, M. Stepien, J.M. Mäkelä, J.J. Saarinen, M. Toivakka, J. Kuusipalo, Review on liquid flame spray in paper converting: Multifunctional superhydrophobic nanoparticle coatings, *Nordic Pulp and Paper Research Journal*, Vol. 29, Iss. 4, 2014, pp. 747-759.

- [82] M. Tuominen, H. Teisala, M. Aromaa, M. Stepien, J.M. Mäkelä, J.J. Saarinen, M. Toivakka, J. Kuusipalo, Creation of superhydrophilic surfaces of paper and board, *Journal of Adhesion Science and Technology*, Vol. 28, Iss. 8-9, 2014, pp. 864-879.
- [83] M. Gunell, **J. Haapanen**, K.J. Brobbey, J.J. Saarinen, M. Toivakka, J.M. Mäkelä, P. Huovinen, E. Eerola, Antimicrobial characterization of silver nanoparticle-coated surfaces by “touch test” method, *Nanotechnology, Science and Applications*, Vol. 10, 2017, pp. 137-145.
- [84] P. Juuti, **J. Haapanen**, C. Stenroos, H. Niemelä-Anttonen, J. Harra, H. Koivuluoto, H. Teisala, J. Lahti, M. Tuominen, J. Kuusipalo, P. Vuoristo, J.M. Mäkelä, Achieving a slippery, liquid-infused porous surface with anti-icing properties by direct deposition of flame synthesized aerosol nanoparticles on a thermally fragile substrate, *Applied Physics Letters*, Vol. 110, Iss. 16, 2017.
- [85] K.J. Brobbey, **J. Haapanen**, M. Gunell, J.M. Mäkelä, E. Eerola, M. Toivakka, J.J. Saarinen, One-step flame synthesis of silver nanoparticles for roll-to-roll production of antibacterial paper, *Applied Surface Science*, Vol. 420, 2017, pp. 558-565.
- [86] H. Keskinen, J.M. Mäkelä, M. Aromaa, J. Keskinen, S. Areva, C.V. Teixeira, J.B. Rosenholm, V. Pore, M. Ritala, M. Leskelä, M. Raulio, M.S. Salkinoja-Salonen, E. Levänen, T. Mäntylä, Titania and titania-silver nanoparticle deposits made by Liquid Flame Spray and their functionality as photocatalyst for organic- and biofilm removal, *Catalysis Letters*, Vol. 111, Iss. 3-4, 2006, pp. 127-132.
- [87] A. Tricoli, M. Righettoni, A. Teleki, Semiconductor gas sensors: Dry synthesis and application, *Angewandte Chemie - International Edition*, Vol. 49, Iss. 42, 2010, pp. 7632-7659.
- [88] H. Koivuluoto, M. Honkanen, P. Vuoristo, Cold-sprayed copper and tantalum coatings - Detailed FESEM and TEM analysis, *Surface and Coatings Technology*, Vol. 204, Iss. 15, 2010, pp. 2353-2361.
- [89] M. Honkanen, M. Hoikkanen, M. Vippola, J. Vuorinen, T. Lepistö, P. Jussila, H. Ali-Löytty, M. Lampimäki, M. Valden, Characterization of silane layers on modified stainless steel surfaces and related stainless steel-plastic hybrids, *Applied Surface Science*, Vol. 257, Iss. 22, 2011, pp. 9335-9346.
- [90] M. Sillanpää, T.-. Paunu, P. Sainio, Aggregation and deposition of engineered TiO₂ nanoparticles in natural fresh and brackish waters, *Journal of Physics: Conference Series*, Institute of Physics Publishing.

- [91] M. Rezaee, Y. Yamini, M. Faraji, Evolution of dispersive liquid-liquid microextraction method, *Journal of Chromatography A*, Vol. 1217, Iss. 16, 2010, pp. 2342-2357.
- [92] M. Rochkind, S. Pasternak, Y. Paz, Using dyes for evaluating photocatalytic properties: A critical review, *Molecules*, Vol. 20, Iss. 1, 2015, pp. 88-110.
- [93] E. Gogolides, K. Ellinas, A. Tserepi, Hierarchical micro and nano structured, hydrophilic, superhydrophobic and superoleophobic surfaces incorporated in microfluidics, microarrays and lab on chip microsystems, *Microelectronic Engineering*, Vol. 132, 2015, pp. 135-155.
- [94] W.-G. Bae, H.N. Kim, D. Kim, S.-. Park, H.E. Jeong, K.-I. Suh, 25th anniversary article: Scalable multiscale patterned structures inspired by nature: The role of hierarchy, *Advanced Materials*, Vol. 26, Iss. 5, 2014, pp. 675-699.
- [95] Z. Chu, S. Seeger, Superamphiphobic surfaces, *Chemical Society Reviews*, Vol. 43, Iss. 8, 2014, pp. 2784-2798.
- [96] K. Liu, L. Jiang, Bio-inspired design of multiscale structures for function integration, *Nano Today*, Vol. 6, Iss. 2, 2011, pp. 155-175.
- [97] H.-J. Choi, S. Choo, J.-H. Shin, K.-I. Kim, H. Lee, Fabrication of superhydrophobic and oleophobic surfaces with overhang structure by reverse nanoimprint lithography, *Journal of Physical Chemistry C*, Vol. 117, Iss. 46, 2013, pp. 24354-24359.
- [98] X. Gou, Z. Guo, Surface topographies of biomimetic superamphiphobic materials: design criteria, fabrication and performance, *Advances in Colloid and Interface Science*, Vol. 269, 2019, pp. 87-121.
- [99] J. Fang, Y. Wang, J. Kangasluoma, M. Attoui, H. Junninen, M. Kulmala, T. Petäjä, P. Biswas, The initial stages of multicomponent particle formation during the gas phase combustion synthesis of mixed SiO₂/TiO₂, *Aerosol Science and Technology*, Vol. 52, Iss. 3, 2018, pp. 277-286.
- [100] M. Stepien, G. Chinga-Carrasco, J.J. Saarinen, H. Teisala, M. Tuominen, M. Aromaa, **J. Haapanen**, J. Kuusipalo, J.M. Mäkelä, M. Toivakka, Wear resistance of nanoparticle coatings on paperboard, *Wear*, Vol. 307, Iss. 1-2, 2013, pp. 112-118.
- [101] M. Vorbau, L. Hillemann, M. Stintz, Method for the characterization of the abrasion induced nanoparticle release into air from surface coatings, *Journal of Aerosol Science*, Vol. 40, Iss. 3, 2009, pp. 209-217.

[102] Y. Liu, Q. Xu, A.M. Lyons, Durable, optically transparent, superhydrophobic polymer films, *Applied Surface Science*, Vol. 470, 2019, pp. 187-195.

PAPER

I

**On the limit of superhydrophobicity: defining the minimum amount of
TiO₂ nanoparticle coating**

Janne Haapanen, Mikko Aromaa, Hannu Teisala, Paxton Juuti, Mikko
Tuominen, Markus Sillanpää, Milena Stepien, Jarkko J. Saarinen, Martti
Toivakka, Jurkka Kuusipalo, Jyrki M. Mäkelä

Materials Research Express 6 (2019), 035004

DOI: 10.1088/2053-1591/aaf2ee

Publication reprinted with the permission of the copyright holders.

Materials Research Express



PAPER

On the limit of superhydrophobicity: defining the minimum amount of TiO₂ nanoparticle coating

RECEIVED

14 August 2018

REVISED


13 November 2018

ACCEPTED FOR PUBLICATION

22 November 2018

PUBLISHED

5 December 2018

Janne Haapanen^{1,9} , Mikko Aromaa¹, Hannu Teisala^{2,3}, Paxton Juuti¹, Mikko Tuominen^{2,4}, Markus Sillanpää⁵, Milena Stepien^{6,7}, Jarkko J Saarinen⁶, Martti Toivakka⁶, Jurkka Kuusipalo² and Jyrki M Mäkelä¹

¹ Aerosol Physics, Laboratory of Physics, Faculty of Natural Sciences, Tampere University of Technology, Tampere, Finland

² Packaging Technology Research Team, Laboratory of Materials Science, Tampere University of Technology, Tampere, Finland

³ Department of Physics at Interfaces, Max Planck Institute for Polymer Research, Mainz, Germany

⁴ Bioscience and Materials/Surface, Process and Formulation, RISE Research Institutes of Sweden, Stockholm, Sweden

⁵ Laboratory Centre, Finnish Environment Institute, Helsinki, Finland

⁶ Laboratory for paper Coating and Converting, Abo Akademi University, Turku, Finland

⁷ Academic Centre for Materials and Nanotechnology, AGH University of Science and Technology, Krakow, Poland

⁸ Department of Chemistry, University of Eastern Finland, Joensuu, Finland

⁹ Author to whom any correspondence should be addressed

E-mail: janne.haapanen@tut.fi

Keywords: nanoparticles, nanocoatings, liquid flame spray, wetting, superhydrophobic, titanium dioxide, TiO₂

Supplementary material for this article is available online

Abstract

Fabrication of superhydrophobic surfaces in large scale has been in high interest for several years, also titanium oxide nanostructures having been applied for the purpose. Optimizing the amount and structure of the TiO₂ material in the coating will play a key role when considering upscaling. Here, we take a look at fabricating the superhydrophobic surface in a one-step roll-to-roll pilot scale process by depositing TiO₂ nanoparticles from a Liquid Flame Spray onto a moving paperboard substrate. In order to find the minimum amount of nanomaterial still sufficient for creating superhydrophobicity, we varied nanoparticle production rate, flame distance from the substrate and line speed. Since the deposited amount of material sideways from the flame path was seen to decrease gradually, spatial analysis enabled us to consistently determine the minimum amount of TiO₂ nanoparticles on the substrate needed to achieve superhydrophobicity. Amount as low as 20–30 mg m⁻² of TiO₂ nanoparticles was observed to be sufficient. The scanning electron microscopy revealed that at this amount, the surface was covered with nanoparticles only partially, but still sufficiently to create a hierarchical structure to affect wetting significantly. Based on XPS analysis, it became apparent that TiO₂ gathers hydrocarbons on the surface to develop the surface chemistry towards hydrophobic, but below the critical amount of TiO₂ nanoparticles, the chemistry could not enable superhydrophobicity anymore. While varying the deposited amount of TiO₂, besides the local spatial variance of the coating amount, also the overall yield was studied. Within the text matrix, a yield up to 44% was achieved. In conclusion, superhydrophobicity was achieved at all tested line speeds (50 to 300 m min⁻¹), even if the amount of TiO₂ varied significantly (20 to 230 mg m⁻²).

1. Introduction

Generation of superhydrophobic surfaces has been of high interest to both scientific and industrial fields. There are various methods for manufacturing superhydrophobic surfaces, such as laser etching [1], photocatalytic lithography [2], wet-chemical route [3, 4], electrochemical deposition [5, 6], electrospinning [7], chemical vapor deposition (CVD) [8] and sol-gel method [9]. Using nanoparticles in surface functionalization has several advantages: e.g. high purity, wide range of coating materials and that amount of material is extremely low compared to macroscopic surface treatment methods. Usually high-speed fabrication of functional coatings

refers to a roll-to-roll coating process, where a substrate unwinds from one roll and winds to another. In this process, a coating is applied in one or several steps on the substrate between the two rolls. When discussing about roll-to-roll nanocoating processes, line speeds in most cases are in the range of a meter to few meters per minute [10–14]. It is a big advantage if coating is performed in one-step process with high nanoparticle production rate, which requires only a simple modification to the roll-to-roll process and enables faster line speeds. Finding the minimum amount of TiO₂ needed for superhydrophobicity is in the key role for future development and aiming for more efficient manufacturing of superhydrophobic surfaces.

Gas-phase synthesis methods for nanoparticle production are widely used in industrial and scientific fields, and especially flame based methods are considered to be optimal for up-scaling [15–17]. Produced nanoparticles can either be collected as powder and subsequently applied on surfaces by various methods [18] or deposited directly onto surfaces forming functional nanocoatings [19, 20]. Similarly to other flame synthesis methods [21, 22], Liquid Flame Spray (LFS) method has also been widely used in nanoparticle generation [23]. Recently, LFS has been used for manufacturing functional nanocoatings in a roll-to-roll process [24–27]. These nanocoated paperboard surfaces can be used e.g. in micro fluidics [28] or as anti-microbial surfaces [29]. In previous studies, roll-to-roll line speed of 50 m min⁻¹ has been used for producing superhydrophobic and superhydrophilic surfaces [24, 25, 30, 31]. To our knowledge, higher line speeds than 150 m min⁻¹ have not been reported before. Higher line speed can be used to minimize coating amount without changing other process parameters. We used pilot scale paper converting machine with line speeds of 50, 100, 200 and 300 m min⁻¹ aiming for superhydrophobic surfaces, with minimal amount of nanocoating on the surface. Especially for industrial scale applications, there is a demand for high line speeds. Commercially available pigment coated paperboard (200 g m⁻²) was chosen as the substrate to be able to compare the results to previous studies with lower line speeds. It has been shown that LFS-generated TiO₂ nanoparticles produce superhydrophobic surfaces with line speed of 50 m min⁻¹, but the effect of higher line speeds to nanocoating behavior need to be analyzed more closely. With the line speed of 50 m min⁻¹, paperboard surface is covered with excess amount of nanoparticles, therefore our aim is to achieve a superhydrophobic surface with a lower amount of nanoparticles and find out what is the minimum amount of TiO₂ needed for superhydrophobicity. Here the TiO₂ nanoparticles produced with the LFS consists mainly of anatase, with a small fraction of rutile [30]. Different LFS process parameters were used in the paperboard coating and they were also optimized to achieve superhydrophobicity with an adequate process yield. Here the yield is defined as the share of produced nanoparticles that adhere on the paperboard.

2. Experimental section

2.1. Liquid flame spray for nanoparticle production

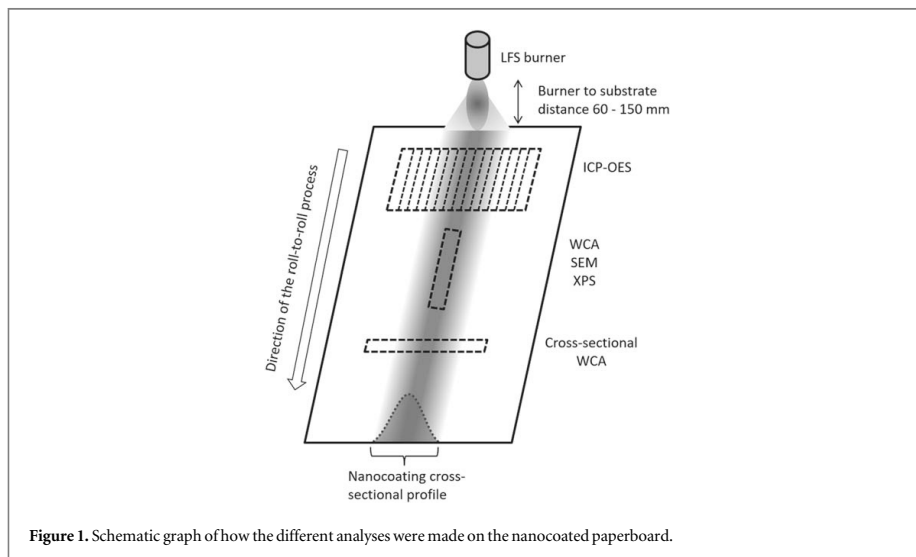
Liquid Flame Spray (LFS) is a versatile aerosol synthesis method for nanoparticle production. In LFS method, liquid precursor solution is injected into a turbulent hydrogen-oxygen flame. Precursor evaporates in the hot flame and due to subsequent rapid cooling, precursor containing gas becomes supersaturated, which leads to nucleation. The aerosol processes of the LFS method have been described in more detail previously [27, 30, 32]. By adjusting the process parameters, such as the precursor concentration and feed rate, and the flow rates of the burner gases, properties of the produced nanoparticle aerosol can be tuned. With high production rates, nanoparticles form agglomerates, consisting of multiple primary nanoparticles. Originally, LFS was developed for coloring art glass by nanoparticles [33]. In past years, LFS has been used more and more to fabricate functional nanocoatings for various substrates [25, 34–37], but also as a tool for test aerosol production [38] and to create optimal surface structure for superamphiphobic surface treatments [39, 40]. In this study, Titanium (IV)-isopropoxide (TTIP, Alfa Aesar 98%+) was pre-mixed with 2-propanol (VWR, HiPerSolv CHROMANORM, HPLC grade) resulting metallic Ti-concentration of 50.0 mg ml⁻¹ in liquid precursor solution. Two different LFS coating parameters were used for paperboard coating: LFS1 and LFS2. Precursor feed rate was fixed at 32.0 ml min⁻¹ for LFS1 and 11.6 ml min⁻¹ for LFS2, resulting in TiO₂ production rates of 2670 and 968 mg min⁻¹, respectively. Gas flow rates for H₂ and O₂ in all experiments were fixed at 50 l min⁻¹ and 15 l min⁻¹, respectively. Process parameters are summarized in table 1. All of the LFS-generated nanocoatings were applied on commercially available pigment coated paperboard (200 g m⁻²) in a pilot scale roll-to-roll paper converting machine, located at Tampere University of Technology. Both LFS1 [27, 41, 42] and LFS2 [24, 25, 30, 43, 44] parameters have been previously used in several publications in nanocoatings for paper and paperboard.

2.2. Spatial distribution of deposited mass

The deposited line of nanoparticles from single pass of the LFS flame nozzle is limited in width due to the evident finite size of the flame itself. Based on a visual inspection of the deposited line for darker nanoparticle material

Table 1. Five process parameters of LFS1 and LFS2 applied in this study.

	Precursor concentration (Ti mg ml ⁻¹)	Precursor feed rate (ml min ⁻¹)	Burner to substrate distance (mm)	Production rate of TiO ₂ (mg min ⁻¹)	Line speeds (m min ⁻¹)
LFS1	50.0	32.0	150	2670	50, 100, 150
LFS2	50.0	11.6	60	968	50, 100, 200, 300



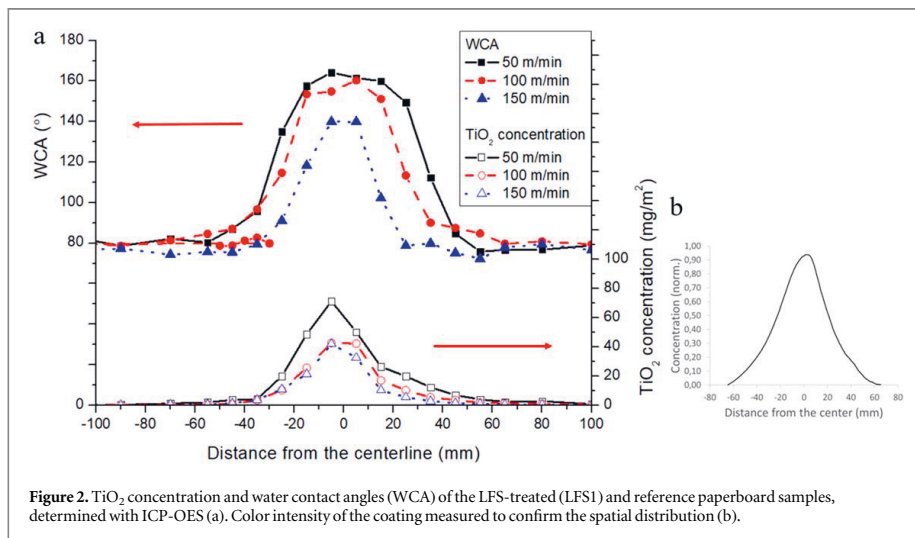
than TiO₂, such as Ag or Fe_xO_y, it is expected that the flame generates a deposited line of nanoparticles with higher concentration in the middle, which decreases towards the edges. A feasible assumption is that this deposited mass distribution follows spatially a normal distribution. The spatial distribution also arises from the fact that the cross section of the flame is round, and also from having slightly hotter parts in the middle. It evidently produces higher temperature gradient between the flame and substrate in the middle, which in turn, furthermore, causes higher deposition velocity of the particles and thus higher concentrations of deposited mass in the center part of the line (figure 2(b)). We approached this phenomenon as follows: we measure certain properties of the coating in the center of the deposited line, and later we continue performing the analyses at different points towards the edges of the pattern. Additionally, a total amount of the integrated cross section of the deposited mass can be analyzed.

2.3. Water contact angle measurement

Water contact angles (WCA) were determined using KSV CAM 200 Optical Contact Angle Meter (KSV Instruments Oy, Helsinki, Finland). The treated samples were stored and the measurements were performed in controlled atmosphere ($50 \pm 2\%$ RH, 23 ± 2 °C). Distilled water (H₂O, surface tension 72.8 mN m^{-1}) was used as the probe liquid. Each WCA value is an average of five individual measurements taken from the centerline of a coating (figure 1). The contact angle value was measured approximately 3 s after the droplet placement to allow the vibrations of the droplet to settle down, but before evaporation and possible penetration of liquid into the substrate did not dramatically affect the droplet volume or the contact angle. The droplet volume used for contact angle measurements was $5 \mu\text{l}$. WCA measurement were carried out in several different time spans: immediately after the coating process and after 1, 2, 7, 30, 90 and 365 days, in order to observe aging effect on the wettability of the nanocoated surface. Also, cross-sectional WCA profile was determined as described in figure 1, with a total width of 110 mm.

2.4. X-Ray photoelectron spectroscopy

The degree of oxidation and chemical composition of the treated samples were determined by XPS using a Physical Electronics Quantum 200 ESCA instrument, equipped with a monochromatic Al K α x-ray source operating at 25 W of power. The pass energy for the survey spectra was 117.4 eV. The charge compensation was



carried out with a combination of a low-energy electron flood gun and a low-energy ion source (Ar). The XPS measurements were performed one day and 90 days after the LFS treatments to analyze chemical changes on the surface. Each XPS measurement value is an average of three individual measurements taken from the centerline of a coating (figure 1). Details of the XPS analysis are described more detailed in previous publications [24, 42].

2.5. Field emission scanning electron microscopy

The surfaces were imaged with ultra-high resolution field emission gun scanning electron microscope (FE-SEM, Zeiss ULTRAplus). Due to the resistive nature of paperboard and TiO₂ nanoparticles, the samples were sputter coated with a thin carbon film prior to FE-SEM imaging for better conductivity. FE-SEM analysis was performed on the centerline of the nanocoating (figure 1).

2.6. Inductively coupled plasma optical emission spectrometry

For the titanium analysis, the paperboard samples with and without TiO₂ nanoparticle coating were first placed into the quartz test tubes for the extraction. Prior to microwave digestion (Milestone, Italy), 2 ml of nitric acid and 2 ml of sulphuric acid were added. The digestion was operated at 240 °C and 40 bar for 45 min. After 15-min cooling, deionized milli-Q water was added until 30 ml total volume was reached. Titanium concentration was determined by using an Inductively Coupled Plasma Optical Emission Spectrometer (ICP-OES; Varian Vista PRO Radial, Australia). For the ICP-OES analysis of LFS2, 30 cm wide cross sectional paperboard strip was analyzed (figure 1) to define total yield of the process. ICP-OES analysis for LFS1 was carried out from the centerline to confirm the spatial distribution of the LFS nanocoating in a roll-to-roll process.

3. Results and discussion

3.1. Titanium analysis

The spatial distribution of the TiO₂ nanocoating was verified by cutting the coated paperboard into 10 mm slices along the coating line and analyzing them by ICP-OES. Results of the ICP-OES is presented in figure 2 along with measured WCA values. The spatial distribution of the TiO₂ nanocoating shows a dependency between the TiO₂ amount and the wetting behavior. Correlation between the TiO₂ mass on the surface and the WCA is illustrated in more detail in figure 3. Results show that as low amount as 20 mg m⁻² of TiO₂ nanoparticles is enough to produce superhydrophobic nanocoating with line speeds of 50 and 100 m min⁻¹. Excess amount of TiO₂ does not depress wettability and the surface is still superhydrophobic even with high TiO₂ concentrations.

With the knowledge of the coating parameters LFS1, the improved coating parameters LFS2 were used to carry out roll-to-roll coating with line speeds of 50, 100, 200 and 300 m min⁻¹. The aim was to get the superhydrophobic nanocoating with less nanoparticles and with relatively good yield. 30 cm wide pieces of the nanocoated paperboard were analyzed by ICP-OES to obtain the yield of the process. Such a wide sample size was chosen to ensure measuring the total mass of deposited nanoparticles. This information is useful in the

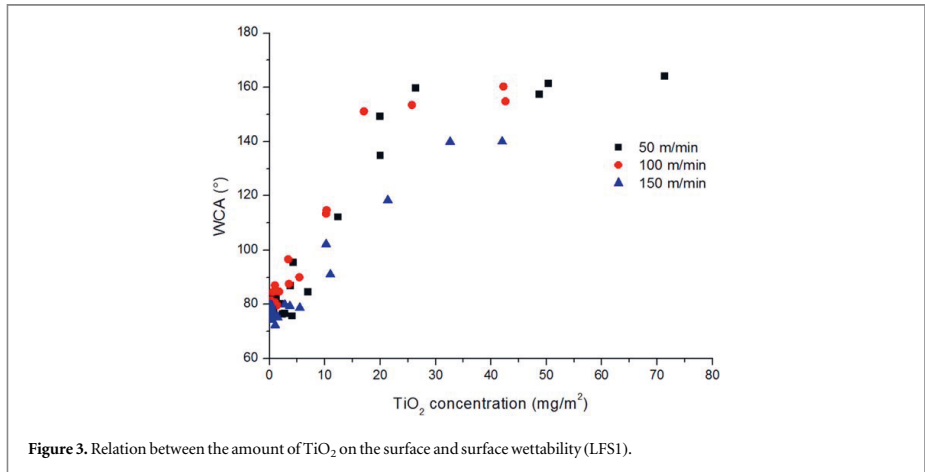


Figure 3. Relation between the amount of TiO_2 on the surface and surface wettability (LFS1).

Table 2. The amount of TiO_2 from the LFS treatment and the yield of the process with different line speeds (LFS2).

Line speed (m/min)	50	100	200	300
Amount of TiO_2 in the coating (mg m^{-2})	23.6	9.2	7.1	4.1
Coated area ($\text{m}^2 \text{min}^{-1}$) from a 30 cm wide sample	15	30	60	90
Yield of the process (%)	36.4	28.4	43.8	38.0

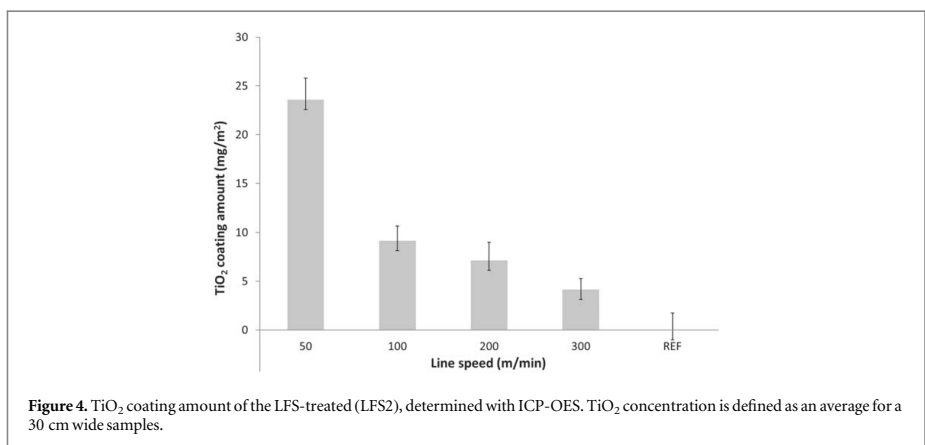


Figure 4. TiO_2 coating amount of the LFS-treated (LFS2), determined with ICP-OES. TiO_2 concentration is defined as an average for a 30 cm wide samples.

future studies when coating is carried out with several burners in a row. Results of the ICP-OES with line speeds of 50, 100, 200 and 300 m min^{-1} are presented in table 2 and in figure 4. The coated area in table 2 means the completely analyzed area: most of the coating is distributed into a smaller area. ICP-OES analysis presents results of the total TiO_2 concentration of the analyzed area, thus the coated area is presented as such a large value. Since the substrate material is pigment coated paperboard, the substrate itself contains TiO_2 as a white pigment. Amount of TiO_2 from the substrate is deducted from the results in table 2. Reference paperboard has TiO_2 concentration of 41.4 mg m^{-2} . After deduction of the reference concentration from the LFS treated samples, deposited TiO_2 amounts are 23.6 mg m^{-2} , 9.2 mg m^{-2} , 7.1 mg m^{-2} and 4.1 mg m^{-2} for line speeds of 50 m min^{-1} , 100 m min^{-1} , 200 m min^{-1} and 300 m min^{-1} , respectively. Total production rate of TiO_2 from the LFS treatment was 968 mg min^{-1} with all line speeds. Yield of the process is relatively good with all tested line speeds.

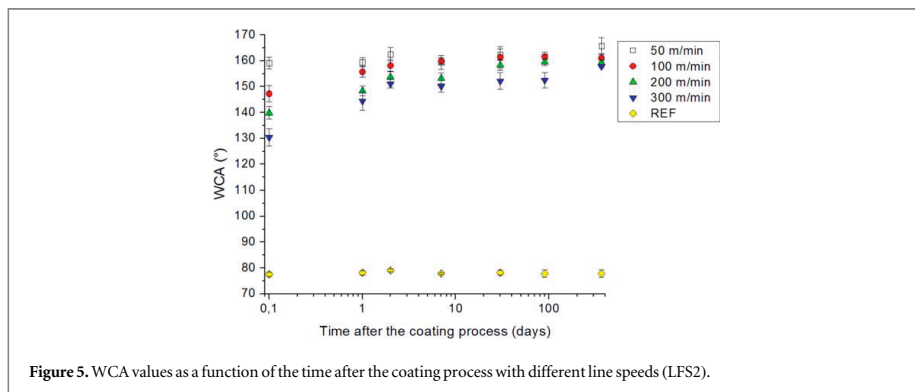


Figure 5. WCA values as a function of the time after the coating process with different line speeds (LFS2).

Highest yield is achieved with line speed of 200 m min^{-1} , as 43.8% of the produced TiO_2 nanoparticles are deposited on the paperboard surface. This is a significant improvement in the yield compared to previously reported 9%–20% yield with LFS1 parameters with different line speeds [27]. Lower distance between the burner and the substrate is the most important yield improving difference between LFS1 and LFS2, mainly due to increased temperature gradient between the flame and the substrate, which improves thermophoretic deposition efficiency.

3.2. Surface wettability

Wettability of the coating was evaluated by measuring a static water contact angle (WCA) several times after the coating process. WCA measurements were performed immediately after the coating process as well as 1, 2, 7, 30, 90 and 365 days after the coating. The observed wetting behavior undergoes changes over time, as the material ages after the coating. This effect is mostly due to accumulation of carbonaceous matter from air and has been previously reported in several studies [24, 45, 46].

With all tested line speeds, level of hydrophobicity increases during time, as presented in figure 5. With a line speed of 50 m min^{-1} , the surface is superhydrophobic ($\text{WCA} > 150^\circ$) immediately after the LFS treatment. With higher line speeds, superhydrophobicity is achieved after one week. WCA values in figure 2 are determined from the center line of the LFS coating. The WCA value of the reference paperboard remains stable at 78° .

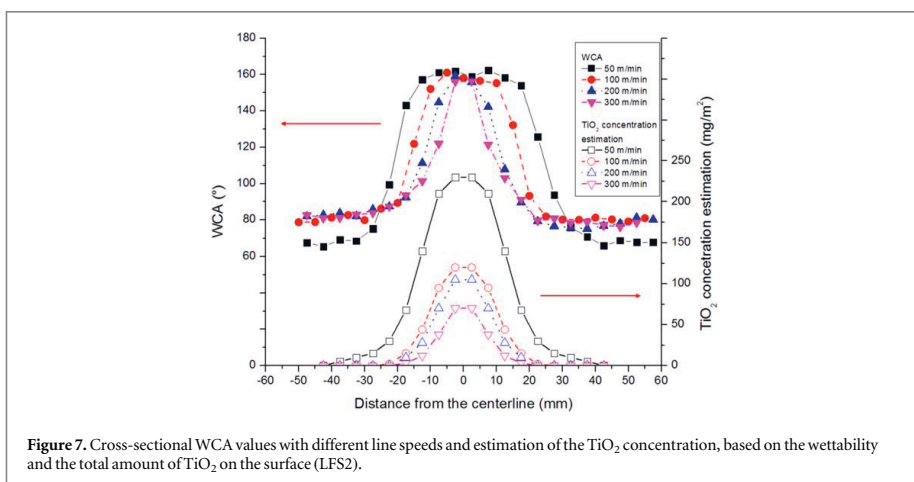
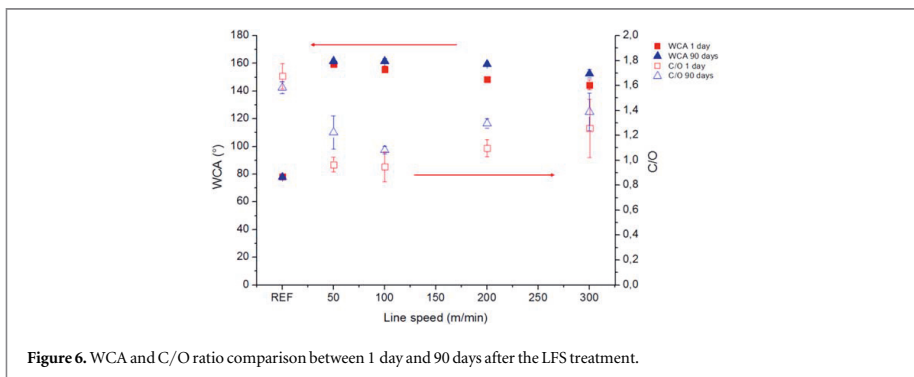
Superhydrophobicity of the TiO_2 -nanocoated paperboard was measured at different time points after the coating process. WCA measurements were carried out immediately after as well as 1, 2, 7, 30, 90 and 180 days after the coating process. The WCA values increase from the initial measurement after the coating and they stabilize in a few days after the coating.

3.3. Chemical changes on the surface with time

The hydrophobicity of the LFS-treated area of the paperboard surface increases with time. Based on the XPS measurements, this is due to chemical changes on the surface. TiO_2 has a tendency to accumulate carbonaceous matter that builds up on top of the nanoparticles as time goes by. These changes in the chemical composition of the LFS-treated surfaces were analyzed by XPS from the centerline of the nanocoating. In the previous studies, carbon to oxygen ratio (C/O) has shown a strong correlation with wettability [24, 42]. In the figure 6, C/O is presented at different line speeds. The LFS-treated surfaces were analyzed after one day and after 90 days of the coating process. Carbon to oxygen ratio increases in 90 days with all the line speeds, indicating accumulation of carbonaceous compounds on the surface. Similar increase in the C/O ratio is not observed in reference paperboard. Additionally, the hydrophobicity also increases as C/O ratio increases with time.

Additionally, the line speed has an effect on the coating width. As is to be expected, coating width gets narrower as the line speed increases. Cross-sectional wetting behavior with different line speeds was analyzed to determine the width of the superhydrophobic area. Cross-sectional WCA values with different line speeds are presented in figure 7. With line speed of 50 m min^{-1} , increased hydrophobicity is achieved in approximately 50 mm and superhydrophobicity in 40 mm cross-sectional area. Width of the superhydrophobic area with line speeds of 100, 200 and 300 m min^{-1} are 20, 15 and 10 mm, respectively. Cross-sectional WCA analysis was performed 365 days after the LFS treatment to maximize the difference between the hydrophobic and non-hydrophobic areas.

Information about spatial distribution and the total mass of the coating were used to estimate distribution of the mass in the coating line with LFS2 parameters. Measured cross-sectional wetting behavior and estimated

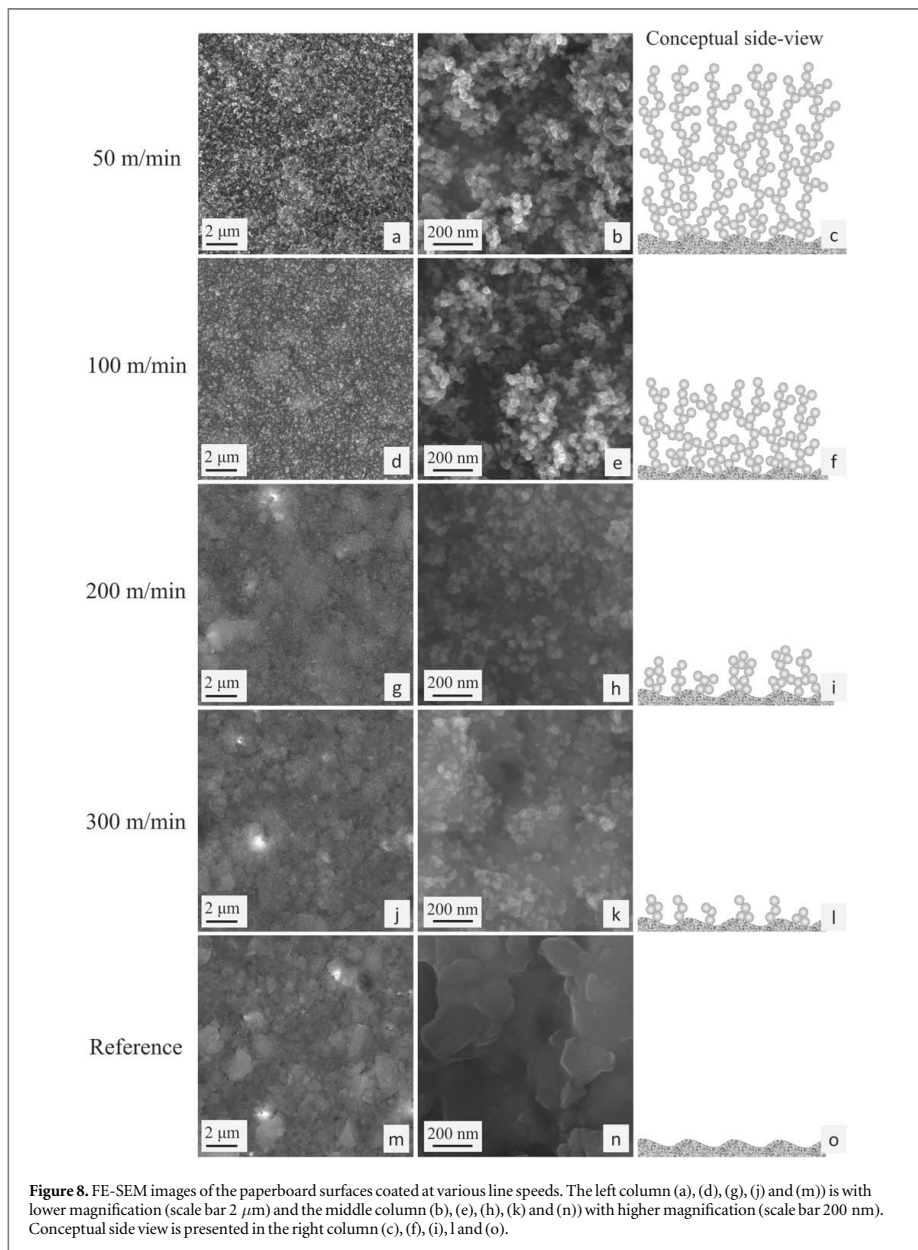


TiO_2 distribution are presented in figure 7. Width of the superhydrophobic line gets narrower as the line speed increases. This is an expected phenomenon, as the coating amount decreases and sufficient amount of TiO_2 is not deposited on the edges of the coating line.

3.4. SEM analysis

FE-SEM graphs with two different magnifications are presented in figure 8. By comparing these graphs with the different line speeds, it is possible to determine the decreasing amount of TiO_2 nanoparticles on top of the paperboard as the line speed increases. With line speeds of 50 and 100 m min^{-1} , the surface is fully covered by TiO_2 nanoparticles, but with a line speed of 200 m min^{-1} , the paperboard surface is partially visible and with 300 m min^{-1} line speed approximately half of the paperboard is visible and the other half is covered by TiO_2 nanoparticles. By comparing these results with the WCA measurements, it is noticeable that the surface is capable of repelling water even if the surface is not fully covered by the TiO_2 nanoparticles and superhydrophobicity was achieved with line speeds of 200 and 300 m min^{-1} . In our previous study [43], cross-sectional SEM image of TiO_2 nanocoated paperboard surface was presented with a coating thickness above 500 nm, which gave a strong indication of full coverage of the paperboard surface with a line speed of 50 m min^{-1} , and explains why full coverage of the surface was also achieved with the line speed of 100 m min^{-1} .

Nanocoatings in figure 8 consist of agglomerates of TiO_2 nanoparticles with primary particle size of approximately 20–30 nm. The production rate of TiO_2 in the LFS process is sufficiently high (968 mg min^{-1}) such that agglomeration cannot be avoided. Some micro-scale roughness is observable on the reference paperboard and with the addition of TiO_2 nanoparticles. The surface has multi-scale roughness, which enables the superhydrophobic behavior. Conceptual side view of the nanocoating in figure 8 is based on the previous publications about porous nanoparticle coatings [43, 47, 48].



3.5. Interpretation of nanoparticle amount

Based on the ICP-OES data, the minimum TiO_2 concentration on the surface to ensure superhydrophobicity is approximately $20\text{--}30\text{ mg m}^{-2}$, which is equivalent to approximately 5–6 nm thick solid layer of TiO_2 on the surface. It is apparent that in our case, the layer consisting of minimum amount of nanoparticles is not hermetically solid, but the substrate is actually peeking through. In principle, the experimentally determined minimum amount, e.g. 20 mg m^{-2} , can be considered to be distributed on the surface in several different ways. For conceptual visualization, and for clarification of what can actually be observed in figure 8(k), three example alternatives for the coverage of 20 mg m^{-2} are presented in figure 9. By comparing figure 8(k) and figure 9, the TiO_2 nanocoating with line speed of 300 m min^{-1} (50 mg m^{-2}) can be interpreted to consist mainly of agglomerates of 3–5 primary nanoparticles. Here, the average distance between agglomerates can be estimated to

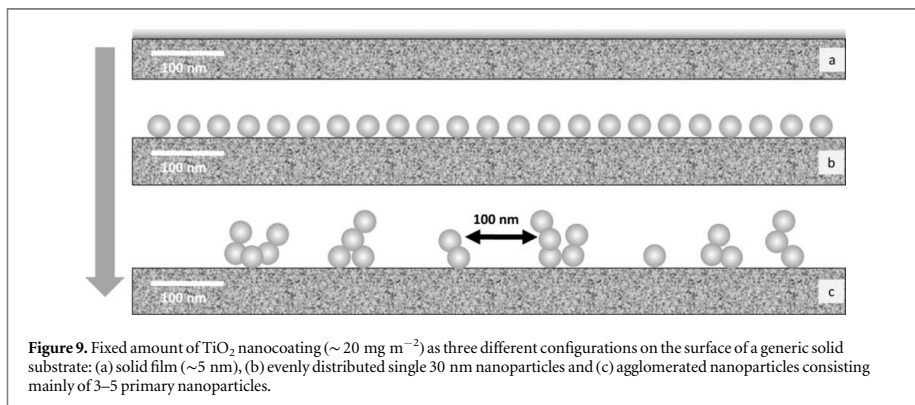


Figure 9. Fixed amount of TiO_2 nanocoating ($\sim 20 \text{ mg m}^{-2}$) as three different configurations on the surface of a generic solid substrate: (a) solid film ($\sim 5 \text{ nm}$), (b) evenly distributed single 30 nm nanoparticles and (c) agglomerated nanoparticles consisting mainly of 3–5 primary nanoparticles.

be approximately 100 nm . This distance between nanoparticles is interpreted to be sufficient to obtain superhydrophobic behavior. To support the estimate, the alternative distribution shown in figure 9(c) is consistent with the info on the amount of TiO_2 . The minimum amount of material to suffice for superhydrophobicity has not been widely discussed in the literature. The recognized references presenting the phenomena of superhydrophobicity and superoleophobicity deal with similar re-entrant structures such as microposts and micro-hoodoo like patterning, but these papers focus merely on micron sized scale [49–51]. Here, we have obviously fabricated structures in the order of $10\text{--}100 \text{ nm}$, but still with similar wetting behaviour. It is generally assumed that superhydrophobicity requires a hierarchical, fractal like structure with both micro and nano structures present [52]. Our result suggests that, at least in the case of our pigment coated paperboard, even a random array with agglomerates of primary nanoparticles, average mutual distances between the agglomerates in the order of 100 nm would be sufficient for superhydrophobicity.

Based on figure 3, the threshold value for superhydrophobic behavior can be estimated to be ca. 20 mg m^{-2} , but since there is relatively large fluctuation in measured data, it may be concluded that 50 mg m^{-2} is definitely enough to ensure superhydrophobic behavior. Surface is superhydrophobic also with relatively thick TiO_2 nanoparticle coating. With line speed of 50 m min^{-1} , paperboard surface is fully covered with TiO_2 nanoparticles with porous layer of several hundreds of nanometers. This information is necessary for future studies as the thickness of the nanocoating layer can have large variation in coating amount and still the surface is superhydrophobic. This enables easier manufacture of a coating system with several parallel LFS burners.

The observed minimum amount of nanocoating required for superhydrophobicity gives a tool to optimize the design of the coating. Furthermore, it opens up new possibilities for manufacturing low-cost superhydrophobic surfaces in large quantities. Superhydrophobic paperboard can be used in several applications, e.g. as a packaging material or as a substrate for low cost microfluidistic devices [28].

4. Conclusions

In this paper, we demonstrated a method for fabricating superhydrophobic surfaces in roll-to-roll process with up to 300 m min^{-1} line speeds. With ever-increasing line speeds, it will become relevant which amount of TiO_2 would be sufficient to ensure hydrophobicity. Here, nanocoating was performed successfully with all tested line speeds and superhydrophobicity was achieved even if the paperboard surface was only partially covered by TiO_2 nanoparticles, which was verified by SEM imaging. A threshold amount of TiO_2 nanoparticles to provide the superhydrophobicity was approximately 20 mg m^{-2} . With this coverage, the surface is only partly covered by the nanoparticles, but the gaps between nanoparticles/agglomerates are small enough ($\sim 100 \text{ nm}$) for superhydrophobic behavior, the structures resembling the surface patterned re-entrant structures presented previously in the literature, but in micron sized scale. To fabricate superhydrophobic surfaces the coating thickness can have great variations since the superhydrophobicity was observed with all coating amounts exceeding 20 mg m^{-2} . Superhydrophobicity of the nanocoated surfaces remained and the level of hydrophobicity even increased during the course of 365-day investigation. XPS analysis showed that C/O ratio increased in all samples during the course of 90-day investigation, which indicates accumulation of organic compounds on the surface. This observation is in line with previous studies and explains the increased hydrophobicity in all analyzed samples. Reference paperboard has some micro scale roughness and with


addition of TiO₂ nanoparticles, the surface has multi-scale roughness, which enables the superhydrophobic behavior.

While searching for the minimum coating amount of deposited TiO₂ required for superhydrophobicity, the process yield was estimated by the characterization of the total deposited TiO₂ mass. ICP-OES analysis verified the total yield of the LFS nanocoating process (deposited TiO₂/produced TiO₂) can be with the current setup as high as 43.8%, depending on the line speed. Total yield and amount of TiO₂ nanoparticles on the LFS treated surface increases significantly from previous studies with optimization of the process parameters, e.g. by tuning the precursor flow rate and decreasing the distance between burner and the substrate (LFS1 versus LFS2). Minimized amount of nanocoating is economically and environmentally beneficial in most application areas of superhydrophobic surfaces, such as self-cleaning, anti-icing, anti-fogging and anti-biofouling surfaces. Also macro- and microfluidic devices as well as oil separation from water and packaging applications would benefit from low-cost manufacturing of superhydrophobic surfaces.

Acknowledgments

This work was supported by the Finnish Funding Agency for Innovation (Tekes) under the project 'Liquid flame spray nanocoating for flexible roll-to-roll materials' (Nanorata 2). J Haapanen wishes to thank also Jenny and Antti Wihuri foundation for the financial support. P Juuti would like to acknowledge TUT graduate school for financial support. Dr Mari Honkanen (TUT, Laboratory of Materials Science) is acknowledged for the SEM imaging and MSc Pauliina Saloranta (ÅA, Laboratory of Paper Coating and Converting) for the XPS analysis.

ORCID iDs

Janne Haapanen  <https://orcid.org/0000-0003-0654-0609>

References

- [1] Jin M, Feng X, Xi J, Zhai J, Cho K, Feng L and Jiang L 2005 Super-hydrophobic PDMS surface with ultra-low adhesive force *Macromol. Rapid Commun.* **26** 1805–9
- [2] Notsu H, Kubo W, Shitanda I and Tatsuma T 2005 Super-hydrophobic /super-hydrophilic patterning of gold surfaces by photocatalytic lithography *J. Mater. Chem.* **15** 1523–7
- [3] Wu X, Zheng L and Wu D 2005 Fabrication of superhydrophobic surfaces from microstructured ZnO-based surfaces via a wet-chemical route *Langmuir* **21** 2665–7
- [4] Karapanagiotis I, Grosu D, Aslanidou D and Aifantis K E 2015 Facile method to prepare superhydrophobic and water repellent cellulosic paper *Journal of Nanomaterials* **2015**
- [5] Shi F, Wang Z and Zhang X 2005 Combining a layer-by-layer assembling technique with electrochemical deposition of gold aggregates to mimic the legs of water striders *Adv. Mater.* **17** 1005–9
- [6] Zhao N, Shi F, Wang Z and Zhang X 2005 Combining layer-by-layer assembly with electrodeposition of silver aggregates for fabricating superhydrophobic surfaces *Langmuir* **21** 4713–6
- [7] Acatay K, Simsek E, Ow-Yang C and Menciloglu Y Z 2004 Tunable, superhydrophobically stable polymeric surfaces by electrospinning *Angew. Chem. Int. Ed.* **43** 5210–3
- [8] Liu H, Feng L, Zhai J, Jiang L and Zhu D 2004 Reversible wettability of a chemical vapor deposition prepared ZnO film between superhydrophobicity and superhydrophilicity *Langmuir* **20** 5659–61
- [9] Karapanagiotis I, Pavlou A, Manoudis P N and Aifantis K E 2014 Water repellent ORMOSIL films for the protection of stone and other materials *Mater. Lett.* **131** 276–9
- [10] Choi H W, Zhou T, Singh M and Jabbour G E 2015 Recent developments and directions in printed nanomaterials *Nanoscale* **7** 3338–55
- [11] Dam H F, Andersen T R, Madsen M V, Mortensen T K, Pedersen M F, Nielsen U and Krebs F C 2015 Roll and roll-to-roll process scaling through development of a compact flexo unit for printing of back electrodes *Solar Energy Mater. Solar Cells* **140** 187–92
- [12] Hwang K, Jung Y, Heo Y, Scholes F H, Watkins S E, Subbiah J, Jones D J, Kim D and Vak D 2015 Toward large scale roll-to-roll production of fully printed perovskite solar cells *Adv. Mater.* **27** 1241–7
- [13] Luo C, Wang J, Fan X, Zhu Y, Han F, Suo L and Wang C 2015 Roll-to-roll fabrication of organic nanorod electrodes for sodium ion batteries *Nano Energy* **13** 537–45
- [14] Polsen E S, McNerny D Q, Viswanath B, Pattinson S W and John Hart A 2015 High-speed roll-to-roll manufacturing of graphene using a concentric tube CVD reactor *Sci. Rep.* **5**
- [15] Kammiller H K, Mädler L and Pratsinis S E 2001 Flame synthesis of nanoparticles *Chem. Eng. Technol.* **24** 583–96
- [16] Stark W J and Pratsinis S E 2002 Aerosol flame reactors for manufacture of nanoparticles *Powder Technol.* **126** 103–8
- [17] Mueller R, Mädler L and Pratsinis S E 2003 Nanoparticle synthesis at high production rates by flame spray pyrolysis *Chem. Eng. Sci.* **58** 1969–76
- [18] Loher S, Schneider O D, Maienfisch T, Bokorny S and Stark W J 2008 Micro-organism-triggered release of silver nanoparticles from biodegradable oxide carriers allows preparation of self-sterilizing polymer surfaces *Small* **4** 824–32
- [19] Blattmann C O, Sotiriou G A and Pratsinis S E 2015 Rapid synthesis of flexible conductive polymer nanocomposite films *Nanotechnology* **26** 12
- [20] Rudin T, Tsougeni K, Gogolides E and Pratsinis S E 2012 Flame aerosol deposition of TiO₂ nanoparticle films on polymers and polymeric microfluidic devices for on-chip phosphopeptide enrichment *Microelectron. Eng.* **97** 341–4
- [21] Mädler L 2004 Liquid-fed aerosol reactors for one-step synthesis of nano-structured particles *KONA Powder Part. J.* **22** 107–20

- [22] Teoh W Y, Amal R and Mädler L 2010 Flame spray pyrolysis: An enabling technology for nanoparticles design and fabrication *Nanoscale* **2** 1324–47
- [23] Mäkelä J M, Haapanen J, Harra J, Juuti P and Kujanpää S 2017 Liquid flame spray—a hydrogen-oxygen flame based method for nanoparticle synthesis and functional nanocoatings *KONA Powder Part. J.* **2017** 141–54
- [24] Teisala H, Tuominen M, Stepien M, Haapanen J, Mäkelä J M, Saarinen J J, Toivakka M and Kuusipalo J 2013 Wettability conversion on the liquid flame spray generated superhydrophobic TiO₂ nanoparticle coating on paper and board by photocatalytic decomposition of spontaneously accumulated carbonaceous overlayer *Cellulose* **20** 391–408
- [25] Teisala H, Tuominen M, Haapanen J, Aromaa M, Stepien M, Mäkelä J M, Saarinen J J, Toivakka M and Kuusipalo J 2014 Review on liquid flame spray in paper converting: multifunctional superhydrophobic nanoparticle coatings *Nord Pulp Pap Res J* **29** 747–59
- [26] Stepien M, Saarinen J J, Teisala H, Tuominen M, Aromaa M, Kuusipalo J, Mäkelä J M and Toivakka M 2011 Adjustable wettability of paperboard by liquid flame spray nanoparticle deposition *Appl. Surf. Sci.* **257** 1911–7
- [27] Mäkelä J M, Aromaa M, Teisala H, Tuominen M, Stepien M, Saarinen J J, Toivakka M and Kuusipalo J 2011 Nanoparticle deposition from liquid flame spray onto moving roll-to-roll paperboard material *Aerosol Sci. Technol.* **45** 817–27
- [28] Songok J, Tuominen M, Teisala H, Haapanen J, Mäkelä J, Kuusipalo J and Toivakka M 2014 paper-based micro fluidics: fabrication technique and dynamics of capillary-driven surface flow *ACS Appl. Mater. Interfaces* **6** 20060–6
- [29] Brobbey K J, Haapanen J, Gunell M, Mäkelä J M, Eerola E, Toivakka M and Saarinen J J 2017 One-step flame synthesis of silver nanoparticles for roll-to-roll production of antibacterial paper *Appl. Surf. Sci.* **420** 558–65
- [30] Haapanen J, Aromaa M, Teisala H, Tuominen M, Stepien M, Saarinen J J, Heikkilä M, Toivakka M, Kuusipalo J and Mäkelä J M 2015 Binary TiO₂/SiO₂ nanoparticle coating for controlling the wetting properties of paperboard *Mater. Chem. Phys.* **149** 230–7
- [31] Tuominen M, Teisala H, Aromaa M, Stepien M, Mäkelä J M, Saarinen J J, Toivakka M and Kuusipalo J 2014 Creation of superhydrophilic surfaces of paper and board *J. Adhes. Sci. Technol.* **28** 864–79
- [32] Tikkanen J, Gross K A, Berndt C C, Pitkänen V, Keskinen J, Raghu S, Rajala M and Karthikeyan J 1997 Characteristics of the liquid flame spray process *Surf. Coat. Technol.* **90** 210–6
- [33] Gross K A, Tikkanen J, Keskinen J, Pitkänen V, Eerola M, Siikamäki R and Rajala M 1999 Liquid flame spraying for glass coloring *J. Therm. Spray Technol.* **8** 583–9
- [34] Ejenstam L, Tuominen M, Haapanen J, Mäkelä J M, Pan J, Swerin A and Claesson P M 2015 Long-term corrosion protection by a thin nano-composite coating *Appl. Surf. Sci.* **357** 2333–42
- [35] Moghaddam M S, Heydari G, Tuominen M, Fielden M, Haapanen J, Mäkelä J M, Wälinder M E P, Claesson P M and Swerin A 2016 Hydrophobisation of wood surfaces by combining liquid flame spray (LFS) and plasma treatment: dynamic wetting properties *Holzforschung* **70** 527–37
- [36] Saarinen J J, Valtakari D, Haapanen J, Salminen T, Mäkelä J M and Uozumi J 2014 Surface-enhanced raman scattering active substrates by liquid flame spray deposited and inkjet printed silver nanoparticles *Opt. Rev.* **21** 339–44
- [37] Juuti P et al 2017 Achieving a slippery, liquid-infused porous surface with anti-icing properties by direct deposition of flame synthesized aerosol nanoparticles on a thermally fragile substrate *Appl. Phys. Lett.* **110** 16
- [38] Mäkelä J M, Aromaa M, Rostedt A, Krinke T J, Janka K, Marjamäki M and Keskinen J 2009 Liquid flame spray for generating metal and metal oxide nanoparticle test aerosol *Hum. Exp. Toxicol.* **28** 421–31
- [39] Tuominen M, Teisala H, Haapanen J, Mäkelä J M, Honkanen M, Vippola M, Bardage S, Wälinder M E P and Swerin A 2016 Superamphiphobic overhang structured coating on a biobased material *Appl. Surf. Sci.* **389** 135–43
- [40] Teisala H, Geyer F, Haapanen J, Juuti P, Mäkelä J M, Vollmer D and Butt H 2018 Ultrafast processing of hierarchical nanotexture for a transparent superamphiphobic coating with extremely low roll-off angle and high impalement pressure *Adv. Mater.* **30** 1706529
- [41] Stepien M, Saarinen J J, Teisala H, Tuominen M, Aromaa M, Haapanen J, Kuusipalo J, Mäkelä J M and Toivakka M 2013 ToF-SIMS analysis of UV-switchable TiO₂-nanoparticle-coated paper surface *Langmuir* **29** 3780–90
- [42] Stepien M, Saarinen J J, Teisala H, Tuominen M, Aromaa M, Kuusipalo J, Mäkelä J M and Toivakka M 2012 Surface chemical analysis of photocatalytic wettability conversion of TiO₂ nanoparticle coating *Surf. Coat. Technol.* **208** 73–9
- [43] Stepien M, Saarinen J J, Teisala H, Tuominen M, Haapanen J, Mäkelä J M, Kuusipalo J and Toivakka M 2013 Compressibility of porous TiO₂ nanoparticle coating on paperboard *Nanoscale Res. Lett.* **8** 1–6
- [44] Stepien M, Chinga-Carrasco G, Saarinen J J, Teisala H, Tuominen M, Aromaa M, Haapanen J, Kuusipalo J, Mäkelä J M and Toivakka M 2013 Wear resistance of nanoparticle coatings on paperboard *Wear* **307** 112–8
- [45] Kanta A, Sedeo R and Ralston J 2005 Thermally- and photoinduced changes in the water wettability of low-surface-area silica and titania *Langmuir* **21** 2400–7
- [46] Takeda S, Fukawa M, Hayashi Y and Matsumoto K 1999 Surface OH group governing adsorption properties of metal oxide films *Thin Solid Films* **339** 220–4
- [47] Castillo J L, Martín S, Rodríguez-Perez D, Perea A and García-Ybarra P L 2014 Morphology and nanostructure of granular materials built from nanoparticles *KONA Powder Part. J.* **31** 214–33
- [48] Mädler L, Lall A A and Friedlander S K 2006 One-step aerosol synthesis of nanoparticle agglomerate films: simulation of film porosity and thickness *Nanotechnology* **17** 4783–95
- [49] Tuteja A, Choi W, Ma M, Mabry J M, Mazzella S A, Rutledge G C, McKinley G H and Cohen R E 2007 Designing superoleophobic surfaces *Science* **318** 1618–22
- [50] Liu T and Kim C 2014 Turning a surface superrepellent even to completely wetting liquids *Science* **346** 1096–100
- [51] Choi H, Choo S, Shin J, Kim K and Lee H 2013 Fabrication of superhydrophobic and oleophobic surfaces with overhang structure by reverse nanoimprint lithography *J. Phys. Chem. C* **117** 24354–9
- [52] Teisala H, Tuominen M and Kuusipalo J 2014 Superhydrophobic coatings on cellulose-Based materials: fabrication, properties, and applications *Adv. Mater. Interfaces* **1** 1300026

PAPER

II

Binary TiO₂/SiO₂ nanoparticle coating for controlling the wetting properties of paperboard

Janne Haapanen, Mikko Aromaa, Hannu Teisala, Mikko Tuominen, Milena Stepien, Jarkko J. Saarinen, Mikko Heikkilä, Martti Toivakka, Jurkka Kuusipalo, Jyrki M. Mäkelä

Materials Chemistry and Physics 149-150 (2015), pp. 230-237

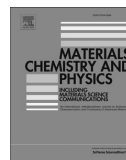
DOI: 10.1016/j.matchemphys.2014.10.011

Publication reprinted with the permission of the copyright holders.



Contents lists available at ScienceDirect

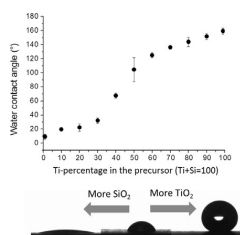
Materials Chemistry and Physics

journal homepage: www.elsevier.com/locate/matchemphysBinary TiO₂/SiO₂ nanoparticle coating for controlling the wetting properties of paperboardJ. Haapanen^{a,*}, M. Aromaa^a, H. Teisala^b, M. Tuominen^{b,c}, M. Stepien^d, J.J. Saarinen^d, M. Heikkilä^e, M. Toivakka^d, J. Kuusipalo^b, J.M. Mäkelä^a^a Aerosol Physics Laboratory, Department of Physics, Tampere University of Technology, P.O. Box 692, FI-33101 Tampere, Finland^b Paper Converting and Packaging Technology, Department of Materials Science, Tampere University of Technology, P.O. Box 589, FI-33101 Tampere, Finland^c SP, Swedish Technical Research Institute, Chemistry, Materials and Surfaces, P.O. Box 5607, SE-11486 Stockholm, Sweden^d Laboratory for Paper Coating and Converting, Abo Akademi University, Porthansgatan 3, FI-20500 Turku, Finland^e Laboratory of Inorganic Chemistry, Department of Chemistry, University of Helsinki, P.O. Box 55, FI-00014 Helsinki, Finland

HIGHLIGHTS

- Liquid Flame Spray (LFS) process was used for TiO₂/SiO₂ coatings on paperboard.
- LFS-made nanoparticles were deposited on paperboard in roll-to-roll process.
- Wetting of the surface was controlled by varying Ti/Si ratio in the precursor.
- Non-linear wetting curve with different TiO₂/SiO₂ ratios were achieved.
- Formed nanoparticles were mixture of TiO₂ and SiO₂ in fast LFS coating process.

GRAPHICAL ABSTRACT



ARTICLE INFO

Article history:

Received 18 September 2013

Received in revised form

4 September 2014

Accepted 9 October 2014

Available online 19 October 2014

Keywords:

Coatings
Composite materials
Nanostructures
Surfaces
Thin films

ABSTRACT

We introduce a flame based aerosol method to fabricate thin films consisting of binary TiO₂/SiO₂ nanoparticles deposited directly from the flame onto the paperboard. Nanocoatings were prepared with Liquid Flame Spray (LFS) in a roll-to-roll process with the line speed of 50 m/min. Surface wetting behavior of nanocoated paperboard was studied for different Ti/Si ratios in the precursor, affecting TiO₂/SiO₂ ratio in the coating. Wettability could be adjusted to practically any water contact angle between 10 and 160° by setting the Ti/Si ratio in the liquid precursor. Structure of the two component nanocoating was analysed with FE-SEM, TEM, EDS, XPS and XRD. The porous thin film coating was concluded to consist of ca. 10 nm sized mixed oxide nanoparticles with segregated TiO₂ and SiO₂ phases. Accumulation of carbonaceous compounds on the surface was seen to be almost linearly dependent on the Ti/Si ratio, indicating of each species being exposed in corresponding amount. However, wetting of the surface was observed to follow merely an S-shaped curve, caused by the roughness of the nanocoated surface. Reasons for the observed superhydrophobicity and superhydrophilicity of these binary nanocoatings on paperboard are discussed.

© 2014 Elsevier B.V. All rights reserved.

* Corresponding author.

E-mail address: janne.haapanen@tut.fi (J. Haapanen).

1. Introduction

Nanoparticles can be synthesized with several different methods, by solid, liquid and gaseous routes [1]. Gaseous aerosol methods are simple and widely used for high purity nanoparticles with high production rates [2,3]. With correctly chosen methods and materials, multicomponent and composite nanoparticles can be synthesized in a single step [4]. Liquid Flame Spray (LFS) is an atmospheric gas phase synthesis method for various nanoparticles, used previously in many applications e.g. glass colouring and synthesis of functional thin films by depositing nanoparticles directly from the flame onto surface [5–7].

From industrial point of view, different wetting properties are needed by different applications. While high hydrophobicity is beneficial for self-cleaning applications [8], highly hydrophilic surfaces can be used to maximize the liquid–solid contact area leading to enhanced mechanical and chemical bonding at the liquid–solid interfaces, e.g. in lamination and coating processes [9]. In some cases a superhydrophilic surface is not the optimal situation but rather controlled wettability is desired. e.g., in many paper and paperboard applications adjustable wetting properties are useful. When using water-based inks, improved print quality and lower ink demand can be achieved by controlling the wettability [10]. In functional printing, maintaining the ink on paper surface by controlling the wettability and ink penetration improves functionality of fabricated devices [11].

In general, different wetting properties result from a combination of chemistry and topography of the surface [12–16]. One of the most well-known hydrophobic self-cleaning surfaces can be found in nature on the leaves of Lotus plant having optimal micro and nanostructure [12,17,18]. Paperboard surface has a microroughness by default, and nanoroughness may be achieved e.g. with LFS generated nanoparticles. In our previous studies, we have introduced a novel surface modification technique for paper and paperboard substrates using Liquid Flame Spray [5,19], obtaining different extreme wetting properties for TiO₂ coated and SiO₂ coated paperboard [20–24]. With LFS-generated TiO₂ nanocoating, paperboard surface is superhydrophobic [20–22], and superhydrophilic with LFS generated SiO₂ nanocoating [22,25]. LFS generated nanocoating has a certain surface roughness with tendency to improve both hydrophilic and hydrophobic properties, depending on the nanoparticles used on the nanocoating.

With pure LFS generated SiO₂ coating, paperboard surface is superhydrophilic. In principle, the water contact angle (WCA) could be increased to a desired level with addition of TiO₂ as a dopant to the nanocoating. In LFS method, this TiO₂ doping can be carried out in a one phase process. LFS-generated TiO₂ nanocoating has been observed to have a tendency to accumulate carbonaceous matter on top of the nanoparticles, whereas LFS-generated SiO₂ has not [22,26]. Therefore, it is assumed that when combining the two species in a single coating, it will both create interesting novel properties, such as potentially highly controllable wetting properties, and give new information about the surface.

As a default, it is assumed that in a flame process, where the precursors evaporate and react, the final products TiO₂ and SiO₂ nucleate and tend to be segregated within each binary nanoparticle generated [27,28]. Different studies for fabricating mixed TiO₂ and SiO₂ oxide nanopowders from gas phase have revealed that in fact a large variety of arrangements between the species, ranging from complete solubility to totally segregated species, and even to core–shell structures, can be obtained by setting appropriate synthesis conditions [27,29–32]. Mixture of TiO₂ and SiO₂ has also been already applied for nanocoating [31–33], but to our knowledge the wetting properties of the coating for different atomic ratios have never been studied so far. Neither has the binary coating been

previously applied for flexible roll-to-roll materials such as paperboard.

In this study, we will scan through different atomic ratios of Ti and Si and determine the wetting properties of the fabricated coatings along with their ability to accumulate carbonaceous compounds. It is important to note that although LFS-made superhydrophobic single component TiO₂ coating can be transformed into superhydrophilic by UV-treatment [21,23,26,34], the same treatment for the mixed oxide coating would be very interesting, but we will omit UV-treatments here and study only the surfaces as prepared.

Target of this study was to create paperboard surfaces with a wide range of different WCA values by changing the atomic ratio of titanium and silicon in the LFS precursor. Furthermore, the benefits and limitations of this method will be discussed.

2. Materials and methods

2.1. Materials

The substrate used in this study is commercially available pigment-coated paperboard (200 g/m²). All nanoparticle coatings were performed in roll-to-roll process in the pilot line of the Laboratory of Paper Converting and Packaging Technology at Tampere University of Technology.

The precursor for the SiO₂ was tetraethyl orthosilicate (TEOS, 98% pure, Alfa Aesar) and the precursor for the TiO₂ was Titanium(IV) isopropoxide (TTIP, 97% pure, Alfa Aesar). Solvent used in all solutions was isopropanol (IpA, technical grade, Neste).

2.2. Methods

Liquid Flame Spray (LFS) is a versatile method for nanoparticle production [5,19,35,36]. With LFS, different metal and metal oxides can be produced with high production rate, ranging from micrograms to several grams of nanoparticles per minute. With high production rates, LFS is a suitable method for industrial scale roll-to-roll process. Nanoparticle size range can be tuned between 2 and 100 nm. In Liquid Flame Spray, liquid precursor solution is fed into the turbulent hydrogen–oxygen flame through an annular tube. Hydrogen gas flow with high velocity disperses the fed liquid precursor solution to micrometer scale droplets. Droplets evaporate in the hot flame; hottest part of the flame is approximately 2500 °C. After the hot part, flame cools down rapidly and evaporated gas becomes supersaturated, producing nanoparticles by homogenous and heterogeneous nucleation. Aerosol processes are described more detailed in Fig. 1. Depending on the process parameters, particle size and production rate can be tuned. Rate of agglomeration of nanoparticles depends on the particle material and process parameters. In this study, production rate of nanoparticles is such high, resulting highly agglomerated nanoparticles. Produced nanoparticles can be deposited directly onto different substrates or collected as nanopowder. Direct deposition onto substrate surface is a result of thermophoresis, diffusion and particle transportation by gas flows [2,37]. With heat sensitive materials, such as paperboard, thermophoresis is the main deposition method since the temperature difference between the flame and the substrate remains high. Distance between the burner and the substrate as well as the line speed can be varied, making it possible to apply the LFS technique also for heat sensitive materials. Direct nanoparticle deposition with LFS has been carried out for paper, paperboard, silicon wafers, plastics, glass, ceramics, metals and painted surfaces. Nanopowders can be collected e.g. with filter systems or with electrostatic precipitator (ESP).

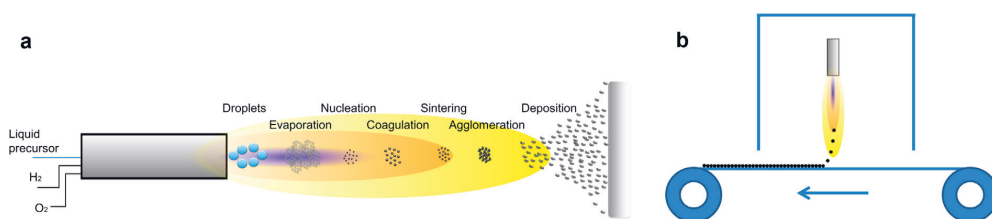


Fig. 1. Schematic picture of the Liquid Flame Spray (LFS) and the LFS coating process. Aerosol processes in the LFS in image a, and the roll-to-roll coating process explained in image b.

2.2.1. Water contact angle (WCA) measurement

Water contact angles (WCA) were determined using KSV CAM 200 Optical Contact Angle Meter (KSV Instruments Oy, Helsinki, Finland). The treated samples were stored and the measurements were performed in controlled atmosphere ($50 \pm 2\%$ RH, 23 ± 2 °C) one day after the coating. The probe liquid used was distilled water (H_2O , surface tension 72.8 mN/m). Each WCA value was an average of five simultaneous measurements taken from the center line of coating. The contact angle value was taken approximately 3 s after droplet placement, because during 3 s the vibration of the droplet had settled down, but evaporation and penetration of liquid into the substrate did not dramatically affect the droplet volume and the contact angle. The droplet volume used for contact angle values was $2 \mu\text{l}$.

2.2.2. X-ray photoelectron spectroscopy (XPS)

The degree of oxidation and chemical composition of the treated samples were determined by XPS using a Physical Electronics Quantum 200 ESCA instrument, equipped with a monochromatic Al $K\alpha$ X-ray source operating at 25 W of power. The pass energy for the survey spectra was 117.4 eV. The charge compensation was carried out with a combination of low-energy electron flood gun and low-energy ion source (Ar). The measurements were performed one day after LFS treatments. Each XPS measurement value was an average of three simultaneous measurements taken from the center line of coating.

2.2.3. Field emission scanning electron microscopy (FE-SEM)

The surfaces were imaged with ultra-high resolution field emission gun scanning electron microscope (FE-SEM), using Zeiss ULTRaplus equipment. Due to the resistive nature of paperboard the samples were sputter coated twice with a thin carbon or gold film prior to FE-SEM imaging for better conductivity. Some samples were charging during the imaging even after multiple gold coatings.

2.2.4. Transmission electron microscopy (TEM)

Transmission electron microscopy (TEM) of the $\text{TiO}_2/\text{SiO}_2$ nanoparticles was performed with Jeol JEM 2010 instrument. Analysed TEM-grids (Lacey grid, Cu-mesh, Agar) were attached onto paperboard in order to get the same interaction with the substrate and nanoparticles. In our previous studies we have shown the effect of the volatile organic compounds from the paperboard surface due to the heat of the LFS process.

2.2.5. X-ray diffraction (XRD)

Crystallinity and phase composition of the films was studied by measuring XRD using PANalytical X'Pert Pro MPD diffractometer in Bragg–Brentano geometry. Constant illuminated length of 10 mm was used and measurements were performed in the angular range of 10 – 100 ° 2θ with a step size of $0.053^\circ/\text{step}$. Measured

diffraction patterns were interpreted using ICDD database and PDF cards 21-1272 for anatase and 21-1276 for rutile forms of TiO_2 .

2.2.6. Energy-dispersive X-ray spectroscopy (EDS, EDX)

Chemical composition and Ti/Si ratio of the single nanoparticles were studied using EDS-analysis with JEOL JEM-2200FS. Same Agar Lacey TEM-grids were analysed as in the TEM analysis. EDS-analysis was carried out for TEM grid samples to reveal nano-scale composition of $\text{TiO}_2/\text{SiO}_2$ -nanoparticles.

3. Experimental

Liquid Flame Spray generated nanocoating was carried out using single nozzle type burner [38]. Combustion gases of LFS were Hydrogen and Oxygen, with gas flow rates of 50 l/min and 15 l/min, respectively. Precursor solution feed rate was fixed at 12 ml/min and distance between the burner and the substrate in 60 mm. Line speed of the substrate was fixed at 50 m/min for the comparison with the previous experiments. Paperboard line speed of 50 m/min is high enough to prevent substrate damaging due to heat, i.e. temperature of the substrate stays below 150 °C. Precursor solutions were different mixtures of TTIP and TEOS, diluted in isopropanol. In all solutions the concentration was fixed in 50 mg of metallic titanium and silicon combined per ml. With the precursor feed rate of 12 ml/min, this equals production rate of 600 mg of Ti + Si per minute. Ratio of Ti and Si was varied between 1 and 99 percent. Total of 11 different ratios of Ti/Si were analysed more detailed in this experiment. Produced nanoparticles are TiO_2 and SiO_2 .

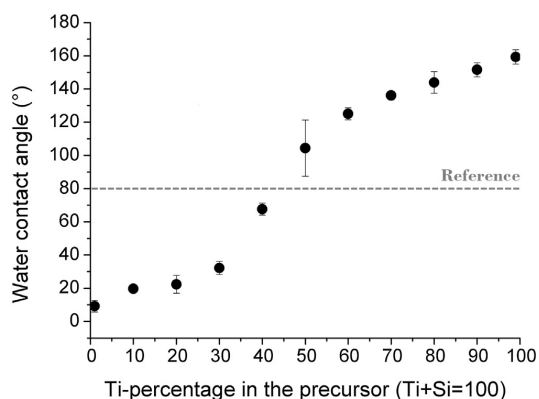


Fig. 2. Dependence of water contact angle (WCA) on Ti-percentage in the precursor. Value 100 in the x-axis indicates 100% of Ti and 0% of Si.

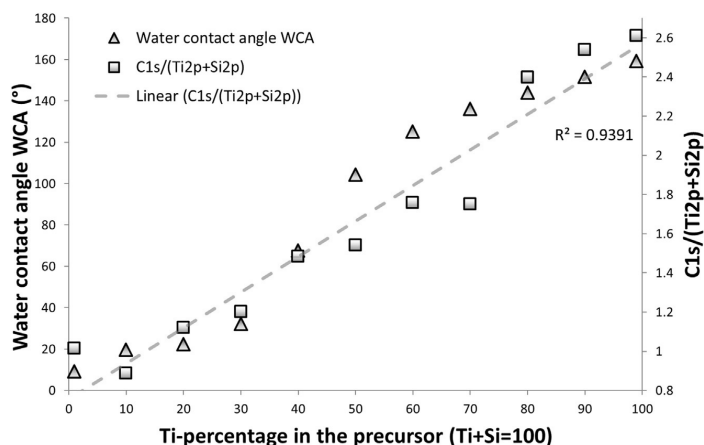


Fig. 3. Water contact angle and C1s/(Ti2p + Si2p) ratio as a function of Ti/Si ratio in the precursor with the linear fitting for C1s/(Ti2p + Si2p).

All nanocoatings were prepared in one phase procedure. All used equipment and vital parts of the pilot scale paper converting machine were cleaned between different coating parameters in order to avoid contaminations from the previous coatings. All the liquid precursor solutions had been prepared at the same day as the coating was carried out.

Nanopowder samples for the XRD measurements were collected using a custom-made plate type ESP. In this ESP, charging plates and collection plates were combined. Charging plate was with negative charge and collection plate was grounded. The distance between these two steel plates was 65 mm and the voltage 20 kV. On the lower end of the charging plate, corona needles are attached on the plate before the collection section.

4. Results and discussion

4.1. Water contact angle

Water contact angle (WCA) measurements show that Ti/Si ratio in the used precursor has a significant effect on the WCA. Coatings with high Ti/Si ratio are superhydrophobic, i.e. WCA exceeds 160°. Coatings with low Ti/Si ratio are superhydrophilic with WCA below 10°. WCA values are shown in Fig. 2. WCA of the uncoated reference paperboard is around 80°.

WCA measurements of coated surfaces with different TiO₂/SiO₂ ratios show a clear difference in the wetting behavior. With a higher Ti/Si ratio in the liquid precursor, the TiO₂/SiO₂ ratio is higher in the coating. With our analysed 11 different Ti/Si ratios from 1/99 to 99/1 in the precursor, WCA consistently increased with Ti/Si ratio without exception in the measured data.

Surface roughness affects wettability of the surface both in hydrophilic and hydrophobic domains. This results in S-shaped wetting curve on rough surfaces, while smooth surfaces possess linear wetting curve. This effect is well known, and was firstly demonstrated by Onda et al. [39]. Also, on the rough LFS nanoparticle coatings the changed surface chemistry results to S-shaped wetting curve. To our knowledge, such wetting behavior with different TiO₂/SiO₂ ratios has not been observed nor published before.

4.2. XPS

Our previous studies have shown a clear correlation with WCA and carbon to oxygen ratio on the surface with LFS generated TiO₂

coating [23]. With high WCA values, there is more carbon and less oxygen on the surface. This is most probably combination of carbonaceous material originating from the flame and from the substrate, and decreased amount of hydroxyl groups on the surface. Pure TiO₂ is hydrophilic, but TiO₂ has a tendency to adsorb carbonaceous material on the surface [40]. SiO₂ coating does not have similar property. In this study, XPS measurement was carried out to confirm the chemical differences of the different nanocoatings. With increased amount of Si in the precursor solution, LFS generated nanoparticle coating becomes more hydrophilic. This can be partly explained by carbon-free SiO₂ coverage on the surface. Correlation with the Ti/Si ratio in the precursor solution and XPS-measured C/(Ti + Si) ratio on the surface can be seen in Fig. 3. Higher ratio of C/(Ti + Si) refers to higher carbon concentration on the surface. From Fig. 3 can be observed somewhat clear correlation between Ti/Si ratio in the precursor and measured C/(Ti + Si) ratio on the nanocoated surface. With higher Ti/Si ratio, also the C/(Ti + Si) ratio is higher.

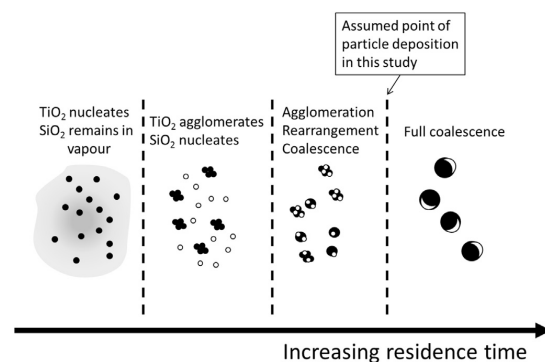


Fig. 4. Proposed species arrangement in the binary TiO₂/SiO₂-aerosol formed in the LFS-flame (black:TiO₂; white:SiO₂). Based on observed linear dependency of the amount of accumulated carbon on the Ti/Si ratio, observed particle morphology in TEM-graphs, consistent dependency of XRD peak of TiO₂ on the Ti/Si ratio and potential species arrangement mechanisms within the particles described in earlier literature [27,32,33]. Particle deposition onto paperboard is assumed to take place before full coalescence.

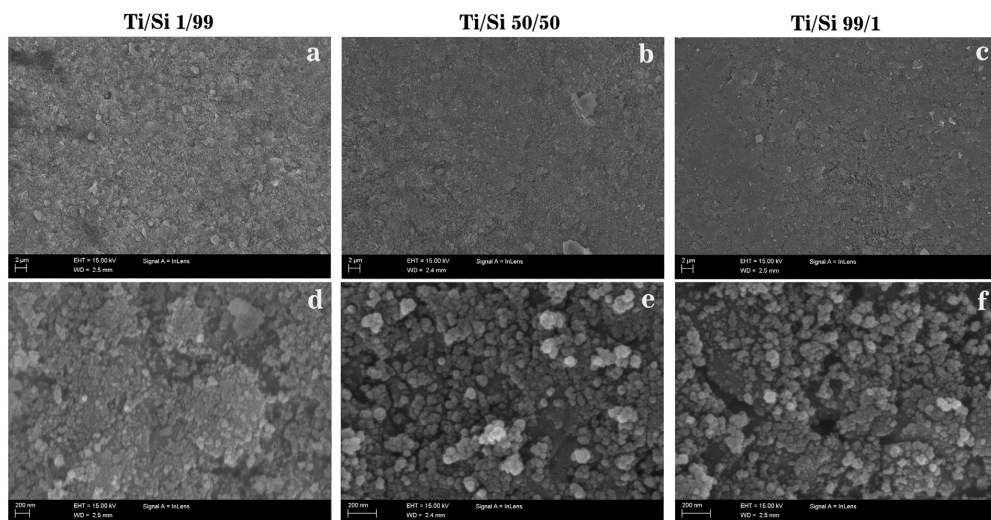


Fig. 5. Scanning electron microscopy (SEM) graphs of paperboard with different Ti/Si ratios in the precursor solution. Images a and d are with Ti/Si ratio of 1/99, images b and e with Ti/Si ratio 50/50 and images c and f with Ti/Si ratio of 99/1.

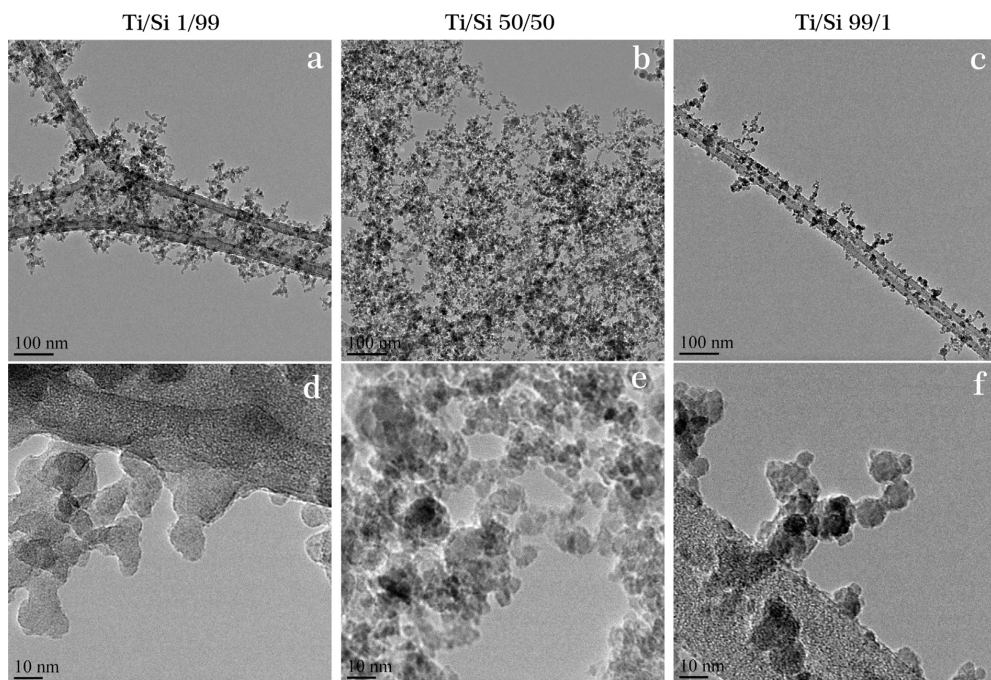


Fig. 6. Transmission electron microscopy (TEM) images with different Ti/Si ratios in the precursor solution. Images a and d are with Ti/Si ratio of 1/99, images b and e with Ti/Si ratio 50/50 and images c and f with Ti/Si ratio of 99/1. With higher Ti-ratios, nanoparticles are more spherical.

XPS measurement was carried out to collect information about the chemical differences of the different nanocoatings. In previous studies it was discovered that the topmost layer of TiO_2 coating has higher carbon content than SiO_2 . Higher WCA value of TiO_2 -coated

board correlates with the lower surface energy in comparison with SiO_2 . However, pure TiO_2 has a higher surface energy than pure SiO_2 , which has an effect on the contamination of the nanocoated surface [40–42]. In our case, carbonaceous material is partly from the

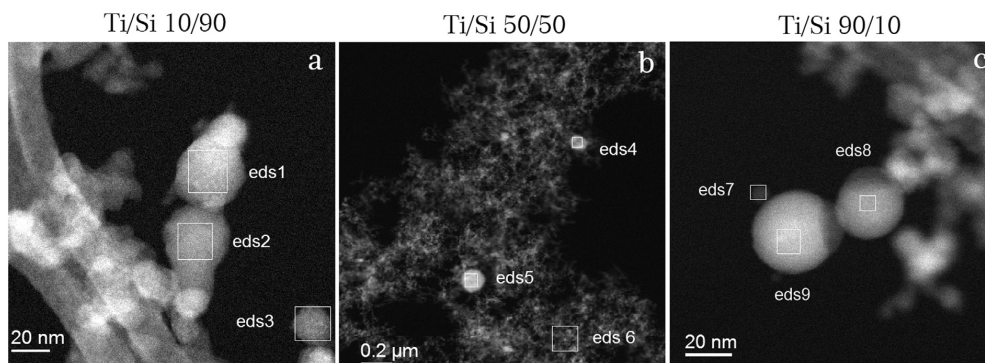


Fig. 7. EDS analysis of TEM grid samples with different Ti/Si ratios. Results of different measurement points are listed in Table 1.

evaporating hydrocarbons from the substrate and partly from the insufficient combustion of the precursor. TiO_2 has a tendency to accumulate carbonaceous material, carbon and hydrocarbons, on top of the TiO_2 nanoparticles. XPS results with different Ti/Si ratios were in line with this hypothesis. With higher Ti/Si ratio in the precursor, C/(Ti + Si) ratio was also higher. Behavior of C/(Ti + Si) was almost linear as a function of Ti/Si ratio, indicating that TiO_2 and SiO_2 nanoparticles cover the surface evenly, and are exposed on top of the coating in the same ratio. With higher Ti/Si ratio, more TiO_2 will be exposed on the surface and more carbonaceous content will be accumulated on top of the nanocoating. It is important to note that the consistent linear dependency of the C/(Ti + Si) ratio on the Ti/Si-ratio in fact practically excludes the possibility of potential core-shell structures with TiO_2 in the core and SiO_2 on the shell. Since TiO_2 has lower vapour pressure than SiO_2 , TiO_2 is assumed to nucleate first in the cooling flame and nucleation of SiO_2 will follow. In the case of ideal core shell structure, a certain fraction of SiO_2 would eventually be sufficient to cover all the TiO_2 , and assumedly also accumulation of carbonaceous species on the surface would be completely blocked. In our case this does not occur. Based on earlier studies, we know that core shell structure is obtained only in a relatively slow process, where the SiO_2 particles will have enough time to rearrange and to cover the surface [29,32]. Our LFS process

with direct deposition of nanoparticles already within the flame is most apparently sufficiently fast to keep the species segregated in separate patches, as has been concluded in Fig. 4.

As a result of the S-curve type of WCA results and almost linear shape of C/(Ti + Si) results, it is clear that to affect the wetting there is also some other factor than the chemical composition only. There have been studies indicating that certain roughness is increasing both hydrophilicity and hydrophobicity [12,14,15]. This explains why WCA values change more rapidly with Ti/Si ratio between 30/70–70/30. On the contrary, it is possible to achieve good level of hydrophobicity even with Ti/Si ratio of 70/30 and good hydrophilicity with Ti/Si ratio of 30/70. Similar S-shaped curve of wetting behavior has been published before to prove the importance of surface roughness [39].

4.3. FE-SEM

Paperboard with different nanoparticle coatings were analysed with SEM. All analysed surfaces were similar if roughness and topography of the surfaces are observed, but severe charging of the SiO_2 -rich samples made it difficult to analyse images with higher magnifications. With higher relative amount of SiO_2 nanocoating, uneven parts of the paperboard are covered more completely even if the coating amount is approximately same. SEM images with different Ti/Si ratios are presented in Fig. 5.

Analysis of SEM images shows similar behavior with all Ti/Si ratios, as a result a good coverage on the paperboard surface is achieved. Nanocoating has a porous structure, similar to our previous studies. SEM samples with lower Ti/Si ratio were charging during the imaging, even with multiple carbon or gold coatings as a sample preparation.

Thickness of the LFS-made nanoparticle coating on paperboard was determined in our previous study [43]. LFS generated nanoparticles form porous layer with thickness of ca. 600 nm.

4.4. TEM

From the TEM samples high level of agglomeration of nanoparticles can be observed. In most LFS applications the production rate of nanoparticles is sufficiently high for agglomeration. Primary nanoparticle size with all precursor solutions was observed to be in the scale of 10 nm, but the agglomerated particle size is much larger. As can be observed in Fig. 6, SiO_2 -rich nanoparticles are more sintered and TiO_2 -rich primary nanoparticles maintain more

Table 1

EDS analysis results of samples with different Ti/Si ratios. Measurement points are displayed in Fig. 7.

Measure point	Precursor Ti/Si mass ratio	Element (keV)	Mass-%	Error-%	Atom-%
EDS 1	10/90	Ti K	4.508 13.40	0.26	8.32
		Si K	1.739 86.60	0.03	91.68
EDS 2	10/90	Ti K	4.508 11.50	0.30	7.08
		Si K	1.739 88.50	0.03	92.92
EDS 3	10/90	Ti K	4.508 13.04	0.32	8.09
		Si K	1.739 86.96	0.04	91.91
EDS 4	50/50	Ti K	4.508 76.88	1.35	66.10
		Si K	1.739 23.12	1.38	33.90
EDS 5	50/50	Ti K	4.508 54.66	1.60	41.42
		Si K	1.739 45.34	1.64	58.58
EDS 6	50/50	Ti K	4.508 60.07	2.01	46.88
		Si K	1.739 39.93	2.06	53.12
EDS 7	90/10	Ti K	4.508 96.07	5.44	93.48
		Si K	1.739 3.93	5.57	6.52
EDS 8	90/10	Ti K	4.508 96.94	1.59	94.88
		Si K	1.739 3.06	1.63	5.12
EDS 9	90/10	Ti K	4.508 97.95	1.45	96.56
		Si K	1.739 2.05	1.49	3.44

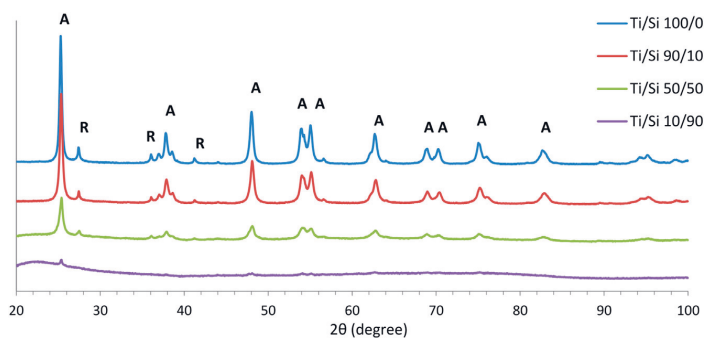


Fig. 8. X-ray diffraction measurement results with different Ti/Si ratios in the precursor. For the clarification, peaks of anatase (A) and rutile (R) are marked in the graph.

spherical form, even when agglomerated. With the ratio 50/50 both forms, sintered and spherical, are present.

Analysis of TEM images gives information from different shapes of LFS-generated TiO₂ and SiO₂ nanoparticles. To collect the nanoparticles as similar as possible as they are on the paperboard surface, Lacey-type TEM grids were attached on paperboard. LFS-made TiO₂ form agglomerates of spherical TiO₂ nanoparticles but LFS-made SiO₂ is more sintered. With higher Ti/Si ratio, more spherical shaped nanoparticles are present in TEM images. According to TEM images, TiO₂ and SiO₂ nanoparticles are separated and cover the surface with same ratio as they are present. There are not clear core–shell structures visible. Even if the XPS revealed remarkable carbon content, there were not any visible carbon shells present in TEM images. Compared to other studies with flame-made TiO₂/SiO₂ composites [44], any nanowire structures were not observed.

4.5. EDS

EDS analysis was performed from TEM samples with three different Ti/Si ratios in the liquid precursor. EDS analysis was carried out to find out if single nanoparticles have similar Ti/Si ratio to precursor. Fig. 7 shows total of nine different points analysed more closely for this study. Results of these nine points are listed in Table 1. All analysed single nanoparticles are consisting both Ti and Si. In Fig. 7b, one TiO₂-rich area (eds 4) was analysed. There were some traces of these TiO₂-rich areas in other samples too, but the fraction was so small it does not affect the wetting behavior.

TEM and EDS analysis confirmed there are similar ratios of Ti and Si in single nanoparticles as in the precursor. None of the used analysis methods gave any indication of the core–shell type structures.

4.6. XRD

XRD measurement was performed to observe differences in TiO₂ crystalline form. As can be observed in Fig. 8, LFS-made TiO₂ nanocoating consisted mainly of anatase, but also some small fraction 10–15% was rutile. Anatase is preferred since it is more photocatalytic than rutile. There was no significant change in the anatase/rutile ratio with different Ti/Si-ratios in the coating. Small fraction of rutile was visible in all measured samples. SiO₂ was amorphous in all measured samples.

XRD analysis was made to confirm high anatase crystallinity form of TiO₂ and amorphous form of SiO₂. In previous studies anatase has been confirmed as preferred crystallinity form of TiO₂ in flame synthesis. Even if the rutile is thermodynamically favored phase for TiO₂, mainly anatase is formed due short residence time

in the flame [45,46]. There have been some studies where presence of SiO₂ prevents TiO₂ anatase from transforming to rutile [31]. In our samples, any significant change in the anatase/rutile was not observed with increasing amount of SiO₂ present. Anatase content of TiO₂ with used parameters was approximately 85%. XRD analysis confirmed also that SiO₂ is amorphous with all Ti/Si ratios.

5. Conclusions

In this paper, we demonstrated a method to fabricate TiO₂/SiO₂ mixed oxide nanocoating consisting of binary nanoparticles. With different ratios of Ti/Si in the precursor, any WCA value between 10° and 160° can be achieved. Surface roughness has an effect on wettability behavior, resulting in an S-shaped graph. This observation is confirmed by C/(Ti + Si) results from XPS measurement. Carbon to oxygen ratio is nearly linear, confirming carbonaceous material accumulating on top of the TiO₂-coating. With higher amount of TiO₂ in the coating, more carbonaceous matter is accumulated on top of the nanocoating. S-shape of WCA-graph is partly a result of roughness of the LFS-generated nanoparticle coating. SEM- and TEM-images indicate even coverage of nanoparticles with similar ratio of TiO₂/SiO₂ as used in the precursor. LFS-made SiO₂ is amorphous and TiO₂ mainly anatase, measured with XRD.

Acknowledgements

This work was supported by the Finnish Funding Agency for Technology and Innovation (Tekes) Grant no. 40094/11 under the project “Liquid flame spray nanocoating for flexible roll-to-roll materials” (Nanorata 2). J. Haapanen wishes to thank also Jenni and Antti Wihuri foundation for the financial support. Dr. Mari Honkanen (TUT, Department of Materials Science) is acknowledged for the SEM and TEM imaging, M.Sc. Pauliina Saloranta (ÅA, Laboratory for Paper Coating and Converting) for the XPS analysis and Dr. Hua Jiang (Aalto University, Department of Applied Physics) for the EDS analysis.

References

- [1] T.T. Kodas, M.J. Hampden-Smith, *Aerosol Processing of Materials*, 1999.
- [2] S.E. Pratsinis, *Prog. Energy Combust. Sci.* 24 (1998) 197–219.
- [3] R. Strobel, S.E. Pratsinis, *J. Mater. Chem.* 17 (2007) 4743–4756.
- [4] E. Jud, L. Gauckler, S. Halim, W. Stark, *J. Am. Ceram. Soc.* 89 (2006) 2970–2973.
- [5] K.A. Gross, J. Tikkanen, J. Keskinen, V. Pitkanen, M. Eerola, R. Siikamaki, M. Rajala, *J. Therm. Spray Technol.* 8 (1999) 583–589.
- [6] H. Keskinen, J.M. Mäkelä, M. Aromaa, J. Keskinen, S. Areva, C.V. Teixeira, J.B. Rosenholm, V. Pore, M. Ritala, M. Leskelä, M. Raulio, M.S. Salkinoja-Salonen, E. Levänen, T. Mäntylä, *Catal. Lett.* 111 (2006) 127–132.

- [7] J.M. Mäkelä, M. Aromaa, H. Teisala, M. Tuominen, M. Stepien, J.J. Saarinen, M. Toivakka, J. Kuusipalo, *Aerosol Sci. Technol.* 45 (2011) 817–827.
- [8] L. Feng, S. Li, Y. Li, H. Li, L. Zhang, J. Zhai, Y. Song, B. Liu, L. Jiang, D. Zhu, *Adv. Mater.* 14 (2002) 1857–1860.
- [9] J. Kuusipalo (Ed.), Book 12, second ed., 2008.
- [10] M. Pykönen, H. Sundqvist, M. Tuominen, J. Lahti, J. Preston, P. Fardim, M. Toivakka, *Nord. Pulp Pap. Res. J.* 23 (2008) 181–188.
- [11] R. Bollström, D. Tobjörk, P. Dolietis, P. Salminen, J. Preston, R. Österbacka, M. Toivakka, *Chem. Eng. Process. Process Intensif.* 68 (2013) 13–20.
- [12] D. Quéré, *Annu. Rev. Mater. Res.* 38 (2008) 71–99.
- [13] A.B.D. Cassie, S. Baxter, *Trans. Faraday Soc.* 40 (1944) 546–551.
- [14] M. Ma, R.M. Hill, *Curr. Opin. Colloid Interface Sci.* 11 (2006) 193–202.
- [15] J. Bico, U. Thiele, D. Quéré, *Colloids Surf. A Physicochem. Eng. Asp.* 206 (2002) 41–46.
- [16] E. Balaur, J.M. MacAk, L. Taveira, P. Schmuki, *Electrochem. Commun.* 7 (2005) 1066–1070.
- [17] W. Barthlott, C. Neinhuis, *Planta* 202 (1997) 1–8.
- [18] K. Koch, B. Bhushan, W. Barthlott, *Prog. Mater. Sci.* 54 (2009) 137–178.
- [19] J.M. Mäkelä, H. Keskinen, T. Forsblom, J. Keskinen, *J. Mater. Sci.* 39 (2004) 2783–2788.
- [20] H. Teisala, M. Tuominen, M. Aromaa, M. Stepien, J.M. Mäkelä, J.J. Saarinen, M. Toivakka, J. Kuusipalo, *Colloid Polym. Sci.* 291 (2013) 447–455.
- [21] H. Teisala, M. Tuominen, M. Stepien, J. Haapanen, J.M. Mäkelä, J.J. Saarinen, M. Toivakka, J. Kuusipalo, *Cellulose* 20 (2013) 391–408.
- [22] M. Aromaa, A. Arffman, H. Suhonen, J. Haapanen, J. Keskinen, M. Honkanen, J.-P. Nikkanen, E. Levänen, M.E. Messing, K. Deppert, H. Teisala, M. Tuominen, J. Kuusipalo, M. Stepien, J.J. Saarinen, M. Toivakka, *J.M. Mäkelä, J. Aerosol Sci.* 52 (2012) 57–68.
- [23] M. Stepien, J.J. Saarinen, H. Teisala, M. Tuominen, M. Aromaa, J. Kuusipalo, J.M. Mäkelä, M. Toivakka, *Surf. Coat. Technol.* 208 (2012) 73–79.
- [24] H. Teisala, M. Tuominen, M. Aromaa, M. Stepien, J.M. Mäkelä, J.J. Saarinen, M. Toivakka, J. Kuusipalo, *Langmuir* 28 (2012) 3138–3145.
- [25] M. Tuominen, H. Teisala, M. Aromaa, M. Stepien, J. Mäkelä, J. Saarinen, M. Toivakka, J. Kuusipalo, *J. Adhes. Sci. Technol.* (2012) 1–16.
- [26] M. Stepien, J.J. Saarinen, H. Teisala, M. Tuominen, M. Aromaa, J. Kuusipalo, J.M. Mäkelä, M. Toivakka, *Appl. Surf. Sci.* 258 (2012) 3119–3125.
- [27] S.H. Ehrman, S.K. Friedlander, M.R. Zachariah, *J. Mater. Res.* 14 (1999) 4551–4561.
- [28] R.C. DeVries, R. Roy, E.F. Osborn, *Trans. Br. Ceram. Soc.* 53 (1954) 525–540.
- [29] C. Hung, J.L. Katz, *J. Mater. Res.* 7 (1992) 1861–1869.
- [30] S. Vemury, S.E. Pratsinis, *J. Am. Ceram. Soc.* 78 (1995) 2984–2992.
- [31] K. Cho, H. Chang, J.H. Park, B.G. Kim, H.D. Jang, *J. Ind. Eng. Chem.* 14 (2008) 860–863.
- [32] F. Qi, A. Moiseev, J. Deubener, A. Weber, *J. Nanoparticle Res.* 13 (2011) 1325–1334.
- [33] W.J. Stark, S.E. Pratsinis, A. Baiker, *J. Catal.* 203 (2001) 516–524.
- [34] M. Stepien, J.J. Saarinen, H. Teisala, M. Tuominen, M. Aromaa, J. Kuusipalo, J.M. Mäkelä, M. Toivakka, *Appl. Surf. Sci.* 257 (2011) 1911–1917.
- [35] J. Tikkanen, K.A. Gross, C.C. Berndt, V. Pitkänen, J. Keskinen, S. Raghu, M. Rajala, J. Karthikeyan, *Surf. Coat. Technol.* 90 (1997) 210–216.
- [36] M. Aromaa, H. Keskinen, J.M. Mäkelä, *Biomol. Eng.* 24 (2007) 543–548.
- [37] A. Gurav, T. Kodas, T. Pluyim, Y. Xiong, *Aerosol. Sci. Technol.* 19 (1993) 411–452.
- [38] H. Keskinen, M. Aromaa, M.C. Heine, J.M. Mäkelä, *At. Sprays* 18 (2008) 619–644.
- [39] T. Onda, S. Shibuichi, N. Satoh, K. Tsujii, *Langmuir* 12 (1996).
- [40] A. Kanta, R. Sedev, J. Ralston, *Langmuir* 21 (2005) 2400–2407.
- [41] G.D. Parfitt, *Pure Appl. Chem.* 48 (1976) 415–418.
- [42] A. Navrotsky, *Geochem. Trans.* 4 (2003) 34–37.
- [43] M. Stepien, G. Chinga-Carrasco, J.J. Saarinen, H. Teisala, M. Tuominen, M. Aromaa, J. Haapanen, J. Kuusipalo, J.M. Mäkelä, M. Toivakka, *Wear* 307 (2013) 112–118.
- [44] A. Tricoli, M. Righettoni, S.E. Pratsinis, *Langmuir* 25 (2009) 12578–12584.
- [45] A. Kobata, K. Kusakabe, S. Morooka, *AIChE J.* 37 (1991) 347–359.
- [46] S.H. Ehrman, S.K. Friedlander, M.R. Zachariah, *J. Aerosol Sci.* 29 (1998) 687–706.

PAPER
III

Superamphiphobic overhang structured coating on a biobased material

Mikko Tuominen, Hannu Teisala, Janne Haapanen, Jyrki M. Mäkelä, Mari Honkanen, Minnamari Vippola, Stig Bardage, Magnus E.P. Wälinder, Agne Swerin

Applied Surface Science, Volume 389 (2016), pp. 135-143
DOI: 10.1016/j.apsusc.2016.05.095

Publication reprinted with the permission of the copyright holders.



Superamphiphobic overhang structured coating on a biobased material

Mikko Tuominen^{a,*}, Hannu Teisala^c, Janne Haapanen^d, Jyrki M. Mäkelä^d,
Mari Honkanen^e, Minnamari Vippola^e, Stig Bardage^f, Magnus E.P. Wålinder^g,
Agne Swerin^{a,b}

^a SP Technical Research Institute of Sweden—Chemistry, Materials and Surfaces, Box 5607, SE-114 86 Stockholm, Sweden

^b KTH Royal Institute of Technology, Department of Chemistry, Surface and Corrosion Science, SE-100 44 Stockholm, Sweden

^c Tampere University of Technology, Paper Converting and Packaging Technology, Department of Materials Science, P.O. Box 589, FI-33101 Tampere, Finland

^d Tampere University of Technology, Aerosol Physics Laboratory, Department of Physics, P.O. Box 692, FI-33101 Tampere, Finland

^e Tampere University of Technology, Material Characterization, Department of Materials Science, P.O. Box 589, FI-33101 Tampere, Finland

^f SP Technical Research Institute of Sweden, Sustainable Built Environment, Biobased Materials and Products, Box 5609, SE-114 86 Stockholm, Sweden

^g KTH Royal Institute of Technology, Department of Civil and Architectural Engineering, Building Materials, SE-100 44 Stockholm, Sweden

ARTICLE INFO

Article history:

Received 15 January 2016

Received in revised form 15 May 2016

Accepted 18 May 2016

Available online 7 July 2016

Keywords:

Biobased material

Wood

Coating

Plasma

Deposition

Titania

Nanoparticle

Perfluorohexane

Wetting

Superamphiphobic

Superhydrophobic

Superoleophobic

Water repellency

Oil repellency

Self-cleaning

ABSTRACT

A superamphiphobic coating on a biobased material shows extreme liquid repellency with static contact angles (CA) greater than 150° and roll-off angles less than 10° against water, ethylene glycol, diiodomethane and olive oil, and a CA for hexadecane greater than 130°. The coating consisting of titania nanoparticles deposited by liquid flame spray (LFS) and hydrophobized using plasma-polymerized perfluorohexane was applied to a birch hardwood. Scanning electron microscopy (SEM) imaging after sample preparation by UV laser ablation of coated areas revealed that capped structures were formed and this, together with the geometrically homogeneous wood structure, fulfilled the criteria for overhang structures to occur. The coating showed high hydrophobic durability by still being non-wetted after 500 000 water drop impacts, and this is discussed in relation to geometrical factors and wetting forces. The coating was semi-transparent with no significant coloration. A self-cleaning effect was demonstrated with both water and oil droplets. A self-cleanable, durable and highly transparent superamphiphobic coating based on a capped overhang structure has a great potential for commercial feasibility in a variety of applications, here exemplified for a biobased material.

© 2016 Elsevier B.V. All rights reserved.

1. Introduction

Wood plays an important role in society, as a heat source, as a raw material for paper and as a construction material. Due to its superior mechanical properties, light weight, easy converting and aesthetic appearance it is extensively used in buildings, bridges, furniture and so forth [1,2]. However, a drawback in exterior building material applications is that wood often has poor weathering

properties. Weathering is a surface change caused mainly by solar radiation, moisture and microbial degradation [1,2]. Wood, as a hydrophilic, hygroscopic, porous and fibrous material, is especially vulnerable to water sorption because of its rapid penetration into the structure of wood causing swelling and eventually a loss of mechanical strength as well as providing conditions for biological degradation. Water repellency is one of the main reasons why wood products for external use are coated [3–6].

In recent years, superhydrophobic surfaces inspired by nature, e.g. the lotus leaf, have attracted much attention in fundamental and applied research. Numerous studies have shown how to increase the water repellency of wooden surfaces using novel

* Corresponding author.

E-mail address: mikko.tuominen@sp.se (M. Tuominen).

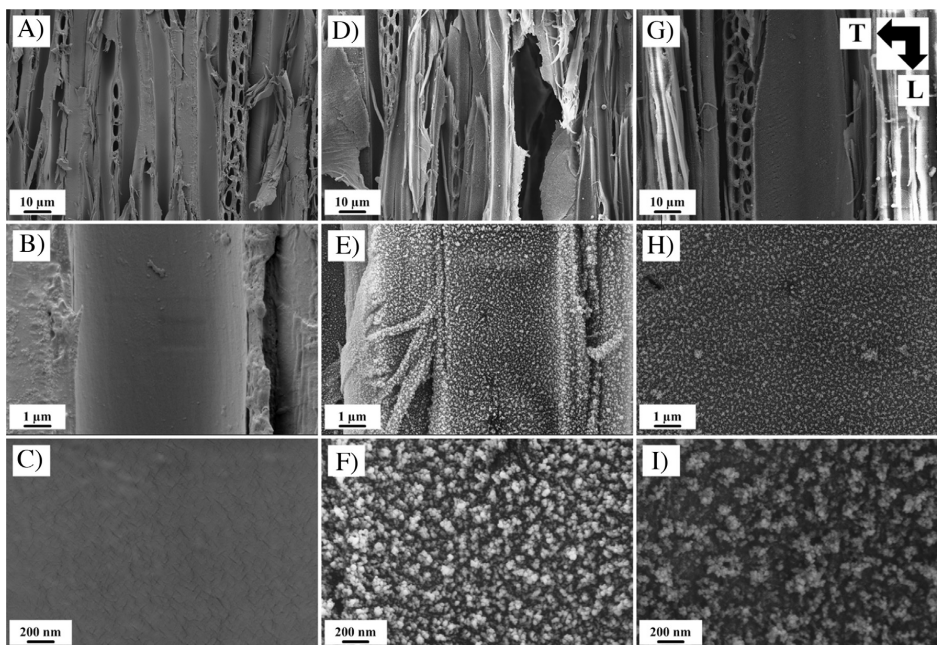


Fig. 1. FEG-SEM images of wood (A–C), $1 \times \text{TiO}_2\text{-PFH}$ (D–F) and $3 \times \text{TiO}_2\text{-PFH}$ (G–I) coated wood. The wood fibers are oriented in the longitudinal direction (L).

surface modification techniques, such as multi-layer deposition followed by fluorination [7], mild pyrolysis in an inert atmosphere [8], covalent grafting of a polymer [9], and silylation [10]. Nanosized metal oxide particles, like TiO_2 [11,12], CeO_2 [2], and ZnO [6,13], as well as SiO_2 [3,14,15] have also been utilized to create extremely water-repellent superhydrophobic coatings on wood. The function of the oxide particles is to increase the surface roughness which, together with a low surface energy coating, can give a superhydrophobic surface. Roughness combined with hydrophobicity results in air/vapor pockets trapped between the solid and liquid (composite interface) described by Cassie and Baxter [16] leading to a significant decrease in the solid–liquid adhesion and an increase in the contact angle [17–19]. It can also result in a solid–liquid interface with very high apparent contact angles of water but which is wetted at the roughness interstices as described by Wenzel [20]. Superhydrophobic surfaces have a water contact angle of 150° or above and a sliding or roll-off angle below 10° [21–23].

Not only water but also other liquids are known to affect wood [3]. In spite of numerous natural superhydrophobic surfaces, there are no known naturally occurring surfaces that can show high contact angles ($>150^\circ$) and low roll-off angles ($<10^\circ$) with sessile drops of oils and non-polar liquids. In the present study, we call the combination of superhydrophobicity (extreme water repellency) and superoleophobicity (extreme oil repellency) ‘superamphiphobicity’. Alternative terminology and notations used in the literature for these type of surfaces are superomniphobicity [23], superamphiphobicity [21,22,24] or ultralyophobicity [25]. The choice of ‘superamphiphobicity’ is natural because it shows the duality of repelling both water and oil and seems to be the most widely used term in recent literature. Superoleophobicity has been found in fish scales and shark skin in nature, but such oil repellency was found to occur only under water [17,24]. To make a superamphiphobic surface, it is not sufficient to use a material with low surface energy and to roughen the surface. Since oils have a lower surface ten-

sion than water, no oil shows a contact angle greater than 90° on any smooth solid surface, and overhang/high re-entrant curvature structures are therefore required to fabricate a superamphiphobic surface [19,21,26–28]. Manufacturing techniques, substrates, coatings and potential end applications of superamphiphobic surfaces have recently been discussed in several papers [21,23,29]. In most cases, the design of a superamphiphobic surface is based on a roughened surface, overhang structures and low surface energy, using e.g. fluorochemicals. This principle was also used in the only study, of which we are aware, an oil repellent coating on wood [3] in which fluorine-containing SiO_2 nanoparticles were spray coated on wood and dried at 105°C overnight. The wood surface showed extreme repellency for water and sunflower seed oil, with static contact angles of 168° and 154° , respectively. It was also shown [30] how roughness alone, if achieved with hindering re-entrant structure that enables a very low liquid–solid contact fraction, can change even the surface of hydrophilic silica to a super repellent against all kinds of liquids, including fluorinated solvents. A recent development which leads to amphiphobicity is slippery liquid-infused porous surfaces (SLIPS), which do not utilize the microstructural roughness of the surface to repel liquids directly, but where instead the microstructural roughness is used to infuse a lubricating liquid layer. Well-matched solid and liquid surface energies, combined with the microstructural roughness, create a highly stable state in which the liquid fills the spaces within the texture and forms a continuous smooth overlying film and can be modified to repel both high and low surface tension liquids [31].

The target of the present study was to create a superamphiphobic surface on wood using a two-step approach. The sub-micron and nanostructure on the wood surface was generated by a liquid flame spray (LFS) technique. LFS is a thermal aerosol-based process utilized to deposit nanometre-sized metal and metal oxide particles. LFS uses a liquid precursor fed together with combustion gases into a specially designed burner in which the precursor is atomized

to micron-sized droplets and evaporated in the high temperature flame. Different synthesis reactions of the precursor vapor result in the formation of solid nanoparticles that are then deposited onto the substrate [32–34]. In our previous studies [35–37], LFS has been used on cellulosic surfaces of paper and paperboard. A limitation of a LFS-based superhydrophobic TiO₂ coating has been the poor repellence of low surface tension liquids [38]. We show that these coatings display overhang/high re-entrant curvature structures, which means that a wood sample with the required geometrical homogeneity can exhibit superamphiphobic properties. We use plasma deposition to provide a hydrophobic capping of the TiO₂ nanoparticle coating by a low-surface-energy fluorine plasma polymer coating. To our knowledge, this is the first time superamphiphobicity based on an overhang structure has been demonstrated for a renewable bio-based material. An aim of the plasma polymer layer was also to improve the durability of the TiO₂ coating, since the commercial application of a superamphiphobic surface largely relies on its mechanical and forced wetting durability [23,29,39]. Despite the importance of durability, this aspect has received relatively little attention, especially in wood applications [3,13,14]. The resulting coatings show extreme water and oil repellency and offer a novel and scalable surface modification technique for a variety of substrates, here exemplified on wood surfaces. Wood has an aligned fiber structure, which is favorable for superamphiphobicity, and a significant need for liquid repellency.

2. Experimental

2.1. Sample preparation

Birch (*Betula pendula*) from Finland was used as substrate in study. Wood samples with dimensions of 100 mm in the longitudinal (L) (fiber orientation of wood), 50 mm in the tangential (T) and 2 mm in the radial (R) direction were prepared and coated using LFS and plasma deposition techniques. The LFS coating was achieved with a single nozzle type burner. Hydrogen and oxygen with flow rates of 50 and 15 L/min, respectively, were used as combustion gases. Titanium tetraisopropoxide (Aldrich, 97%) diluted in 2-propanol (VWR, HPLC Grade) was used as the TiO₂ precursor. The concentration of the precursor solution was 50 mg of atomic metal per mL, the feed rate was 12 mL/min, the treatment distance 60 mm and the treatment speed 50 m/min. The samples were treated either once (1 ×) or three times (3 ×) in the tangential direction.

Low-pressure plasma deposition was carried out using an in-house reactor consisting of a glass vessel connected to a double-stage rotary vacuum pump (Leybold-Heraeus D 65 B). Two externally wrapped, capacitively coupled, copper electrode bands were powered by a 13.56 MHz radio-frequency power generator (ENI, Model ACG-3). Perfluorohexane (PFH, Apollo Scientific) monomer was used as a precursor. During plasma deposition the treatment (generator) power was 40 W at a pressure of 18 Pa during 5 min. These plasma deposition parameters were chosen, based on previous experience, to provide a uniform and homogeneous coverage with a thickness of 30 nm.

2.2. Contact and roll-off angles

The static contact angles of water, ethylene glycol (Aldrich), diiodomethane (Aldrich), a household olive oil (Olio Extra Virgine D'oliva Primadonna, Fiorentini Firenze S.p.A., density: 924 kg/m³, dynamic viscosity: 70.5 mPas) and hexadecane (Aldrich) with surface tension of 72.8, 48.3, 50.8, 32.1 and 27.6 mN/m, respectively, were determined using an optical contact angle (OCA) instrument (CAM 200, KSV Instruments Oy). The roll-off angles of water, ethylene glycol, diiodomethane and olive oil were measured using a different OCA instrument (OCA40, DataPhysics GmbH), equipped

with a high speed CCD camera (maximum 2200 images s⁻¹) with 20× magnification. The images were analysed using the SCA 20 (DataPhysics) software. The tilting speed of roll-off angle measurements was 2° s⁻¹. Each CA and roll-off angle value was an average of five independent measurements. The droplet volume used was 5 μL in the static CA-measurements and 10 μL in roll-off-angle-measurements. The treated samples were conditioned and measurements performed at 50 ± 2% RH, 23 ± 2 °C.

2.3. Self-cleaning and drop impact resistance

Self-cleaning of the surfaces was evaluated by dropping water (volume 20 μL) and olive oil (volume 10 μL) onto the surface covered by sand (50–70 mesh size SiO₂ particles from Sigma-Aldrich). The drop heights were 20 mm (impact velocity 0.6 m/s), 50 mm (1.0 m/s) and 100 mm (1.4 m/s) and the tilting angle of the surface was 25° in the longitudinal direction (fiber orientation). The self-cleaning dynamics in the supporting materials was filmed using a Memrecam fx K5 high resolution and high speed video system.

In the drop impact test 5 μL water drops were impinged from a height of 100 mm (impact velocity 1.4 m/s). The tilting angle of the samples was 45° and the dropping frequency was one drop every third second. Water drops were impinged onto the same spot of the coated sample and changes in the wetting dynamics, i.e. droplet pinning and bouncing from the surface, were recorded.

2.4. Surface characterisation

The surfaces were imaged with a field emission gun scanning electron microscope FEG-SEM, model Zeiss ULTRAplus. Prior to the FEG-SEM imaging, the samples were gold sputter coated due to the resistive nature of wood. Prior to the FEG-SEM analysis, some wood specimens were prepared by an ultra violet- (UV-) laser ablation technique [40]. Previously, UV-laser ablation has been successfully used for prepared modified wood samples [41,42]. TiO₂-PFH coated wood samples were subjected to UV laser ablation using a pulsing krypton fluoride (KrF) excimer laser (Lumonix 600LX), emitting radiation with wavelength 248 nm with a pulse width of 20 ns and a frequency variation between 5 and 10 Hz. The energy level of the output ranged between 300 and 400 mJ.

The degree of oxidation and the chemical composition of the treated samples were determined by X-ray photoelectron spectroscopy (XPS), using a Kratos AXIS Ultra^{DL} (Kratos Analytical) equipped with a monochromatic AlX-ray source operated at 150 W. The take-off angle was 90° from to the sample surface. The pressure in the main chambers was maintained at 1.3 × 10⁻⁵ Pa during spectra acquisition. The samples were irradiated by monoenergetic X-rays for 6 min with a pass energy of 160 eV for survey analysis.

Color was measured with an optical spectrophotometer (CM-2600d, Konica Minolta Sensing, Inc.) and the color change was evaluated using L^* , a^* , b^* values and ΔE^* ($= \sqrt{\Delta a^{*2} + \Delta b^{*2} + \Delta L^{*2}}$) based on the CIELAB color scale. The maximum value of L^* is 100, representing the perfectly reflecting diffuser and the minimum is 0, representing black. A positive a^* is red and negative is green, whereas a positive b^* is yellow and negative is blue. ΔE^* is the total color difference between two samples, which takes into account the differences in the L^* , a^* and b^* values [43]. The transmittance spectra of TiO₂- and PFH-coated glass plates were measured using a UV/VIS spectrometer (Lambda 650, Perkin Elmer).

3. Results and discussion

3.1. Surface characterization

Wood has a rather geometrically homogeneous multi-scale structure. This fact, together with the observation that aged wood

Table 1

Atomic concentrations of TiO₂-PFH-coated wood surfaces measured by XPS. There were also trace amounts of N, Ca and P.

Sample	Atomic%			
	C	O	F	Ti
Wood, (reference)	73.0	24.8	–	–
Wood, 1 × TiO ₂ -PFH	32.2	4.0	62.4	1.0
Wood, 3 × TiO ₂ -PFH	35.4	5.8	56.5	1.9

Table 2

Wetting tension of water, ethylene glycol (EG), diiodomethane (DIM), olive oil and hexadecane (Hexa) on uncoated and TiO₂-PFH-coated wood samples.

Sample	Wetting tension ($\gamma_{LV} \cos \theta$), mNm ⁻¹				
	Water	EG	DIM	Olive oil	Hexa
Wood (reference)	-48.1	-9.1	19.3	31.2	27.6 ^a
Wood, 1 × TiO ₂	-65.5	-6.7	49.2	30.6	27.6 ^a
Wood, 3 × TiO ₂	-67.8	-9.5	50.7	31.4	27.6 ^a
Wood, PFH	-61.1	-39.7	-35.5	-21.7	-5.1
Wood, 1 × TiO ₂ -PFH	-67.5	-44.8	-47.0	-29.9	-19.7
Wood, 3 × TiO ₂ -PFH	-68.7	-45.1	-47.0	-29.4	-17.4

^a Based on an estimated static CA of 2°.

has surprisingly high water contact angles, led us to explore whether wood can be made superamphiphobic, repelling both water and oil/alkane, by the overhang/high re-entrant curvature concept. This concept has been explored in theory and in experiments [21,26,44] and, to our knowledge, we show for the first time that this concept gives superamphiphobic properties with a thin, semitransparent coating on a natural, wood material. As shown in the FEG-SEM-images in Fig. 1, the fibrous structure of wood gives a micro-scale roughness, while a uniformly distributed TiO₂ nanoparticle coating containing both particles and agglomerates, provides sub micrometer- and nano-scale roughness.

Such a multi-scale surface roughness together with the correct surface chemistry can provide an air/vapor layer at the interface between the surface and a liquid drop, preventing the liquid from wetting the surface and penetrating through the thin coating into the wood. The surface structures and chemistries of the TiO₂- and perfluorohexane (PFH)-coated wood samples coated both once and three times are very similar, as seen in Fig. 1 and Table 1, except that the amount of TiO₂ particle agglomerates and the thickness seem to be higher on the three-times-coated sample (Fig. 1, D–F vs. G–I). Our previous studies [45–47] have shown that the superhydrophobic properties of a TiO₂ nanoparticle coating are due to a carbonous overlayer which can be removed by UV illumination or plasma activation to give a superhydrophilic surface. According to previous studies [35,46,48], the average TiO₂ particle size is 25–30 nm, the coating amount ~50 mg/m² and the coating thickness ~660 nm (1 × TiO₂) where other cellulosic materials, e.g. paperboard, has been TiO₂-coated using the same LFS conditions.

3.2. Wettability

The wettability of TiO₂- and PFH-coated wood surfaces was evaluated by determining the static contact angles and roll-off angles of water, ethylene glycol, diiodomethane, olive oil and hexadecane with surface tensions of 72.8, 48.3, 50.8, 32.1, 27.6 mNm⁻¹, respectively. Table 2 shows the wetting tension values and Figure 2 shows the static contact angle (CA) together with photographs of water and oil drops on uncoated and fully coated wood.

Fig. 2 shows that the TiO₂ coating alone increased the static CA of water above 150°, but not that of the other liquids. On the other hand, the PFH layer enhanced the repellency of wood against all liquids, but with no values above 150°. Combining TiO₂ and PFH into a composite coating increased the CA values for all the liquids

Table 3

Roll-off angles of water, ethylene glycol (EG), diiodomethane (DIM), olive oil and hexadecane (Hexa) on TiO₂ (1 × and 3 ×) and PFH coated wood.

Sample	Roll-off angle, °				
	Water	EG	DIM	Olive oil	Hexa
Wood, 1 × TiO ₂	L: 7 ± 1 T: 9 ± 2	n.d.	n.d.	n.d.	n.d.
Wood, 3 × TiO ₂	L: 5 ± 1 T: 6 ± 1	n.d.	n.d.	n.d.	n.d.
Wood, 1 × TiO ₂ -PFH	<2 ^a	L: 2 ± 0.5 T: 3 ± 0.5	L: 2° ± 0.5° T: 3° ± 0.5°	L: 4 ± 1 T: 7 ± 2	n.d.
Wood, 3 × TiO ₂ -PFH	<2 ^a	L: 2 ± 0.5 T: 2 ± 0.5	L: 2 ± 0.5 T: 2 ± 0.5	L: 3 ± 0.5 T: 5 ± 1	n.d.

^a Water droplets run away when first placed on the surface. When the droplet becomes pinned, it then rolls off below 2° tilting. The roll-off angles were measured in both longitudinal (L) (fiber orientation of wood) and tangential (T) tilting directions. n.d. means not determined, since the static CA was below 150°.

to above 150° with the exception of hexadecane. The wetting tension $\gamma_{LV} \cos \theta$, being the primary wetting parameter, as shown in Table 3, exhibited strongly negative, non-wetting, values only for the combined TiO₂-PFH coatings. A static contact angle greater than 150° however, was not enough to be defined as a super repellent surface, since the contact angle hysteresis or roll-off angle must also be below 10°. Table 3 shows that the roll-off angles of water, ethylene glycol, diiodomethane and olive oil from the TiO₂ and PFH coated surfaces are indeed below 10°. The number of coating layers and thickness (1 × or 3 ×) or the tilting direction in relation to the wood fibers (longitudinal or tangential) have a minor effect on the static CA and roll-off angle values. A small but consistent difference in the roll-off angle between the different tilting directions can however be observed due to the anisotropic surface structure caused by the fiber orientation in the wood (Fig. 1 and 3). As expected, the drops preferably roll parallel to the direction of the fibers (longitudinal direction). Similar anisotropic dewetting has been observed on natural rice leaf [49] and it probably contributes to the establishment a re-entrant curvature on wood similar to that on oil-repellent electrospun coatings [26,44].

The TiO₂-PFH-coated wood surfaces are superhydrophobic and superoleophobic, since the static CAs of water and oil are above 150° and the roll-off angles below 10°. Surfaces that are both superhydrophobic and superoleophobic have generally been classified as superamphiphobic, even though this definition in some cases has been extended to include liquids with even lower surface tensions than oil, such as alkanes or fluorinated liquids [21,26]. For hexadecane, with a lower surface tension than olive oil, we note a very high CA of 130–135° without any optimization (e.g. the coating thickness) of the coating parameters.

3.3. Self-cleaning effect

Self-cleaning of a surface is a very interesting feature in many practical applications and it has been investigated by spreading sand particles as a contaminant on the surface of the TiO₂-PFH-coated wood samples. It was observed that the rolling water and oil droplets were able to remove the sand from the surface demonstrating a self-cleaning capability of the surfaces (see Fig. 4 I–P and movie clips 3 and 4 in Supporting information).

Although the roll-off angles of water and oil are well below 10°, a clear difference in their wetting dynamics can be observed, especially when the droplets are dropped onto the surface from a height (forced wetting) instead of as sessile drops (spontaneous wetting) as in the roll-off angle measurement. The images in Fig. 4 A–H and the movie clips 1 and 2 provided in the supporting information shows that the water droplet bounces off from the surface in a fraction of a second whereas the oil droplet rests on the surface for a

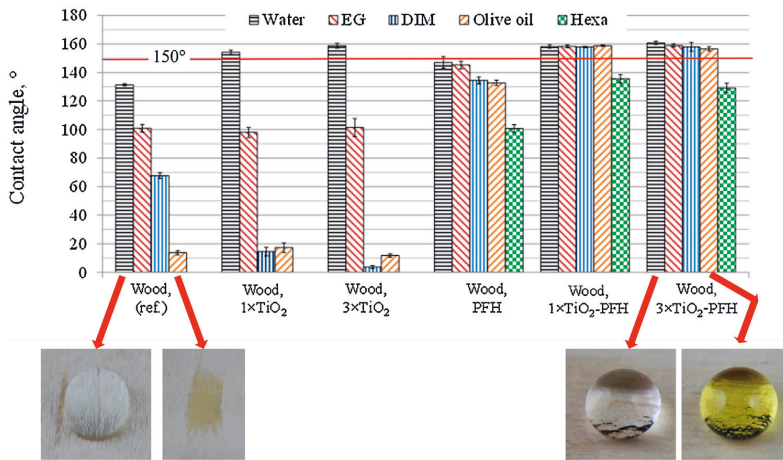


Fig. 2. Static contact angles of water, ethylene glycol (EG), diiodomethane (DIM), olive oil and hexadecane (Hexa) on (1 × and 3 ×) TiO₂-PFH coated wood. Static CA of hexadecane on wood, 1 × and 3 × TiO₂ coated wood is <2°. Inset: ~10 mL drops of water and olive oil on uncoated and fully coated wood.

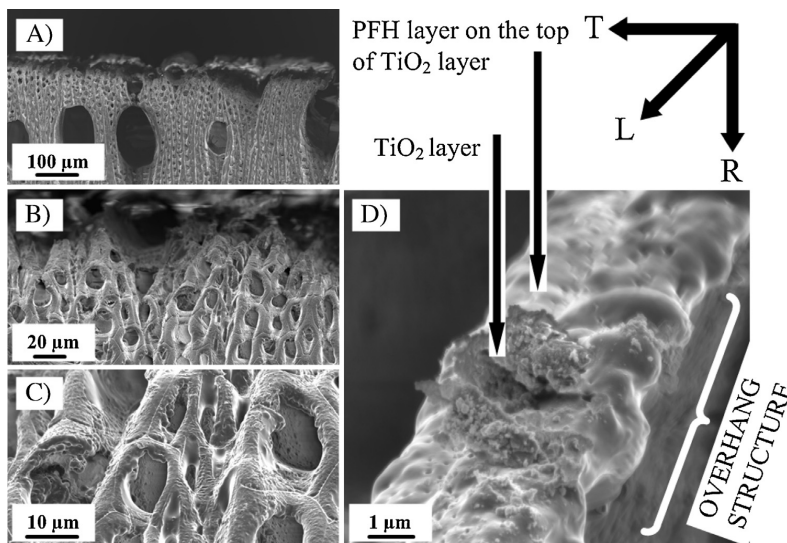


Fig. 3. FEG-SEM images of the cross section of the coated wood samples at successive magnifications of 3 × TiO₂-PFH coated wood. The overhang structure is seen in D. In addition, the individual TiO₂ and PFH layers are clearly seen in a small area where the PFH-TiO₂ coating has been damaged. T: tangential direction, L: longitudinal (fiber orientation of wood) direction and R: radial direction.

short while and then starts to slowly roll along the surface. The advancing and receding CAs were not evaluated from the movies but a clear difference (CA hysteresis) between advancing and receding CA of the rolling oil droplet can be seen, probably due to pinning on the heterogeneous surface. This observation was not further explored, but it is notable since the oil roll-off angles were small.

The PFH coating covers the surface quite uniformly, whereas the fibrous structure of the wood and the coating by nanoparticle agglomerates led to a structural heterogeneity and thus high CAH on the surface. An interesting observation related to the wetting state transition was seen when oil was dropped from different heights onto the once coated and three times coated TiO₂-PFH sam-

ples. The single coated surface repelled the oil when the dropping height was 20 mm, but the oil droplet sticks to the surface when the dropping height was increased to 50 mm. The situation was the same with the three times coated surface, but the oil droplet stuck to the surface when the dropping height was 100 mm not 50 mm. In the case of a dispensed droplet there is forced wetting, in this case leading to a partial transition from the Cassie-Baxter to the Wenzel wetting state. The wetting transition and related droplet pinning can result in droplet penetration deep into the porous coating, where the increase in the liquid-solid contact area between the droplet and the surface gives high adhesion and prevents the droplet from reverting back to Cassie-Baxter wetting state. On the

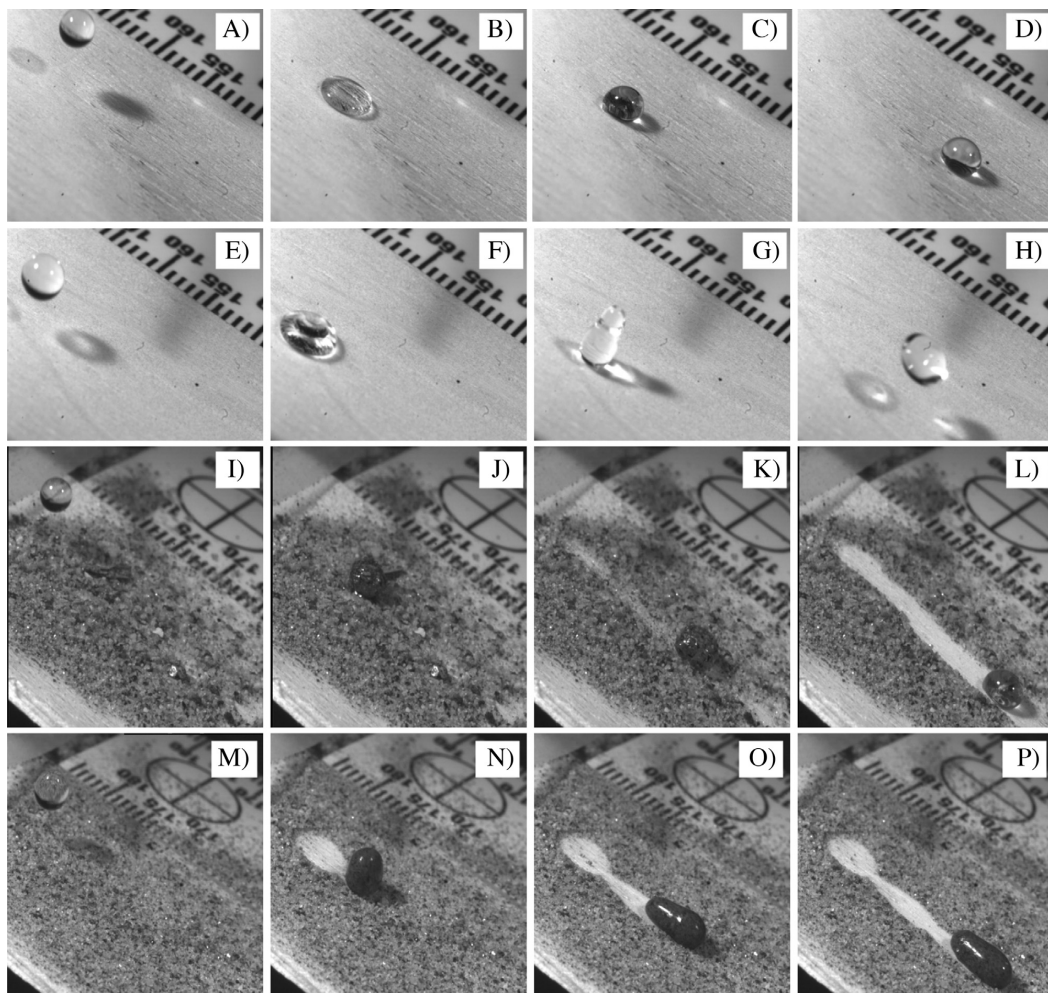


Fig. 4. Photographs from movies (supporting information): A–D: oil droplet on $3 \times \text{TiO}_2$ -PFH coated wood, E–H: water droplet on $3 \times \text{TiO}_2$ -PFH coated wood surface, I–L: self-cleaning using oil droplet on $3 \times \text{TiO}_2$ -PFH coated wood (I and J: 1st droplet, K: 2nd droplet, L: 5th droplet) and M–P: self-cleaning using water droplet in the longitudinal direction on $3 \times \text{TiO}_2$ -PFH coated wood.

other hand, if TiO_2 particles deep in the porous structure are not completely covered by the PFH coating the oil droplet may become pinned anyway, as long as the penetration depth is sufficiently high. There is evidently a limit in impact force for a double coating to be able to repel a falling oil droplet, depending at least on the drop height and on the structure and chemistry of the nanoparticle coating ($1 \times$ or $3 \times$). The XPS spectra in Table 2 showed that the surface chemistries of once coated and three times coated surfaces are very similar, indicating that the difference in TiO_2 coating structure (thickness, porosity, number of agglomerates, etc.) may explain the difference in oil repellence.

3.4. Wetting durability

Poor durability of superamphiphobic coatings is a major limitation for their successful utilization in applications where self-cleaning and liquid repellence are required. In our previous studies,

the durability of TiO_2 -coated paperboard was studied using a tape test [37], a Taber wheel test [48] and calendering [50]. In all of these studies the change in the static CA was followed in relation to different types and levels of abrasion of the coated surface. In all cases, the superhydrophobicity (water $\text{CA} > 150^\circ$) of the TiO_2 coating was lost already after a few abrasion cycles. More severe abrasion removed a part of the nanoparticles, but the surface still maintained its hydrophobicity (water $\text{CA} > 90^\circ$). In the present study, a water drop impact [22] was used to evaluate the wetting durability of the TiO_2 - and PFH-coated wood surfaces. The surface sensitivity of such a method makes it very suitable for studying the wetting dynamics and drop impact resistance of a superamphiphobic surface. Fig. 5 shows the test setup, where water droplets are repeatedly dropped onto the same spot on the coated sample and the change in wetting dynamics is monitored.

No changes in the wetting properties of TiO_2 -PFH-coated surfaces were observed even after 500 000 drop impacts, whereas the

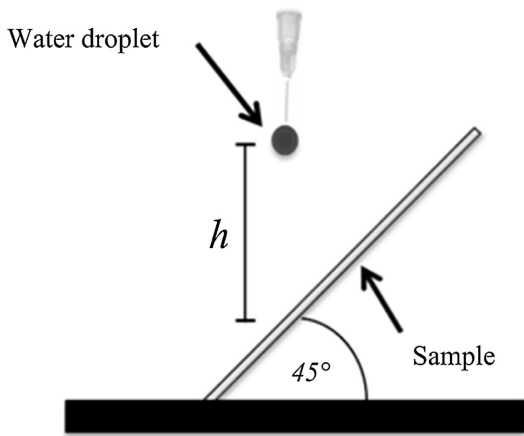


Fig. 5. Sketch of the setup to test water drop impact resistance. 5 μL water drops were dispensed from a height (h) of 10 cm (impact velocity $U = 1.4$ m/s). The tilting angle of the sample was 45° and the sequence was one drop every third second.

wetting of TiO_2 -coated surfaces without the PFH coating changed already after 500 drops, a small fraction of the bouncing water droplets being pinned onto the surface. The size of the pinned droplet increased with increasing number of falling droplets, and eventually the falling droplet no longer bounced off the surface, a result of a gradual transition from the Cassie-Baxter to the Wenzel wetting state. The increasing pressure in the contact area of the repeatedly falling droplets or a chemical change, i.e. a gradual removal of carbonaceous material from the top of the TiO_2 nanoparticles, eventually led to a wetting state transition. The structural changes, i.e. removal of nanoparticles from the TiO_2 coating probably plays a minor role after ~ 500 drop impacts because, if the pinned droplet is allowed to evaporate, the falling droplets again bounce off the surface with no significant change in the wetting (static water CA $> 150^\circ$ and roll-off angle $< 10^\circ$).

It is suggested that the, extremely low wettability, hexadecane is also non-wetting although not super-repellent is due to these overhang hydrophobic capped structures giving a high re-entrant curvature for wetting liquids. This mechanism was suggested in earlier studies [26,44] and experimentally shown for fabricated silicone substrates and for electrospun fluorine polymers, but it has not so far been reported for natural biobased materials using thin coatings. The parameters describing overhang structures have been explored in detail [21]. A requirement for achieving overhang on wood seems to be to prepare the coating on the right wood species and on the right direction of that particular wood in order to fulfill the geometrical requirement of superoleophobicity. The bare wood sample selected here had a very high water contact angle because of ageing under ambient conditions. Only one wood sample has been investigated in this study, but it seems plausible that oil repellence will be easier to achieve if there is already water repellence.

In order to categorize this new coating in relation to several other similar superhydro- and amphiphobic substrates, we have applied the approach suggested by Tuteja et al. [44] to discuss the required geometry in relation to non-wetting robustness in which two dimensionless parameters are introduced, D^* to describe the geometric spacing and H^* for the non-wetting robustness:

$$D^* = [(W + D)]^2; H^* = \left\{ 2 \left[(1 - \cos \theta) R + H \right] \sqrt{\gamma_{LV} / \rho g} \right\} / D^2 \quad (1)$$

where W , D , R and H are geometrical parameters describing the width of the hydrophobic cap, the spacing between the caps, the

Table 4

The CIE $L^*a^*b^*$ color values and color change of TiO_2 - and PFH-coated wood (compared to uncoated wood).

Sample	Color change (compared to uncoated wood)			
	ΔL^*	Δa^*	Δb^*	ΔE^*
Wood (reference)	0	0	0	0
Wood, $1 \times \text{TiO}_2$	1.4	-0.8	1.4	2.1
Wood, $3 \times \text{TiO}_2$	0.4	-0.7	1.9	2.1
Wood, PFH	1.3	-0.2	0.1	1.3
Wood, $1 \times \text{TiO}_2$ -PFH	1.1	-0.8	1.7	2.2
Wood, $3 \times \text{TiO}_2$ -PFH	0.5	-0.6	2.1	2.3

radius of curvature of the overhang cap and the height of the capillary, respectively. Applying values for the superamphiphobic wood estimated from Fig. 3 and optical profilometer data (not shown) gives $D^* = 1.6$, and $H^* = 800$ – 1100 for hexadecane and water respectively. These values place the superamphiphobic wood sample in the upper left-hand corner of different substrates and surfaces displaying extreme liquid repellency as discussed by Tuteja et al. [44], meaning high non-wetting robustness factor but with much smaller geometrical features than to the 'nanonails' and 'micro hoodoo' structures.

The forced wetting durability is of crucial importance in applications. The parameters that govern a transition from non-wetting to wetting can be expressed as a balance between two opposing pressures, $P_{non-wetting}$ describing the non-wetting cavity being formed, proportional to the wetting tension divided by the length of the non-wetted contact line CL (drop contour length) according to:

$$P_{non-wetting} \sim \gamma_{LV} \cos \theta / CL \quad (2)$$

where γ_{LV} is the surface tension and θ the contact angle. The forced wetting pressure is governed by the liquid density ρ , the impacting drop velocity U and the number of drop impacts N_{drop} , i.e.:

$$P_{wetting} \sim \rho U^2 N_{drop} \quad (3)$$

Combining Eqs. (1) and (2) determines the wetting transition and thus the forced wetting durability. There are only seven data points in the present study, but these suffice to conclude that $\log P_{wet} \sim P_{non-wet}$, while indicating that the superamphiphobic wood in the present study seems to have a high forced wetting durability.

3.5. Transparency and color

A natural appearance of wood is desired and it is therefore often protected by a lacquer in many applications, such as buildings, boats and furniture. It is thus vital to assess whether the coatings affect the visual properties of wood. The transparency of the TiO_2 and PFH coatings and their effects on the color of the wood were measured. Generally, the TiO_2 and PFH coatings had only a minor influence on the color of wood, but a smaller change (ΔE^*) was seen when only PFH was used compared with PFH and TiO_2 together ($1 \times$ or $3 \times$), as seen in Table 4 with a single layer (PFH) or a combination of two layers (PFH and TiO_2) on top of the wood.

A large amount of TiO_2 coating ($3 \times$ instead of $1 \times$) makes the color slightly darker and yellower, whereas a PFH layer has no significant influence on the color. The transparency of the coatings on the wood could not be measured directly. Instead, glass plates were coated using the same LFS and plasma deposition parameters as for the wood coatings. Fig. 6 shows the transparency of the different TiO_2 -PFH coatings.

$1 \times \text{TiO}_2$ and $1 \times \text{TiO}_2$ -PFH coatings showed excellent transparency, allowing the transmission of up to 80% of all visible light, whereas $3 \times \text{TiO}_2$ and $3 \times \text{TiO}_2$ -PFH coatings showed poorer transparency with a transmittance of less than 50% at shorter wave-

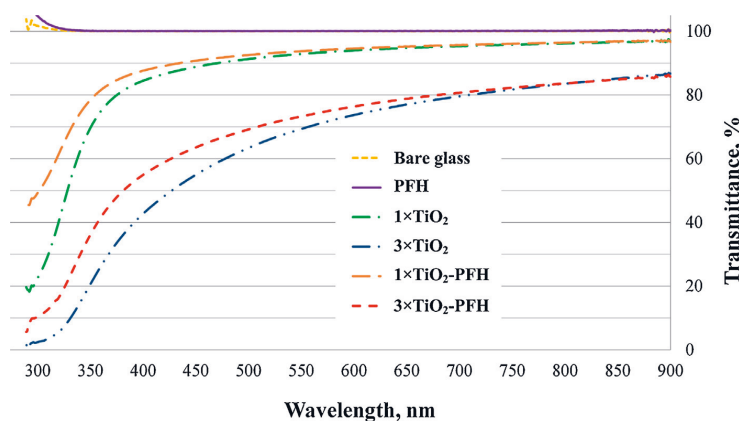


Fig. 6. Transmittance spectra of TiO₂-PFH coated glass plates.

lengths of visible light. The PFH coating itself did not change the transmittance of glass, but it improved the transmittance of TiO₂ coatings slightly, probably due to a reduction in the light scattering by the porous coating.

4. Conclusions

A superamphiphobic coating was created on wood using LFS and plasma polymer deposition techniques. The coated wood surface showed extreme repellence against water, ethylene glycol, diiodomethane and olive oil with static CAs greater than 150° and roll-off angles of less than 10° (and a static CA of 130–135° for hexadecane) enabling the surface to be classified as superamphiphobic, i.e. superhydrophobic (water repellent) and superoleophobic (oil repellent). It is suggested that the superamphiphobicity is due to an overhang hydrophobic capped structure of the TiO₂ nanoparticles combined with a low surface energy perfluorohexane (PFH) layer to form an air/vapor layer at the interface between the surface and the liquid.

The TiO₂-PFH coating shows the potential to become commercially feasible. It had a high transparency and no significant coloring effect, which is vital in many end applications of wood where the natural appearance of the wood is desirable. Moreover, its durability against droplet impact was high. No change in surface wetting performance was observed after 500 000 water drop impacts. A self-cleaning effect was demonstrated using both water and oil droplets.

Acknowledgments

Mikko Tuominen and Agne Swerin thank the Nils and Dorthi Troëdsson Foundation for Scientific Research for financial support. RISE Research Institutes of Sweden AB provided additional funding. Magnus Wälinder thanks the Swedish Research Council Formas (project EnWoBio 2014-172) for financial support. Jari Rämö (TUT) is thanked for the high speed video clips, Johan Andersson for performing the plasma trials at SP and Joachim Seltman for UV laser ablation.

Appendix A. Supplementary data

Supplementary data associated with this article can be found, in the online version, at <http://dx.doi.org/10.1016/j.apsusc.2016.05.095>.

References

- [1] S. Olsson, Enhancing UV Protection of Clear Coated Exterior Wood by Reactive UV Absorber and Epoxy Functional Vegetable Oil, D.Sc. Thesis, KTH Royal Institute of Technology, Stockholm, Sweden, 2014, 87 p.
- [2] Y. Lu, S. Xiao, R. Gao, J. Li, Q. Sun, Improved weathering performance and wettability of wood protected by CeO₂ coating deposited onto the surface, *Holzforschung* 68 (2014) 345–351.
- [3] C.T. Hsieh, B.S. Chang, J.Y. Lin, Improvement of water and oil repellency on wood substrates by using fluorinated silica nanocoating, *Appl. Surf. Sci.* 257 (2011) 7997–8002.
- [4] C. Wang, C. Piao, C. Lucas, Synthesis and characterization of superhydrophobic wood surfaces, *J. Appl. Polym. Sci.* 119 (2011) 1667–1672.
- [5] S. Wang, C. Wang, C. Liu, M. Zhang, H. Ma, J. Li, Fabrication of superhydrophobic spherical-like α-FeOOH films on the wood surface by a hydrothermal method, *Colloids Surf. A: Physicochem. Eng. Aspects* 403 (2012) 29–34.
- [6] Y. Fu, H. Yu, Q. Sun, G. Li, Y. Liu, Testing of the superhydrophobicity of a zinc oxide nanorod array coating on wood surface prepared by hydrothermal treatment, *Holzforschung* 66 (2012) 739–744.
- [7] H. Yang, Y. Deng, Preparation and physical properties of superhydrophobic papers, *J. Colloid Interface Sci.* 325 (2008) 588–593.
- [8] M. Hakkou, M. Pétrissans, A. Zoullalian, P. Gérardin, Investigation of wood wettability changes during heat treatment on the basis of chemical analysis, *Polym. Degrad. Stab.* 89 (2005) 1–5.
- [9] D. Tastet, M. Save, F. Charrier, B. Charrier, J.B. Ledeuil, J.C. Dupin, L. Billon, Functional biohybrid materials synthesized via surface-initiated MADIX/RAFT polymerization from renewable natural wood fiber: grafting of polymer as non leaching preservative, *Polymer* 52 (2011) 606–616.
- [10] I. Mohammed-Ziegler, I. Táncoz, Z. Hörvölgyi, B. Agoston, Water-repellent acylated and silylated wood samples and their surface analytical characterization, *Colloids Surf. A: Physicochem. Eng. Aspects* 319 (2008) 204–212.
- [11] Q. Sun, Y. Lu, Y. Liu, Growth of hydrophobic TiO₂ on wood surface using a hydrothermal method, *J. Mater. Sci.* 46 (2011) 7706–7712.
- [12] L. Gao, Y. Lu, X. Zhan, J. Li, Q. Sun, A robust, anti-acid, and high-temperature-humidity-resistant superhydrophobic surface of wood based on a modified TiO₂ film by fluoroalkyl silane, *Surf. Coat. Technol.* 262 (2015) 33–39.
- [13] S. Wang, J. Shi, C. Liu, C. Xie, C. Wang, Fabrication of a superhydrophobic surface on a wood substrate, *Appl. Surf. Sci.* 257 (2011) 9362–9365.
- [14] F. Liu, S. Wang, M. Zhang, M. Ma, C. Wang, J. Li, Improvement of mechanical robustness of the superhydrophobic wood surface by coating PVA/SiO₂ composite polymer, *Appl. Surf. Sci.* 280 (2013) 686–692.
- [15] C. Wang, M. Zhang, Y. Xu, S. Wang, F. Liu, M. Ma, D. Zang, Z. Gao, One-step synthesis of unique silica particles for the fabrication of bionic and stably superhydrophobic coatings on wood surface, *Adv. Powder Technol.* 25 (2014) 530–535.
- [16] A.B.D. Cassie, S. Baxter, Wettability of porous surfaces, *Trans. Faraday Soc.* 40 (1944) 546–551.
- [17] M. Nosonovsky, B. Bhushan, Superhydrophobic surfaces and emerging applications: non-adhesion energy, green engineering, *Curr. Opin. Colloid Interface Sci.* 14 (2009) 270–280.
- [18] B. He, N.A. Patankar, J. Lee, Multiple equilibrium droplet shapes and design criterion for rough hydrophobic surfaces, *Langmuir* 19 (2003) 4999–5003.
- [19] S. Herminghaus, Roughness-induced non-wetting, *Europhys. Lett.* 52 (2000) 165–170.

- [20] R.N. Wenzel, Resistance of solid surfaces to wetting by water, *Ind. Eng. Chem.* 28 (1936) 988–994.
- [21] H.J. Butt, C. Semperebon, P. Papadopoulos, D. Vollmer, M. Brinkmann, M. Ciccotti, Design principles for superamphiphobic surfaces, *Soft Matter* 9 (2013) 418–428.
- [22] X. Deng, L. Mammen, H.J. Butt, D. Vollmer, Candle soot as a template for a transparent robust superamphiphobic coating, *Science* 335 (2012) 67–70.
- [23] A.K. Kota, W. Choi, A. Tuteja, Superomniphobic surfaces: design and durability, *MRS Bull.* 38 (2013) 383–390.
- [24] J. Zeng, B. Wang, Y. Zhang, H. Zhu, Z. Guo, Strong amphiphobic porous films with oily-self-cleaning property beyond nature, *Chem. Lett.* 43 (2014) 1566–1568.
- [25] W. Chen, A.Y. Fadeev, M.C. Hsieh, D. Öner, J. Youngblood, T.J. McCarthy, Ultrahydrophobic and ultralyophobic surfaces: some comments and examples, *Langmuir* 15 (1999) 3395–3399.
- [26] A. Tuteja, W. Choi, M. Ma, J.M. Mabry, S.A. Mazzella, G.C. Rutledge, G.H. McKinley, R.E. Cohen, Designing superoleophobic surfaces, *Science* 318 (2007) 1618–1622.
- [27] A. Tuteja, W. Choi, J.M. Mabry, G.H. McKinley, R.E. Cohen, Robust omniphobic surfaces, *Proc. Natl. Acad. Sci. U. S. A.* 105 (2008) 18200–18205.
- [28] W. Choi, A. Tuteja, S. Chhatre, J.M. Mabry, R.E. Cohen, G.H. McKinley, Fabrics with tunable oleophobicity, *Adv. Mater.* 21 (2009) 2190–2195.
- [29] Z. Xue, M. Liu, L. Jiang, Recent developments in polymeric superoleophobic surfaces, *J. Polym. Sci. Part B: Polym. Phys.* 50 (2012) 1209–1224.
- [30] T. Liu, C.J. Kim, Turning a surface superrepellent event to completely wetting liquids, *Science* 346 (2014) 1096–1100.
- [31] T.S. Wong, S.H. Kang, S.K.Y. Tang, E.J. Smythe, B.D. Hatton, A. Grinthal, J. Aizenberg, Bioinspired self-repairing slippery surfaces with pressure-stable omniphobicity, *Nature* 477 (2011) 443–447.
- [32] J. Tikkanen, K.A. Gross, C.C. Berndt, V. Pitkänen, J. Keskinen, S. Raghu, M. Rajala, J. Karthikeyan, Characteristics of the liquid flame spray process, *Surf. Coat. Technol.* 90 (1997) 210–216.
- [33] A. Gurav, T. Kodas, T. Pluym, Y. Xiong, Aerosol processing of materials, *Aerosol Sci. Technol.* 19 (1993) 411–452.
- [34] S.E. Pratsinis, Flame aerosol synthesis of ceramic powders, *Prog. Energy Combust. Sci.* 24 (1998) 197–219.
- [35] J.M. Mäkelä, M. Aromaa, H. Teisala, M. Tuominen, M. Stepien, J.J. Saarinen, M. Toivakka, J. Kuusipalo, Nanoparticle deposition from liquid flame spray onto moving roll-to-roll paperboard material, *Aerosol Sci. Technol.* 45 (2011) 817–827.
- [36] M. Stepien, J.J. Saarinen, H. Teisala, M. Tuominen, M. Aromaa, J. Kuusipalo, J.M. Mäkelä, M. Toivakka, Adjustable wettability of paperboard by liquid flame spray nanoparticle deposition, *Appl. Surf. Sci.* 257 (2011) 1911–1917.
- [37] H. Teisala, M. Tuominen, M. Aromaa, J.M. Mäkelä, M. Stepien, J.J. Saarinen, M. Toivakka, J. Kuusipalo, Development of superhydrophobic coating on paperboard surface using the liquid flame spray, *Surf. Coat. Technol.* 205 (2010) 436–445.
- [38] H. Teisala, M. Tuominen, M. Aromaa, M. Stepien, J.M. Mäkelä, J.J. Saarinen, M. Toivakka, J. Kuusipalo, High- and low-adhesive superhydrophobicity on the liquid flame spray-coated board and paper: structural effects on surface wetting and transition between the low- and high-adhesive states, *Colloid Polym. Sci.* 291 (2013) 447–455.
- [39] T. Verho, C. Bower, P. Andrew, S. Franssila, O. Ikkala, R.H.A. Ras, Mechanically durable superhydrophobic surfaces, *Adv. Mater.* 23 (2011) 673–678.
- [40] J. Seltman, Opening the wood structure by UV-irradiation, *Holz als Roh- und Werkstoff* 53 (1995) 225–228.
- [41] M. Wälinder, A. Omidvar, J. Seltman, K. Segerholm, Micromorphological studies of modified wood using a surface preparation technique based on ultraviolet laser ablation, *Wood Mater. Sci. Eng.* 4 (2009) 46–51.
- [42] K. Laine, K. Segerholm, M. Wälinder, L. Rautkari, G. Ormondroyd, M. Hughes, D. Jones, Micromorphological studies of surface densified wood, *J. Mater. Sci.* 49 (2014) 2027–2034.
- [43] Colorimetry. CIE 1976 L*a*b* Colour space, BS EN ISO 11664-4:2011, BSI, 2010, 14.
- [44] A. Tuteja, W. Choi, G.H. McKinley, R.E. Cohen, M.F. Rubner, Design parameters for superhydrophobicity and superoleophobicity, *MRS Bull.* 33 (2008) 752–758.
- [45] J. Haapanen, M. Aromaa, H. Teisala, M. Tuominen, M. Stepien, J.J. Saarinen, M. Heikkilä, M. Toivakka, J. Kuusipalo, J.M. Mäkelä, Binary TiO₂/SiO₂ nanoparticle coating for controlling the wetting properties of paperboard, *Mater. Chem. Phys.* 149 (2015) 230–237.
- [46] H. Teisala, M. Tuominen, M. Stepien, J. Haapanen, J.M. Mäkelä, J.J. Saarinen, M. Toivakka, J. Kuusipalo, Wettability conversion on the liquid flame spray generated superhydrophobic TiO₂ nanoparticle coating on paper and board by photocatalytic decomposition of spontaneously accumulated carbonaceous overlayer, *Cellulose* 20 (2013) 391–408.
- [47] M. Stepien, J.J. Saarinen, H. Teisala, M. Tuominen, M. Aromaa, J. Haapanen, J. Kuusipalo, J.M. Mäkelä, M. Toivakka, ToF-SIMS analysis of UV-switchable TiO₂-nanoparticle-coated paper surface, *Langmuir* 29 (2013) 3780–3790.
- [48] M. Stepien, G. Chinga-Carrasco, J.J. Saarinen, H. Teisala, M. Tuominen, M. Aromaa, J. Haapanen, J. Kuusipalo, J.M. Mäkelä, M. Toivakka, Wear resistance of nanoparticle coatings on paperboard, *Wear* 307 (2013) 112–118.
- [49] L. Feng, S. Li, Y. Li, H. Li, L. Zhang, J. Zhai, Y. Song, B. Liu, L. Jiang, D. Zhu, Super-hydrophobic surfaces: from natural to artificial, *Adv. Mater.* 14 (2002) 1857–1860.
- [50] M. Stepien, J.J. Saarinen, H. Teisala, M. Tuominen, J. Haapanen, J.M. Mäkelä, J. Kuusipalo, M. Toivakka, Compressibility of porous TiO₂ nanoparticle coating on paperboard, *Nanoscale Res. Lett.* 8 (2013) 1–6.

PAPER
IV

**Ultrafast Processing of Hierarchical Nanotexture for a Transparent
Superamphiphobic Coating with Extremely Low Roll-Off Angle and
High Impalement Pressure**

Hannu Teisala, Florian Geyer, Janne Haapanen, Paxton Juuti, Jyrki M. Mäkelä,
Doris Vollmer, Hans-Jürgen Butt

Advanced Materials 30 (2018), 1706529

DOI: 10.1002/adma.201706529

Publication reprinted with the permission of the copyright holders.

Ultrafast Processing of Hierarchical Nanotexture for a Transparent Superamphiphobic Coating with Extremely Low Roll-Off Angle and High Impalement Pressure

Hannu Teisala,* Florian Geyer, Janne Haapanen, Paxton Juuti, Jyrki M. Mäkelä, Doris Vollmer, and Hans-Jürgen Butt*

Low roll-off angle, high impalement pressure, and mechanical robustness are key requirements for super-liquid-repellent surfaces to realize their potential in applications ranging from gas exchange membranes to protective and self-cleaning materials. Achieving these properties is still a challenge with superamphiphobic surfaces, which can repel both water and low-surface-tension liquids. In addition, fabrication procedures of superamphiphobic surfaces are typically slow and expensive. Here, by making use of liquid flame spray, a silicon dioxide–titanium dioxide nanostructured coating is fabricated at a high velocity up to 0.8 m s^{-1} . After fluorosilanization, the coating is superamphiphobic with excellent transparency and an extremely low roll-off angle; $10 \mu\text{L}$ drops of *n*-hexadecane roll off the surface at inclination angles even below 1° . Falling drops bounce off when impacting from a height of 50 cm, demonstrating the high impalement pressure of the coating. The extraordinary properties are due to a pronounced hierarchical nanotexture of the coating.

Superamphiphobic surfaces are characterized by their low adhesion to both polar and nonpolar, low-surface-tension liquids.^[1–5] Drops deposited on such surfaces adapt a spherical shape with a static contact angle larger than 150° . More importantly, when moving the contact line, the apparent receding contact angle^[6] exceeds $\approx 140^\circ$. As a result, drops can roll off the surface at low inclination angles, typically below 10° . The early approaches to design superamphiphobic surfaces were reported by Tsujii et al.^[1] in 1997 and Tuteja et al.^[2] in 2007. After this, superamphiphobic surfaces have been in spotlight of research both from the fundamental and economical aspects. Full comprehension of the super liquid-repellency mechanisms is a prerequisite to realize the potential of superamphiphobic surfaces in applications ranging from protective and self-cleaning materials^[4,7] to medical devices^[8,9] and gas exchange membranes.^[10] In many

of the applications, such as wind screens, window panes, lenses, or protective goggles, the superamphiphobic coating should be optically transparent, mechanically stable, and capable of repelling liquid impalement even under high hydrostatic pressure or drop impact.^[11]


The capability of superamphiphobic surfaces to repel low-surface-tension liquids arises from a combination of their overhang, inward curved surface morphology and low-surface-energy chemistry. Overhanging morphology and low surface energy are required to stabilize an air cushion below the drops and maintain the so-called Cassie–Baxter state.^[12] An exception to this is a doubly re-entrant micropillar surface introduced by Liu and Kim,^[13] where a low-surface-energy chemistry is not needed. The required surface

morphology for superamphiphobic materials can be realized with well-defined, mushroom-like micropillars,^[2,13,14] or with random, sub-micrometer scale surface textures with overhang curvature. The micropillars are typically fabricated by reactive ion etching.^[2,13] Randomly structured superamphiphobic surfaces have a higher potential for scaled up production. Methods to fabricate these surfaces include growth of silicone nanofilaments^[3,10] and templating candle soot.^[4] Because the morphology required for superamphiphobic surfaces is rather complex, the number of suitable approaches is limited. Most methods are energy-, chemical-, or time-consuming with multiple process steps.^[5,7] Furthermore, it is still a challenge to fabricate superamphiphobic surfaces which combine high receding contact angles with high impalement pressure and mechanical robustness.

Spray methods are potential candidates for scaled up fabrication of super liquid-repellent surfaces.^[15,16] Particularly, liquid flame spray (LFS) has been applied to produce superhydrophobic surfaces in high-speed roll-to-roll processes.^[17–19] In LFS, a liquid feedstock is injected and atomized in an oxygen-hydrogen flame. Dissolved in the liquid are organometallic precursor molecules. After evaporating and reacting in the flame they form nanoparticles. These nanoparticles are collected on the surface. With the heat from the flame the particles partially sinter together to form a stable, highly porous film. Advantages of LFS are that the deposition process is solvent-free and takes only fractions of seconds as the sample is rapidly moved

Dr. H. Teisala, F. Geyer, Prof. D. Vollmer, Prof. H.-J. Butt
Department of Physics at Interfaces
Max Planck Institute for Polymer Research
Ackermannweg 10 D-55128, Mainz, Germany
E-mail: teisala@mpip-mainz.mpg.de; butt@mpip-mainz.mpg.de

J. Haapanen, P. Juuti, Prof. J. M. Mäkelä
Laboratory of Physics
Tampere University of Technology
P.O. Box 692 FI-33101, Tampere, Finland

 The ORCID identification number(s) for the author(s) of this article can be found under <https://doi.org/10.1002/adma.201706529>.

DOI: 10.1002/adma.201706529

through the flame spray even at the velocities of the order of m s^{-1} . In addition, a broad range of materials including vulnerable biomaterials, such as cellulose-based paper and wood can be coated.^[16,20] A certain minimal velocity is required to avoid destroying the substrate.

Here we use LFS to fabricate a superamphiphobic and optically transparent silicon dioxide (SiO_2)–titanium dioxide (TiO_2) nanoparticle coating on glass. Our coating shows minimal solid–liquid interactions for both high- and low-surface-tension, polar and nonpolar liquids. Drops of water and *n*-hexadecane (10 μL) deposited on the surface easily roll off the coating at inclination angles $<1^\circ$. To our knowledge, this is the lowest roll-off angle toward hexadecane ever reported. To achieve these superior properties, first, we adjusted the surface morphology by varying the ratio of silicon dioxide and titanium dioxide in the coating. Second, after achieving the right morphology, we applied chemical vapor deposition (CVD) of a 1*H*,1*H*,2*H*,2*H*-perfluorooctyl-trichlorosilane (97% pure, Sigma-Aldrich) to lower the surface energy. In this way, we left the nanoporous morphology of the coating intact. This is necessary to achieve the superamphiphobic properties—already a 20 nm thick additional layer on top of the nanoparticles hinders liquid repellency.

To synthesize the surfaces by LFS, we use hydrogen (50 L min^{-1}) and oxygen (15 L min^{-1}) as combustion gases to achieve a turbulent, high temperature flame ($>2500^\circ\text{C}$),^[19] and inject the liquid feedstock, tetraethyl orthosilicate (TEOS, 98% pure, Alfa Aesar) and titanium(IV) isopropoxide (TTIP, 97% pure, Alfa Aesar) dissolved in isopropanol (technical grade, Neste), into the flame through a custom-made spray torch at a feed rate of 12 mL min^{-1} (the overall Si+Ti atomic concentration in the precursor solution was kept constant at 50 mg mL^{-1}), **Figure 1**. The organometallic precursors react and nucleate in the flame to form nanosized oxide particles. The particles aggregate and are deposited directly on the surface—driven by diffusion and thermophoresis through a boundary layer of air at the substrate^[19]—to form a porous coating. More details of LFS method are given elsewhere.^[17–19] Silicon dioxide and titanium dioxide were selected as coating materials since they are widely used in different coating applications such as painting,^[21] cast-,^[22] dip-,^[23] spray-,^[18] and vapor-phase^[4] deposition. Titanium dioxide is well-known for its photocatalytic activity. This property can be utilized in self-cleaning coatings^[24] and to decompose atmospheric pollutants such as nitrogen oxides (NO_x).^[21]

We first investigate potential of a pure silicon dioxide coating (Si/Ti ratio = 100/0 wt% in the precursor) to form the overhang morphology. From now on, we call this “Si 100 wt% coating.” The coating was synthesized on a smooth glass substrate by injecting TEOS diluted in isopropanol into the upward pointing LFS flame, through which the sample was moved at a velocity of 0.8 m s^{-1} at the distance of 6 cm from the burner face. Scanning electron microscopy shows that the resulting coating is ≈ 100 nm thick and is composed of highly sintered, round sub-micrometer scale clusters evenly distributed on the surface (Figure 1a,g). After fluorination the surface shows moderate liquid repellency with apparent static contact angles of 138° for water (surface tension $\gamma = 72.8 \text{ mN m}^{-1}$), 118° for ethylene glycol ($\gamma = 47.3 \text{ mN m}^{-1}$, 99.8% pure, Sigma-Aldrich), and 83° for *n*-hexadecane ($\gamma = 27.5 \text{ mN m}^{-1}$, 99% pure, Sigma-Aldrich).

To enhance liquid repellency, we use two approaches (Figure 1). First, we substitute part of the silicon dioxide by titanium dioxide in the coating by adding TTIP to the precursor solution (Figure 1, leftmost column). Second, we increase the thickness of the coating by applying 5 LFS coating cycles prior to fluorination (Figure 1, middle column). To gain insight on the individual agglomerate morphology, we collected particles from LFS on transmission electron microscopy grids (Figure 1, rightmost column).

Already 1 wt% addition of titanium atoms with respect to silicon atoms in the precursor (Si/Ti ratio = 99/1 wt%) drastically changes the morphology of the coating. We call this “Si 99 wt% coating,” Figure 1c,h. An energy dispersive X ray spectroscopy (EDS/EDX) analysis indicates that the Si/Ti ratio within the coating is 96.2/3.8 wt% (Figure S1 and Table S1, Supporting Information). The changes become more prominent when the titanium content was increased up to 99 wt% (Si/Ti ratio = 1/99 wt%). We call this “Si 1 wt% coating,” Figure 1e,i,j. Silicon dioxide is no longer aggregated in highly sintered, dense clusters. Instead, the coating shows increasing amount of porous, nanosized particle aggregates with overhang structures. EDS/EDX analysis shows that the Si/Ti ratio within the coating is 2.1/97.9 wt%. Titanium dioxide exists mainly as anatase with small fraction, 10–15%, of rutile independently on the Si/Ti ratio. Anatase is known to be photocatalytically more active than rutile.^[25] Silicon dioxide remains amorphous.^[18] We speculate that these morphological changes are caused by an early nucleation of titanium dioxide in the cooling flame, while silicon dioxide remains still in vapor phase.^[18,19] Titanium dioxide particles thus act as nucleation sites for silicon dioxide and facilitate formation of the porous particle aggregates within the coating. Silicon dioxide, which sinters at lower temperature than titanium dioxide, acts as a “binding agent” within the coating and thus enhances its mechanical stability (see discussion with drop impact and sand abrasion experiments).

Then we increase the coating thickness by moving the samples through the flame spray 5 sequential times at intervals of ≈ 2 s. The growth mechanism of the coating through the boundary layer of air at the surface—driven by thermophoresis and diffusion—induces accumulative growth of large particle aggregates at the surface (Figure S2, Supporting Information). As a consequence, the height of the surface protrusions and hierarchical roughness of the coating increase (Figure 1b,d,f,k; and Figures S3 and S4, Supporting Information). The final height of the surface textures depends on the coating composition. With highly sintered, dense Si 100 wt% coating the highest protrusions reach ≈ 700 nm after 5 coating cycles (Figure S3, Supporting Information). With Si 1 wt% coating the highest peaks of the surface texture are ≈ 700 nm already after the first coating cycle (Figure 1j) and reach a height of at least 7 μm after 5 cycles (Figure 1k; and Figure S4, Supporting Information).

After a single LFS coating cycle, referred to as “thin coating,” the best liquid repellency is given by Si 1 wt% coating. Water drops deposited on the surface adapt a spherical shape with static contact angle $>160^\circ$. 10 μL sized drops roll off the surface as soon as the substrate is inclined by less than $\approx 3^\circ$. With ethylene glycol and *n*-hexadecane, the static contact angles

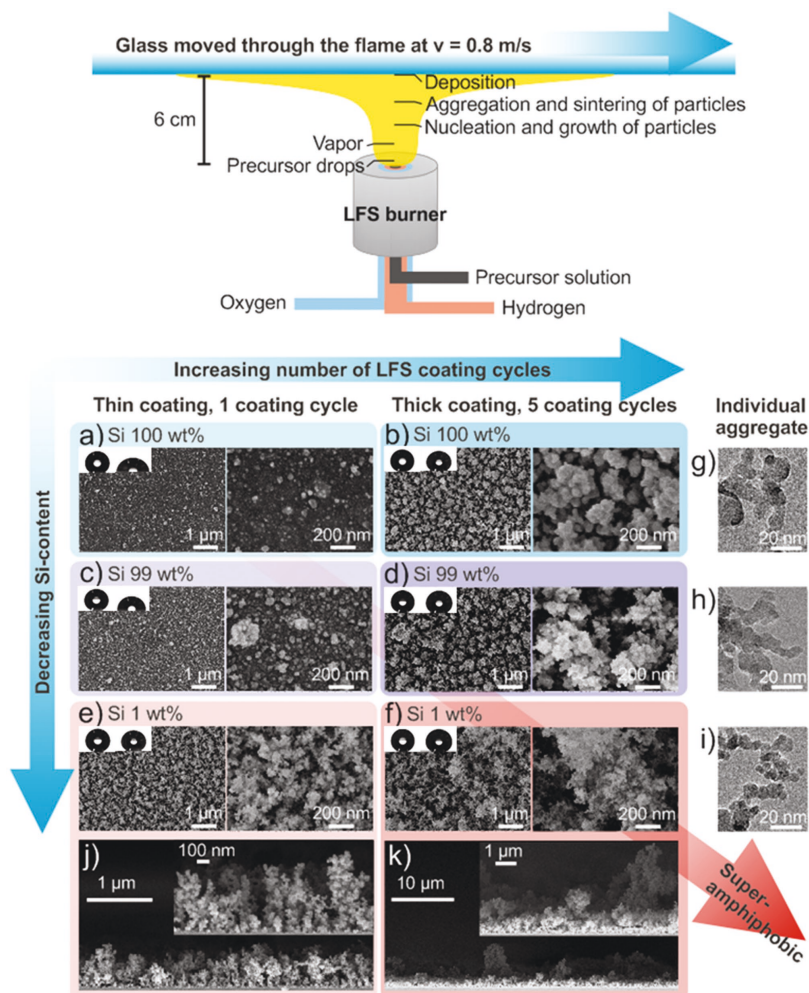


Figure 1. Synthesis and morphology of nanotextured liquid-repellent coatings by LFS. Top: schematic illustration of the coating procedure (not to scale). Bottom: top-view scanning electron microscopy (SEM) images of the coatings with different silicon dioxide content and thickness after chemical vapor deposition (CVD) of the fluorosilane. a,b) Si 100 wt%; c,d) Si 99 wt%; and e,f) Si 1 wt% coating. Insets: the shape of 5 μ L water (left) and *n*-hexadecane (right) drops resting on the respective surfaces. Transmission electron microscopy (TEM) images show different degree of sintering and overhang morphology of the particle aggregates: g) Si 100 wt%, h) Si 99 wt%, and i) Si 1 wt% coating. Side-view SEM images of j) Si 1 wt% thin coating (coated 1 time) and k) Si 1 wt% thick coating (coated 5 times).

approach 150° but the drops pin to the surface, i.e., roll-off angles are typically $>10^\circ$ (Table 1).

A coating with superamphiphobic properties was achieved by coupling the two approaches, i.e., by reducing the amount of Si/Ti ratio in the precursor from 100/0 wt% to 1/99 wt% and by increasing the number of coating cycles from 1 to 5, referred to as “thick coating.” In this way, we obtained a roll-off angle below 1° for 10 μ L *n*-hexadecane drops. Advancing and receding contact angles were 165° with nonmeasurable contact angle hysteresis when the drop volume was increased and decreased between 15 and 25 μ L at the rate of 1 μ L s^{-1} using

a standard contact angle goniometer (Figure S5 and Video S1, Supporting Information).

The superamphiphobic coating developed here shows extremely low interaction with water and even with *n*-hexadecane. To our knowledge, the lowest roll-off angles reported for *n*-hexadecane on superamphiphobic surfaces are 2° – 5° depending on the surface and the drop size.^[2–5,7,9,10,16] Here, 10 μ L drops of *n*-hexadecane typically rolled off the surface as soon as the goniometer needle tip was detached although the substrate was adjusted in horizontal plane without any apparent inclination angle (Video S2, Supporting Information).

Table 1. Wettability of the liquid-repellent coatings. Apparent static contact angles (CA) and roll-off angles (RA) of 10 μL drops of water, ethylene glycol, and *n*-hexadecane on coatings with different silicon dioxide content and thickness after chemical vapor deposition of the fluorosilane. "Thin" refers to a single LFS coating cycle. "Thick" refers to 5 subsequent LFS coating cycles. The standard deviations are given by individual contact angle goniometer measurements. Note that contact angles larger than $\approx 155^\circ$ cannot reliably be measured using the goniometer technique and thus the real error is larger.

Coating	Water CA/RA [°]	Ethylene glycol CA/RA [°]	<i>n</i> -Hexadecane CA/RA [°]
Si 100 wt%, thin	138 \pm 3/–	118 \pm 1/–	83 \pm 1/–
Si 100 wt%, thick	168 \pm 1/<1	154 \pm 3/50 \pm 3	146 \pm 1/–
Si 99 wt%, thin	157 \pm 4/13 \pm 10	126 \pm 5/–	91 \pm 4/–
Si 99 wt%, thick	168 \pm 1/<1	160 \pm 5/6 \pm 1	153 \pm 2/–
Si 1 wt%, thin	163 \pm 2/3 \pm 1	154 \pm 2/12 \pm 1	151 \pm 2/29 \pm 7
Si 1 wt%, thick	167 \pm 1/<1	164 \pm 1/<1	157 \pm 4/1 \pm 1

Our coating consists of random, overhang nanostructures where the diameter of spherical primary particles is $\approx 10\text{--}20$ nm. We investigated the effect of texture size on water repellency by growing an additional 20 nm thick silicon dioxide layer on the surface using a gas-phase Stöber-like reaction.^[4] After growing the silicon dioxide layer (Figure S6, Supporting Information) and modifying the surface with the fluorosilane, the antiwetting performance declined. For all coating compositions (Si 100 wt%, Si 99 wt%, and Si 1 wt%) the water contact angle decreased and the roll-off angle increased due to the increased solid–liquid contact area and smoothed out overhangs as compared to the pristine coatings (Table S2, Supporting Information). This underlines the role of nanosized texture in reducing the solid–liquid interactions on the coating. Coupling this nanosized texture with pronounced hierarchical surface roughness supports the air cushion below the liquids and leads to extremely small overall contact area between the coating and the liquids.

We expect that the extreme liquid repellency of the thick Si 1 wt% layer is caused by the hierarchical surface roughness in addition to the overhanging morphology on the 10 nm scale. A simple estimation on a surface consisting of spherical, randomly aggregated particles shows that this combination ensures low penetration depth and wetted contact area of both polar and nonpolar liquids on the solid substrate, **Figure 2**. Knowing the mean radius of the particles r and the Young contact angle θ on the solid, fluorinated silicon oxide, the penetration depth δ around a single particle on the surface in thermodynamic equilibrium at zero external pressure can be estimated (Figure 2a, Supporting discussion in the Supporting Information) to be $\delta \approx 0.58r$ for

water ($\theta = 115^\circ$) and $\delta \approx 1.29r$ for *n*-hexadecane ($\theta = 73^\circ$). Here, we assumed that the particle is fixed at the bottom. Taking into account the random packing in the porous structure, the number of wetted particles underneath the first layer of particles will increase before reaching θ (Figure 2b). This increase in the wetted contact area is larger for nonpolar liquids than for polar, high-surface tension liquids. That is, overhangs can support the air cushion below low-surface-tension liquids, however, the liquid still wets large surface area and therefore pins to the solid (Supporting discussion, Supporting Information). To reduce the overall wetted area of the solid and thus adhesion of drops, hierarchical roughness needs to be introduced (Figure 2c). Indeed, several surfaces with inherent hierarchical roughness such as paper,^[9] wood,^[16] and fabrics^[7] serve as ideal substrates for randomly structured superamphiphobic coatings where both polar and nonpolar liquid drops can bead up and easily roll off the surface.

To achieve superamphiphobicity, a nanoscopic overhanging structure needs to be combined with roughness on the >1 μm length scale; in the following we call this a hierarchical structure. Such hierarchical structures need a certain minimum coating thickness. Below this minimum thickness, it might not be possible to create a superamphiphobic surface. The overall solid–liquid contact area would become too large.

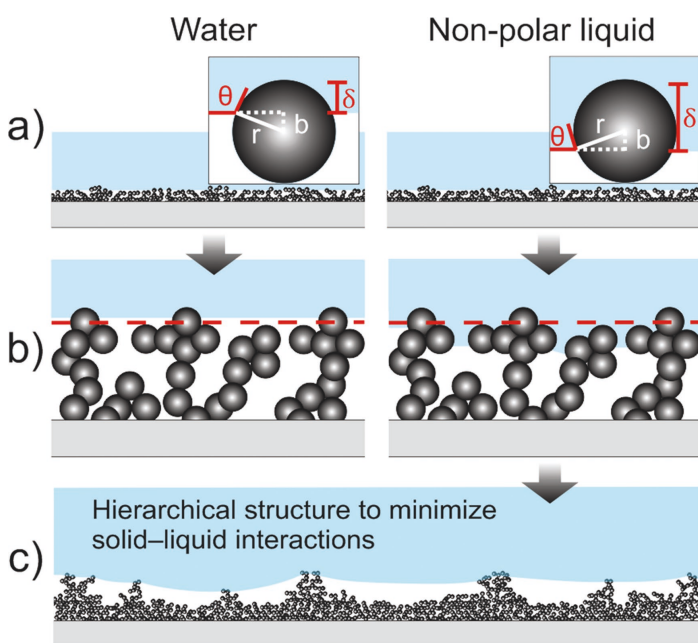


Figure 2. Schematic illustration of wetting of a model surface by water and a nonpolar liquid. The surface consists of spherical particles. Penetration depth δ of the liquid around a single particle with radius r depends on the intrinsic wettability of the material, characterized by the Young contact angle θ . a) Water (large θ) wets small fraction of individual particles within the first particle layer, indicated by the dashed line in (b). A nonpolar liquid (small θ) wets large fraction of individual particles and b) invades from one particle to the other into the texture of the solid until θ is reached at the overhangs. c) Hierarchical roughness of the surface has critically important role in reducing the overall solid–liquid contact area and pinning of low-surface-tension liquids on randomly structured superamphiphobic surfaces.

This condition poses a lower limit to the thickness of a superamphiphobic coating on a smooth substrate such as plain glass. Here the coating was not superamphiphobic after one coating cycle when its thickness was ≈ 700 nm (Figure 1j). However, after 5 coating cycles the coating became superamphiphobic (Figure 1k; and Figure S4, Supporting Information). It is reasonable to assume that with most of the randomly structured superamphiphobic surfaces, the hierarchical surface structure increases with increasing coating thickness. For example, the candle soot templated coating remains superamphiphobic only when the coating is thicker than ≈ 2 μm .^[4,26]

We verify optical transparency of our coatings by ultraviolet–visible light transmittance spectroscopy. All thin coatings (coated 1 time) transmit more than 98% as compared to the transmittance through the pristine glass substrate (for wavelengths higher than 500 nm, Figure S7, Supporting Information). Thick coatings (coated 5 times) transmit 97% of the light for Si 100 wt% coating and 79% for Si 1 wt% coating (Figure 3a). High transmittance of light at the visible light spectrum results in good optical transparency (Figure 3b) of the super liquid-repellent coatings (Figure 3c).

In addition to liquid repellency and optical transparency, the impalement resistance of the coating decides about potential applications. How stable is the Cassie–Baxter state before the whole surface texture is wetted by the liquid and the system goes to the so-called Wenzel state?^[27] We investigate the impalement resistance of our superamphiphobic coating by letting water drops impact the surface from different heights. Water drops of 15 μL volume (radius $R = 1.5$ mm) were released from heights of 1–200 cm leading to impact velocities v between 0.4 and 5.4 m s^{-1} . This approaches the terminal velocity of

falling medium-sized rain drops ($R < 1$ mm).^[28] Such an impact velocity and drop radius corresponds to Weber numbers up to $We = \rho v^2 R / \gamma \approx 600$. Here, ρ is the density of water = 1 g cm^{-3} . The drops always rebounded from the surface and no impalement was observed.

To prevent full or partial penetration of the impinging drops,^[11] the capillary pressure P_C generated within the textures should be higher than the maximal effective hammer pressure P_E , which is the upper limit for the pressure the surface can experience during the impact. For drops impacting on horizontal flat surface, one can estimate the maximal hammer pressure^[29]

$$P_E \approx 0.2\rho C v \quad (1)$$

Here, C is the sound velocity (for water $C = 1497$ m s^{-1}). For an impact velocity $v = 5.4$ m s^{-1} and water the hammer pressure can be estimated to be 1.6 MPa. The maximal capillary pressure developed within the particle-like surface texture to prevent the impalement can be estimated from^[30]

$$P_C \approx \frac{2\gamma r}{d^2} \sin^2 \frac{\theta_{adv}}{2} \quad (2)$$

Here, d is the mean distance between protrusions, r is the radius of the constituting particles, and $\theta_{adv} = 119^\circ$ is the advancing contact angle of water on a smooth fluorosilane coated silicon oxide. When the hammer pressure P_E exceeds P_C , one expects the Cassie–Baxter state to collapse. With roughly $r = 5$ –10 nm and setting $P_E = P_C$ we get a required maximal spacing of protrusions = 18–26 nm. On our coating, the smallest pores between the particles and their aggregates can fulfill this criterion (Figure 1f,i). It is expected that the liquid will penetrate in between the largest protrusions on the surface. These protrusions dampen the impact and relief the pressure experienced by the surface in between them. For comparison, on a rectangular array of the fluorosilane modified SU8 micropillars with solid area fraction of 0.06 (5 μm side wall, 10 μm height, 15 μm spacing, fabricated by photolithography^[31]) impalement of impacting 15 μL water drops occurred already at the hammer pressure of ≈ 240 kPa (release height = 3 cm, impact $v = 0.8$ m s^{-1} , $We = 12$).

The superamphiphobic coating also repels impalement of impacting *n*-hexadecane drops ($R = 1$ mm, $\rho = 0.773$ g cm^{-3} , Figure 4). At 1 cm release height the 5 μL drop bounced 4 times before settling down at the surface ($v = 0.4$ m s^{-1} , $We = 5.4$, Video S3, Supporting Information). At 10 cm release height the drop bounced 6 times before settling down ($v = 1.4$ m s^{-1} , $We = 55$, Video S4, Supporting Information). The *n*-hexadecane drops even rebound when released from a height of 50 cm. The corresponding impact velocity for the drop was 3 m s^{-1} ($We = 250$). Above the release height of 50 cm, the kinetic energy becomes large as compared to the surface tension causing that the rim of the drop breaks up and many satellite drops are generated. Because of the breakdown of the drop, at higher release heights it becomes difficult to reliably determine whether the drop partially impales the coating. Calculating the pressure experienced by the surface during impact of the *n*-hexadecane drop with Equation (1) and a speed of sound

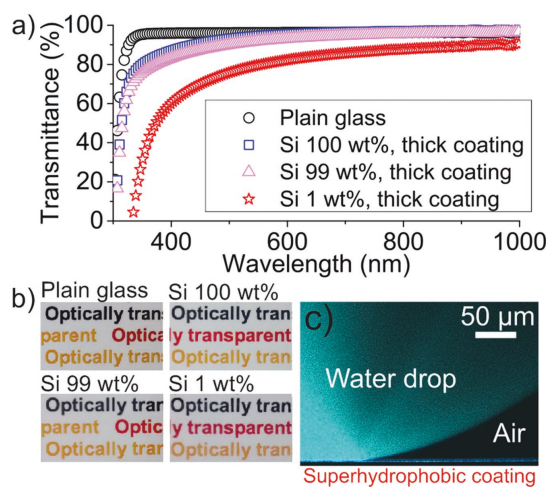


Figure 3. Optical transparency of the liquid repellent coatings. a) Ultraviolet–visible light transmittance spectra of glass before and after the coating. b) Photographs of the thick coatings (coated 5 times) on glass. Printed letters on paper are visible below the liquid repellent coatings. c) Laser scanning confocal microscopy (LSCM) image of a 0.5 μL water drop resting on a ≈ 700 nm thick superhydrophobic coating on a glass substrate (Si 100 wt%, thick coating). The drop was fluorescently labeled with ATTO 488 hydrophilic dye at the concentration of 1 $\mu\text{g mL}^{-1}$.

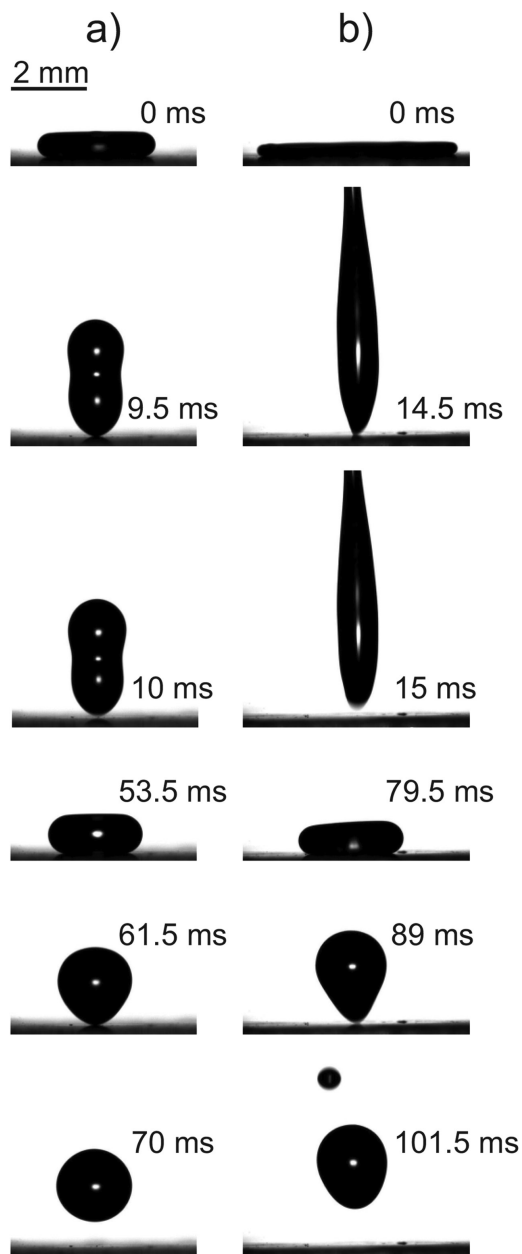


Figure 4. 5 μL *n*-hexadecane drops ($R = 1$ mm) impinging the superamphiphobic surface at different velocities. The snapshot images of a high-speed camera (2000 fps) show the maximum spreading and take off of the drops within the first and the second rebound at the surface at a) impingement velocity $\nu = 0.4$ m s^{-1} (release height = 1 cm, $We = 5.4$) and b) $\nu = 1.4$ m s^{-1} (release height = 10 cm, $We = 55$). At the higher impingement velocity $\nu = 1.4$ m s^{-1} the drop generated a satellite drop within the impact, which is merging with the main drop after the second rebound.

in *n*-hexadecane = 1339 m $\text{s}^{-1[32]}$ we get $P_E = 650$ kPa for the impact from the height of 50 cm. Assuming that this pressure is balanced by the capillary pressure (Equation (2)) a protrusion spacing of maximal $d = 13\text{--}18$ nm is allowed when $\theta_{\text{adv}} = 77^\circ$ is the advancing contact angle of *n*-hexadecane on a smooth fluorosilane coated silicon oxide. This is in the same order of magnitude that we got for the maximal spacing with water.

The mechanical stability of the superamphiphobic coating (Table S3, Supporting Information) was tested by letting 15 μL water drops impact on the surface from the release height of 200 cm at $\nu = 5.4$ m s^{-1} . The sample was tilted by 10° to ensure rapid removal of the impinging drops. The coating could withstand at least 20 000 drop impacts (90 impacts min^{-1}) by completely allowing the impinging drops to bounce off the surface. After the experiment, roll-off angle of 10 μL water drops at the impacted area was 13° . The nanotexture was partially damaged and *n*-hexadecane drops started to pin to the impacted surface (Figure S8, Supporting Information). With increasing silicon dioxide content the mechanical stability of the coating increased against impacting drops. After 20 000 drop impacts on both the Si 100 wt% and Si 99 wt% coating the roll-off angle of 10 μL water drops remained at $3^\circ\text{--}5^\circ$. That is, the surfaces remained superhydrophobic after the exposure to the impacting drops.

To further test the robustness of the superamphiphobic coating (Si 1 wt%, coated 5 times), in particular the adhesion of the coating to the glass substrate, we exposed the surface to steam and continuous water flush. Therefore, water was heated in a beaker on a hot plate at 150°C and the sample was placed face down 5 cm above the water surface for 1 h. In a second set of experiments, the surface was rinsed with Milli-Q water flow at $\nu = 1.7$ m s^{-1} for 1 h. After both treatments, the roll-off angle for 10 μL water drops remained unchanged, i.e., $<1^\circ$, which indicates good adhesion of the coating. Additionally, the adhesion of the coating was tested by adhering and peeling off an adhesive tape (Scotch Magic), applied with the pressure = 2.5 kN m^{-2} for 60 s. After the tape test, the coating maintained low roll-off angle for both water and *n*-hexadecane, $<1^\circ$ and $6^\circ \pm 2^\circ$, respectively.

Abrasion by impacting sand particles can locally damage the superamphiphobic coating (Si 1 wt%, coated 5 times). After impacting the surface with 100–200 μm diameter sand grains from the height of 2 cm for 10 s (5 g of sand; impact $\nu = 0.63$ m s^{-1} ; sample was adjusted at an angle of 45°), *n*-hexadecane drops pinned to the surface. However, water drops kept the high static contact angle = 155° and roll-off angle = 25° after the abrasion. Although the impact of the sand particles damaged the top part of the protrusions, the measurements indicate that the adhesion of the coating to the glass substrate was not compromised, i.e., it exceeded the cohesive strength of the coating. Si 100 wt% coating (coated 5 times) remained superhydrophobic after the sand abrasion test and maintained a low roll-off angle = 2° for 10 μL water drops.

Temperature-stability of the superamphiphobic coating (Si 1 wt%, coated 5 times) was investigated between -200°C and $+500^\circ\text{C}$. Delamination of the coating was not observed even after freezing the sample in liquid nitrogen for ≈ 30 s (Figure S9, Supporting Information). Roll-off angles for water and *n*-hexadecane remained $<1^\circ$ and $10^\circ \pm 5^\circ$, respectively. Heating the sample in an oven at 500°C for 3 h degraded the

fluorosilane layer. After reapplying the fluorosilane, the coating recovered its high static contact angle $>160^\circ$ and low roll-off angle $<1^\circ$ for both water and *n*-hexadecane.

Photosensitivity of the superamphiphobic coating (Si 1 wt%, coated 5 times) was investigated by illuminating the surface with UV-A light ($2.3 \pm 0.3 \text{ mW cm}^{-2}$) up to 4 h. After 40 min of illumination, 10 μL drops of *n*-hexadecane pinned to the surface (Table S4, Supporting Information) because of photodegradation of the fluorosilane coating on top. To delay this, before the fluorination we encapsulated the coating with a $\approx 3 \text{ nm}$ thick silicon dioxide shell by applying a gas-phase Stober-like reaction for 4 h. Such a thin passivation layer did not reduce the superamphiphobic properties of the coating. Moreover, the coating remained superamphiphobic even after the UV-A illumination of 4 h: roll-off angles for 10 μL water, and *n*-hexadecane drops were $<1^\circ$ and $4^\circ \pm 2^\circ$, respectively.

Robustness of the air cushion on the superamphiphobic coating (Si 1 wt%, coated 5 times) under prolonged contact with *n*-hexadecane was investigated by letting 10 μL drops to rest on the surface for 30 min. The static contact angle remained unchanged within the experimental error (Figure S10, Supporting Information). After the period of 30 min, roll-off angle for the *n*-hexadecane drops was $10^\circ \pm 2^\circ$, proving the stability of the air cushion.

In summary, we introduce an up-scalable method to fabricate optically transparent superamphiphobic surfaces with low drop adhesion and high impalement resistance against both high- and low-surface-tension liquids. With LFS and by mixing Si and Ti precursors, surfaces can be fabricated with high apparent contact angles and low roll-off angles below $\approx 1^\circ$ even for *n*-hexadecane. To achieve an ultralow drop adhesion for nonpolar liquids, the superamphiphobic surface needs to fulfill the following criteria: (1) low-surface-energy chemistry, (2) nanoscale, overhang surface structures, (3) hierarchical roughness, and (4) sub-micrometer scale pore size to increase the critical impalement pressure. We show that increasing the Ti content or increasing the number of coating cycles increases porosity, thickness, and hierarchical structure of the coating. Both measures improve the superamphiphobic properties. On the other hand, optical transparency of the coating decreases and better mechanical stability is achieved with a high Si content. The Si/Ti ratio needs to be optimized depending on the specific requirements for the coating.

Experimental Section

Surface Modification: Prior to CVD with the fluorosilane the samples were activated by oxygen plasma (Femto low-pressure plasma system, Diener electronic, Germany) at 300 W for 10 min. The samples were placed in a desiccator together with 100 μL of the fluorosilane and the pressure was reduced to $\approx 200 \text{ mbar}$ for 2 h. After the CVD, the samples were placed in a vacuum oven at 60°C for 2 h to remove unreacted silane. To investigate the effect of the size of surface textures on the wetting properties of the coatings, a gas-phase Stober-like reaction was applied for selected samples (Si 100 wt%, Si 99 wt%, Si 1 wt%, coated 1 time). The samples were placed in a desiccator together with ammonia (3 mL) and TEOS (3 mL) at atmospheric pressure and room temperature for 24 h. This resulted in growth of an additional 20 nm thick porous silicon dioxide shell around the particles.^[4] After the silicon dioxide growth, the samples were sintered in an oven at 500°C for

3 h and subsequently fluorinated by the CVD process. Sintering induces compactification of the silica shell. To delay photocatalytic degradation of the fluorosilane, the superamphiphobic coating (Si 1 wt%, coated 5 times) was passivated by growing a thin, $\approx 3 \text{ nm}$ thick silicon dioxide layer on the surface by applying the gas-phase Stober-like reaction for 4 h. After this, the coating was fluorinated by CVD. The coating was not sintered in the oven.

Microscopy/Spectroscopy: For SEM imaging (LEO 1530 Gemini, Zeiss), the samples were sputter-coated with a nm thick Pt layer to reduce the surface charging. The used sputtering time would yield a layer thickness of $\approx 7 \text{ nm}$ on a smooth substrate. TEM imaging was performed with JEOL JEM-2010 instrument. The samples were collected on lacey carbon film on copper grid (Agar) directly from LFS at the distance of 6 cm from the burner face by moving the grid through the flame at the velocity of 0.8 m s^{-1} . The chemical composition of the coatings was investigated using a Hitachi SU8000 SEM equipped with EDS/EDX. For the analysis, the porous oxide coatings (coated 5 times) were scraped from the glass substrate onto a conductive carbon tape to exclude any Si signal originating from the substrate. At least 3 measurements at different positions were conducted. An inverted laser scanning confocal microscope (Leica TCS SP8 SMD, Leica Microsystems) with HC PL APO CS2 40x/1.10 water objective was used to capture a micrograph of a water drop resting on Si 100 wt% surface.

Wetting Properties: Static contact angles with 5 μL drops and roll-off angles with 10 μL drops of water, ethylene glycol, and *n*-hexadecane were measured by DataPhysics OCA 35 goniometer (DataPhysics Instruments) using 3–5 individual measurements at different positions on each sample. Static contact angles larger than 155° cannot reliably be measured using the goniometer technique as for high contact angles real position of the base line is difficult to determine and even small variation greatly influences the measured values. Although the measured values may be too low, the trend should be correct. Advancing and receding contact angles were measured by increasing the drop volume from 0 to 25 μL and decreasing the volume back to $\approx 0 \mu\text{L}$ at the rate of $1 \mu\text{L s}^{-1}$. The dynamic contact angles were carefully analyzed using Fiji,^[33] an open-source image processing software. Contact angle hysteresis was determined using drop volumes of 15–25 μL to prevent that the goniometer needle affected the results.^[34] Impingement dynamics of 5 μL *n*-hexadecane drops were investigated using Photron Fastcam Mini UX100 high-speed camera (2000 fps).

Illumination and Light Transmittance: To test UV stability, the samples were illuminated by UV-A light (intensity = $2.3 \pm 0.3 \text{ mW cm}^{-2}$) from the distance of 8 cm (light source: LQ-400, Dr. Gröbel UV-Elektronik GmbH). Intensity of the illumination was measured using an UV-radiometer RM-12 with UV-A sensor for spectral range of 315–400 nm (Dr. Gröbel UV-Elektronik GmbH). Ultraviolet–visible light spectrometer (Lambda 25, PerkinElmer) was used to investigate light transmittance of the coatings.

Supporting Information

Supporting Information is available from the Wiley Online Library or from the author.

Acknowledgements

This work was funded by the ERC advanced Grant No. 340391—SUPRO, the Collaborative Research Center 1194, and the European Union's Horizon 2020 research and innovation program LubISS No 722497. H.T. acknowledges Tekes—the Finnish Funding Agency for Innovation (Grant No. 40365/14), Walter Ahlström Foundation (Tutkijat maailmalle—program), and Alexander von Humboldt Foundation for financial support. Dr. Mari Honkanen (Tampere University of Technology) is acknowledged for the TEM images. Gunnar Glasser is acknowledged for the EDS/EDX analysis. Olinka Ramirez and Dr. Jonathan Pham are acknowledged for technical support.

Conflict of Interest

The authors declare no conflict of interest.

Keywords

omniphobic, spray coating, superhydrophobic, superoleophobic, wetting

Received: November 8, 2017

Revised: January 9, 2018

Published online: February 27, 2018

- [1] K. Tsujii, T. Yamamoto, T. Onda, S. Shibuichi, *Angew. Chem., Int. Ed. Engl.* **1997**, 36, 1011.
- [2] A. Tuteja, W. Choi, M. Ma, J. M. Mabry, S. A. Mazzella, G. C. Rutledge, G. H. McKinley, R. E. Cohen, *Science* **2007**, 318, 1618.
- [3] J. Zhang, S. Seeger, *Angew. Chem., Int. Ed. Engl.* **2011**, 50, 6652.
- [4] X. Deng, L. Mammen, H.-J. Butt, D. Vollmer, *Science* **2012**, 335, 67.
- [5] Z. Chu, S. Seeger, *Chem. Soc. Rev.* **2014**, 43, 2784.
- [6] F. Schellenberger, N. Encinas, D. Vollmer, H.-J. Butt, *Phys. Rev. Lett.* **2016**, 116, 096101.
- [7] A. K. Kota, G. Kwon, A. Tuteja, *NPG Asia Mater.* **2014**, 6, e109.
- [8] M. Paven, P. Papadopoulos, S. Schöttler, X. Deng, V. Mailänder, D. Vollmer, H. J. Butt, *Nat. Commun.* **2013**, 4, 2512.
- [9] L. Jiang, Z. Tang, R. M. Clinton, V. Breedveld, D. W. Hess, *ACS Appl. Mater. Interfaces* **2017**, 9, 9195.
- [10] F. Geyer, C. Schönecker, H.-J. Butt, D. Vollmer, *Adv. Mater.* **2017**, 29, 1603524.
- [11] a) D. Bartolo, F. Bouamrine, É. Verneuil, A. Buguin, P. Silberzan, S. Moulinet, *Europhys. Lett.* **2006**, 74, 299; b) M. Reyssat, A. Pépin, F. Marty, Y. Chen, D. Quéré, *Europhys. Lett.* **2006**, 74, 306; c) Y. Liu, L. Moevius, X. Xu, T. Qian, J. M. Yeomans, Z. Wang, *Nat. Phys.* **2014**, 10, 515.
- [12] A. B. D. Cassie, S. Baxter, *Trans. Faraday Soc.* **1944**, 40, 546.
- [13] T. Liu, C.-J. Kim, *Science* **2014**, 346, 1096.
- [14] a) R. Dufour, P. Brunet, M. Harnois, R. Boukherroub, V. Thomy, V. Senez, *Small* **2012**, 8, 1229; b) A. G. Marín, H. Gelderblom, A. Susarrey-Arce, A. van Houselt, L. Lefferts, J. G. Gardeniers, D. Lohse, J. H. Snoeijs, *Proc. Natl. Acad. Sci. USA* **2012**, 109, 16455.
- [15] a) H. Teisala, M. Tuominen, J. Kuusipalo, *Adv. Mater. Interfaces* **2014**, 1, 1300026; b) Y. Si, Z. Guo, *Nanoscale* **2015**, 7, 5922; c) W. S. Wong, G. Liu, N. Nasiri, C. Hao, Z. Wang, A. Tricoli, *ACS Nano* **2017**, 11, 587; d) W. Cui, T. Wang, A. Yan, S. Wang, *Appl. Surf. Sci.* **2017**, 400, 162; e) X. Zhu, Z. Zhang, G. Ren, X. Men, B. Ge, X. Zhou, *J. Colloid Interface Sci.* **2014**, 421, 141.
- [16] M. Tuominen, H. Teisala, J. Haapanen, J. M. Mäkelä, M. Honkanen, M. Vippola, S. Bardage, M. E. P. Wälinder, A. Swerin, *Appl. Surf. Sci.* **2016**, 389, 135.
- [17] H. Teisala, M. Tuominen, M. Aromaa, J. M. Mäkelä, M. Stepien, J. J. Saarinen, M. Toivakka, J. Kuusipalo, *Surf. Coat. Technol.* **2010**, 205, 436.
- [18] J. Haapanen, M. Aromaa, H. Teisala, M. Tuominen, M. Stepien, J. J. Saarinen, M. Heikkilä, M. Toivakka, J. Kuusipalo, J. M. Mäkelä, *Mater. Chem. Phys.* **2015**, 149–150, 230.
- [19] J. M. Mäkelä, M. Aromaa, H. Teisala, M. Tuominen, M. Stepien, J. J. Saarinen, M. Toivakka, J. Kuusipalo, *Aerosol Sci. Technol.* **2011**, 45, 827.
- [20] H. Teisala, M. Tuominen, M. Aromaa, M. Stepien, J. M. Mäkelä, J. J. Saarinen, M. Toivakka, J. Kuusipalo, *Langmuir* **2012**, 28, 3138.
- [21] N. S. Allen, M. Edge, J. Verran, J. Stratton, J. Maltby, C. Bygott, *Polym. Degrad. Stab.* **2008**, 93, 1632.
- [22] R. A. Caruso, *Topics in Current Chemistry: Colloid Chemistry 1*, Vol. 226, Springer-Verlag, Berlin, Germany **2003**, p. 91.
- [23] L. Xu, J. He, *Langmuir* **2012**, 28, 7512.
- [24] a) Y. Paz, Z. Luo, L. Rabenberg, A. Heller, *J. Mater. Res.* **2011**, 10, 2842; b) S. Wooh, N. Encinas, D. Vollmer, H.-J. Butt, *Adv. Mater.* **2017**, 29, 1604637.
- [25] a) L. Liu, H. Zhao, J. M. Andino, Y. Li, *ACS Catal.* **2012**, 2, 1817; b) T. Luttrell, S. Halpegamage, J. Tao, A. Kramer, E. Sutter, M. Batzill, *Sci. Rep.* **2014**, 4, 4043.
- [26] M. Paven, P. Papadopoulos, L. Mammen, X. Deng, H. Sachdev, D. Vollmer, H.-J. Butt, *Pure Appl. Chem.* **2014**, 86, 87.
- [27] R. N. Wenzel, *Ind. Eng. Chem.* **1936**, 28, 988.
- [28] J. O. Laws, *Trans. Am. Geophys. Union* **1941**, 22, 709.
- [29] a) T. Deng, K. K. Varanasi, M. Hsu, N. Bhate, C. Keimel, J. Stein, M. Blohm, *Appl. Phys. Lett.* **2009**, 94, 133109; b) O. G. Engel, *J. Res. Natl. Bur. Stand.* **1955**, 54, 281.
- [30] a) M. Ye, X. Deng, J. Ally, P. Papadopoulos, F. Schellenberger, D. Vollmer, M. Kappl, H.-J. Butt, *Phys. Rev. Lett.* **2014**, 112, 016101; b) H.-J. Butt, C. Semperebon, P. Papadopoulos, D. Vollmer, M. Brinkmann, M. Ciccotti, *Soft Matter* **2013**, 9, 418.
- [31] F. Schellenberger, J. Xie, N. Encinas, A. Hardy, M. Klapper, P. Papadopoulos, H.-J. Butt, D. Vollmer, *Soft Matter* **2015**, 11, 7617.
- [32] S. Outcalt, A. Laesecke, T. J. Fortin, *J. Chem. Thermodyn.* **2010**, 42, 700.
- [33] J. Schindelin, I. Arganda-Carreras, E. Frise, V. Kaynig, M. Longair, T. Pietzsch, S. Preibisch, C. Rueden, S. Saalfeld, B. Schmid, J. Y. Tinevez, D. J. White, V. Hartenstein, K. Eliceiri, P. Tomancak, A. Cardona, *Nat. Methods* **2012**, 9, 676.
- [34] J. T. Korhonen, T. Huhtamäki, O. Ikkala, R. H. A. Ras, *Langmuir* **2013**, 29, 3858.

